Thesis

NMR and NQR Studies of High Temperature Superconductor $La_{2-x}Sr_xCuO_4$

Shigeki Ohsugi

Faculty of Engineering Science, Osaka University

January 1993

CONTENTS

Abstract

In $La_{2-x}Sr_xCuO_4$(LSCO), the superconductivity emerges just after the disappearance of the magnetic ordering, accompanied by the gradual increase of T_c on doping Sr. The superconducting transition temperature reaches a maximum at T_c=38K for x=0.15 and subsequently starts to decrease. The further increase of Sr doping makes T_c decrease, being T_c=0K at around x=0.3. Though many investigations have been made for high temperature superconductors(HTSC), the mechanism and the origins of the T_c-variation upon Sr content in La system have not been understood yet. In this context, we carried out Cu NQR and NMR experiments for superconducting LSCO. In addition, an NMR study of Chevrel phase superconductors(SC) was performed for a comparison with those of HTSC, in order to stress the unusual relaxation behavior for HTSC.

$(T_1T)^{-1}$ of ^{63}Cu in $La_{2-x}Sr_xCuO_4$ in the normal state exhibits a T-dependence of $C/(T+\theta)$ above around θ and approaches a nearly constant value in a narrow T-region just above T_c. This result suggests that the T-dependence of the staggered susceptibility, χ_Q, at around the zone boundary, $Q=(\pi/a, \pi/a)$, follows the Curie-Weiss law. In addition, the decrease of $1/T_1T$ and the increase of the Knight shift perpendicular to the c-axis, $K_\perp$, upon hole doping testify the decrease of χ_Q and the increase of the uniform susceptibility, χ_o, at the zone center, q=0, respectively.

$1/T_1$'s of ^{205}Tl in Chevrel-phase SC $TlMo_6Se_{7.5}$(T_c=12.2K) and of ^{119}Sn in $Sn_{1.1}Mo_6Se_{7.5}$(T_c=4.2K) decrease exponentially below $0.8T_c$ with $2\Delta = 4.5$ and $3.6k_BT_c$ without and with the Hebel and

Slichter peak(coherence peak), respectively. For the former case, the quasiparticle damping by the strong electron-phonon interaction causes the suppression of the coherence peak just below T_c. In contrast, the steep decrease just below T_c and the power-law like T-dependence at low-T of $1/T_1$ in HTSC cannot be interpreted by the s-wave model, whatever the quasiparticle damping is taken into account.

In the superconducting state, the rapid decrease of $1/T_1$ and $K_\perp$ of Cu in LSCO just below T_c have commonly been observed in whole doping level, verifying the existence of superconducting phases with lower T_c's than 38K from a microscopic point of view.

In the lightly doped region, the behavior of a T_1=const. for ^{63}Cu NQR and the large value of ^{63}Cu NMR line width for x=0.10 at low-T far below T_c have been found. Furthermore, T_c decreases with decreasing θ , becoming zero at x=0.05 when θ is extrapolated to zero. From these results, it is considered that the antiferromagnetic(AF) spin fluctuations at considerably low frequency($\omega \sim 0$) is increased near the magnetic phase boundary.

In the over doped region, a gapless feature of superconductivity was found from characteristic behaviors of a T_1T=const. relation and a presence of the residual spin Knight shift of $K_\perp$ increased upon hole doping at low-T far below T_c. These behaviors of T_1 and Knight shift are pointed out to be understood in terms of a d-wave model in which a finite residual density of states associated with a pair breaking effect is taken into account at the Fermi level. The origin of gapless state should be attributed to the crystal structural instability from orthorhombic to tetragonal phase upon hole doping.

Chapter 1. Introduction

In this chapter, we summarize the basic experimental results on the physical properties of La system and Chevrel compounds, and the purpose of our investigation.

1-1. $La_{2-x}Sr_xCuO_4$

Since the discovery of high-T_c superconducting Ba-La-Cu-O system by J.G. Bednortz and K.A. Muller in 1986,[1] many experimental and theoretical works have been carried out in order to elucidate the mechanism of high-T_c superconductivity. Among them, there is a general consensus that the presence of two dimensional CuO_2 plane is essential for the occurrence of high-T_c superconductivity. It has been established that the doped holes destroying the antiferromagnetic(AF) order and causing the superconductivity are predominantly oxygen-2p like rather than Cu-3d like.

(1) Crystal Structure and Phase Diagram

The crystal structure of LSCO is shown in **Fig.1-1-1**. It has layered perovskite structure of K_2NiF_4-type, in which only single CuO_2 plane exists. The Cu atom is surrounded by octahedral oxygens and La(Sr) layers. La_2CuO_4 is an antiferromagnetic insulator with the Néel temperature, T_N, of 240K and the ordered moment of about $0.6\mu_B$ caused by a superexchange interaction between Cu spins. The spin structure is shown in **Fig.1-1-2**.[2]

By substituting divalent ions such as Sr (Ba, Ca etc.) into

the site of trivalent ions La, or by increasing the oxygen content, holes are introduced into the CuO_2 plane. As seen in the phase diagram for $La_{2-x}Sr_xCuO_4$ of **Fig.1-1-3**,[3] T_N is quickly suppressed by the hole doping.

With the substitution of about x=0.02, the AF long range order is destroyed completely, then the glass like phase appears at low-T.[4,5] With further hole doping, a superconducting phase appears at around x=0.05, and the critical temperature, T_c, attains a broad maximum of 38K at around x=0.15. In further doped region, the bulk superconductivity is suppressed and then transforms into the metallic state.[6,7]

The lattice constants at room temperature plotted against the Sr content in $(La_{1-x}Sr_x)_2CuO_4$ are shown in **Fig.1-1-4**.[7] The systematic change of the lattice parameters upon doping is seen in the figure. It has been reported that any trace of line broadening is not observed over the whole Sr content region, and the orthorhombic to tetragonal transition occurs at around x=0.05 at room temperature.

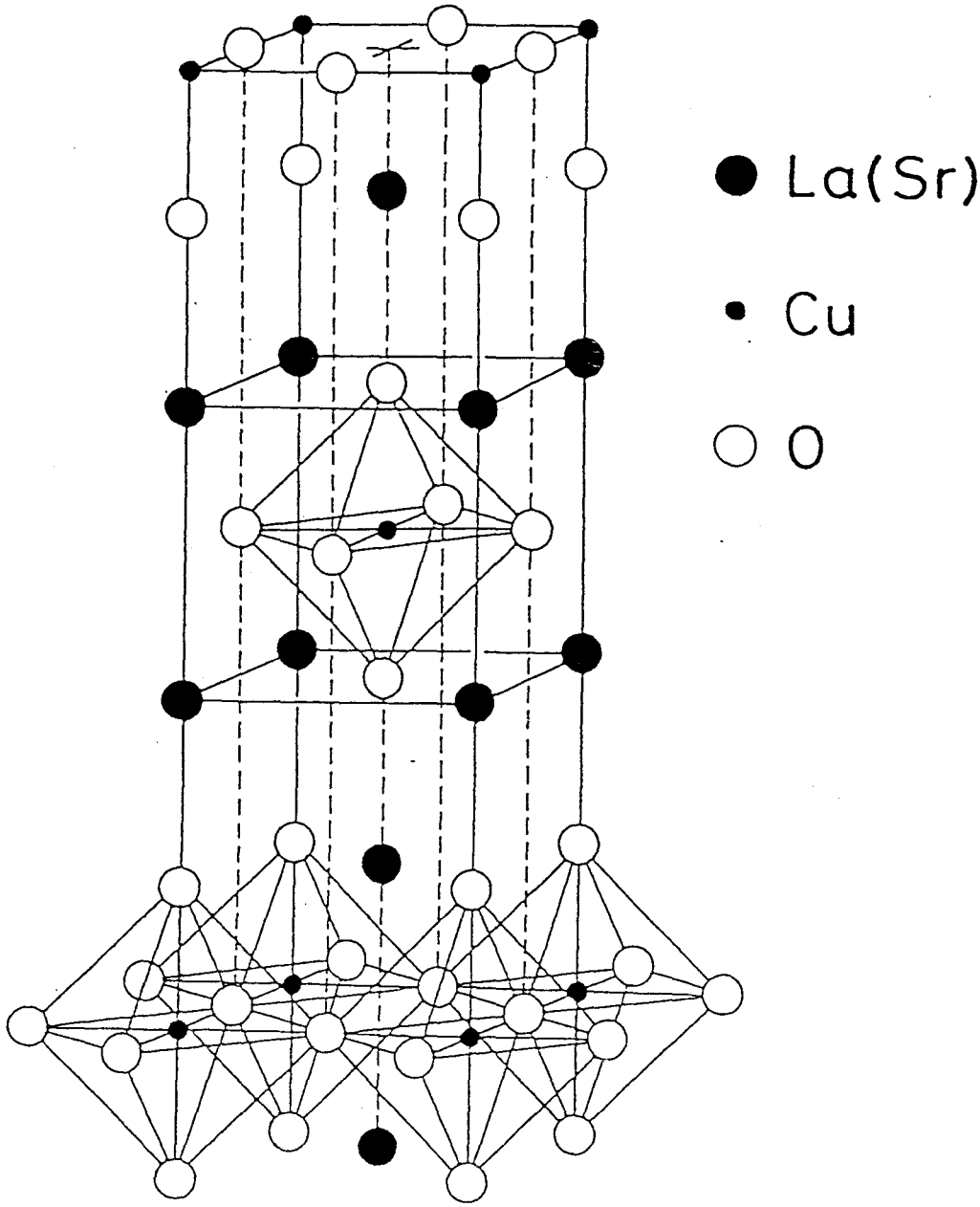

Fig.1-1-1.
Crystal structure of $La_{2-x}Sr_xCuO_4$.

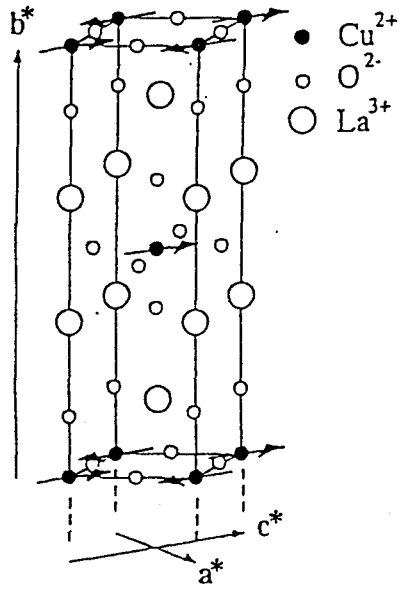

Fig.1-1-2.
Spin structure of La_2CuO_4.[2)]

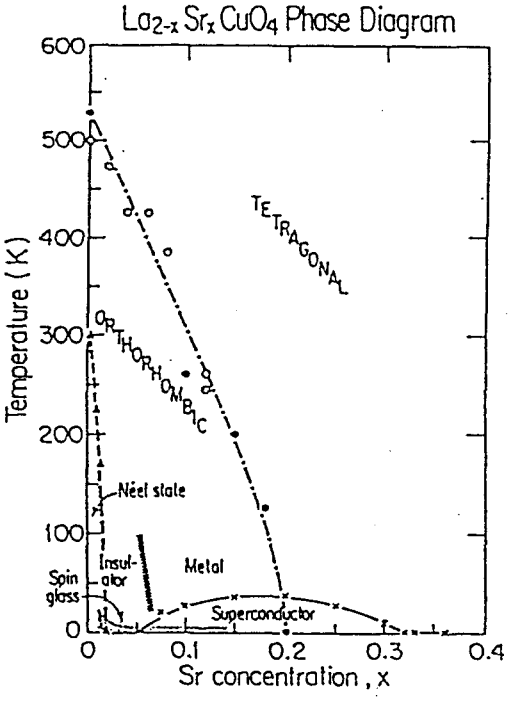

Fig.1-1-3.
Phase diagram of $La_{2-x}Sr_xCuO_4$.[3)]

Fig.1-1-4.
Sr content, x, dependence of the lattice parameters a and c, and oxygen content 4-y determined by the iodometric titration.[7)] For the orthorhombic samples below x=0.05 in $(La_{1-x}Sr_x)_2CuO_4$, normalized lattice parameters $2^{-1/2}a$, $2^{-1/2}b$ and c are shown.

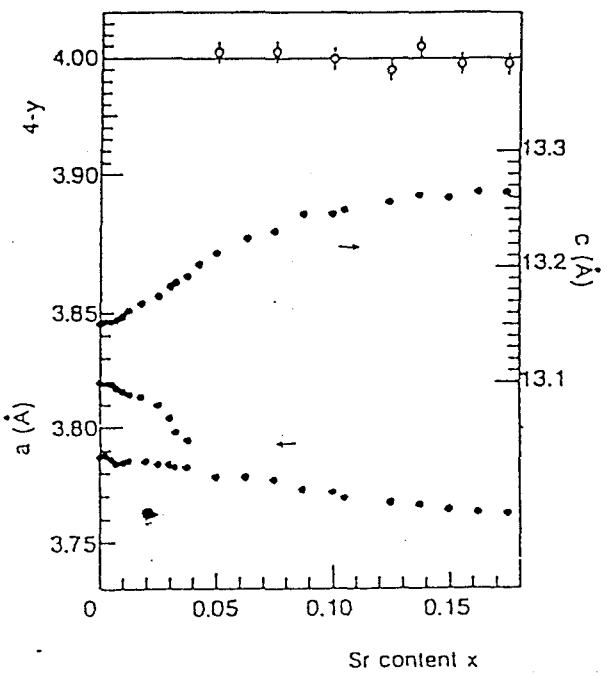

(2) Pysical Properties

One of the anomalous properties in HTSC is the T-dependence of the electrical resistivity. The electrical resistivity changes systematically with hole doping as shown in **Fig.1-1-5.**[8] The resistivity is fairly large and proportional to temperature at high-T below around x=0.075 in $(La_{1-x}Sr_x)_2CuO_4$ as seen in the figure, suggesting that there exists another scattering mechanism such as the spin fluctuations other than the ordinary scattering process with phonons.

The T-dependence of a.c.χ of $(La_{1-x}Sr_x)_2CuO_4$ is shown in **Fig.1-1-6.**[7] T_c's can be determined from these results and the resistivity measurements. Since the magnitude of the Meissner signal is remarkably small at around x=0.03 and 0.125, the presence of inevitable compositional inhomogeneity seems to make the boundary obscure.

In **Fig.1-1-7**, the Hall coefficients of $(La_{1-x}Sr_x)_2CuO_4$ at 80 and 300K are shown against the Sr content, x.[7] The positive Hall coefficient decreases almost in inverse proportion to the Sr content, i.e. 1/x, in the low Sr content region.

In **Fig.1-1-8**, the T-dependence of the bulk static magnetic susceptibility, d.c.χ , is shown for $(La_{1-x}Sr_x)_2CuO_4$.[7] T_N=240K for La_2CuO_4 is demonstrated by the presence of the peak in the T-dependence of d.c.χ . For superconducting LSCO, upon Sr content, the values of d.c.χ are increased. The anomalous behavior is seen in the T-dependence of d.c.χ .

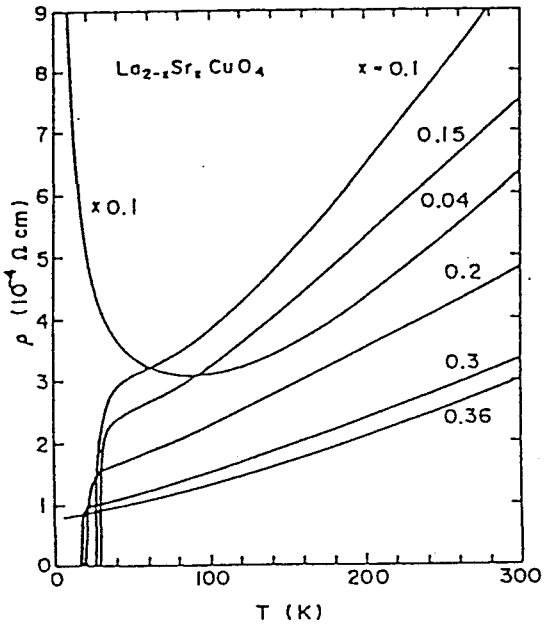

Fig.1-1-5.
T-dependence of the electrical resistivity of $La_{2-x}Sr_xCuO_4$.[8]

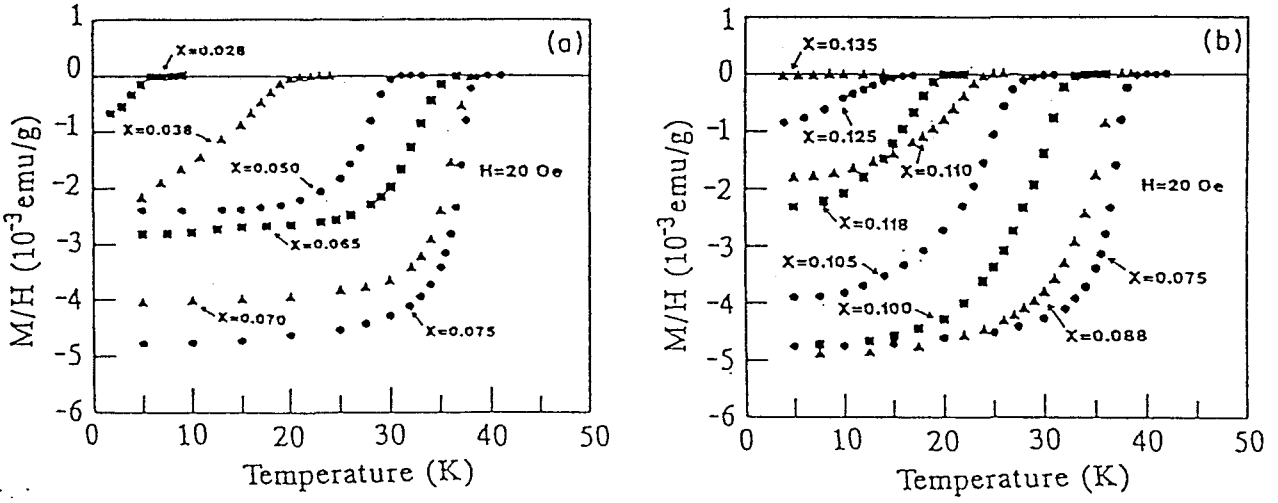

Fig.1-1-6.
T-dependence of a.c.χ of $(La_{1-x}Sr_x)_2CuO_4$.[7]

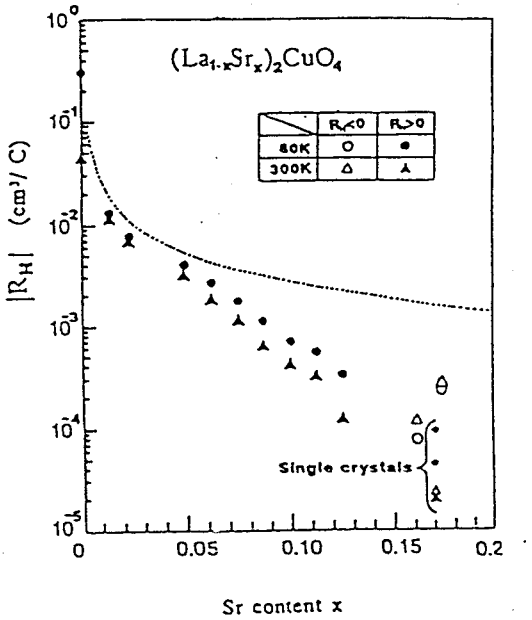

Fig.1-1-7.
Sr content dependence of the Hall coefficients of $(La_{1-x}Sr_x)_2CuO_4$ at 80 and 300K.[7] The positive Hall coefficient decreases almost in inverse proportion to the Sr content, x, i.e. 1/x, in the low Sr content region.

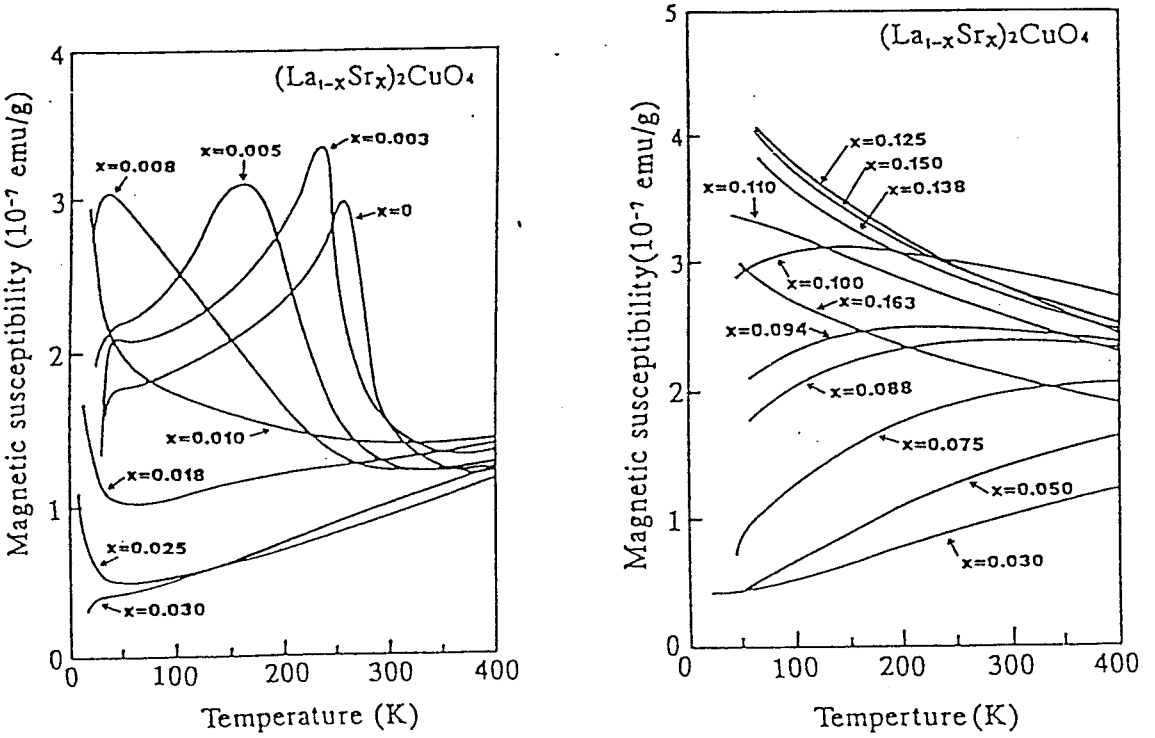

Fig.1-1-8.
T-dependence of the bulk static magnetic susceptibility, d.c. χ .[7]

(3) NMR and NQR Measurements

NMR and NQR measurements have an advantage in obtaining the information for the electronic state at each atomic site, which is important for an investigation of the mechanism of superconductivity.[9]

As seen in **Fig.1-1-9**, the nuclear spin-lattice relaxation rate, $1/T_1$, of ^{63}Cu NQR for x=0.15 in $La_{2-x}Sr_xCuO_4$(LSCO) and that in $YBa_2Cu_3O_7$($YBCO_7$) decrease rapidly below T_c, while change weakly upon temperature at high-T in the normal state.[10] Imai proposed that $1/T_1$ followed a+bT, i.e. $1/T_1$ was proportional to temperature at high-T in the normal state.[11] There exsists a question for the intrinsic behavior of $1/T_1$ in the normal state.

Next the Knight shift of ^{63}Cu NMR in $YBa_2Cu_3O_7$,[12] $La_{1.85}Sr_{0.15}CuO_4$ [13,14] and $Tl_2Ba_2CuO_{6+y}$ [15] are shown in **Fig.1-1-10**. The Knight shift parallel to the c-axis, $K_{||}$, for $YBCO_7$ and LSCO is almost T-independent with the same value of about 1.2% . The anomalous behavior is seen in the T-dependence of the Knight shift perpendicular to the c-axis, $K_{\perp}$, of LSCO in the normal state. The T-dependence of the Knight shift have not been understood yet.

So far, there are lots of NMR and NQR works on ^{63}Cu, ^{17}O and ^{89}Y in $YBa_2Cu_3O_{6+x}$($YBCO_{6+x}$).[9] The most characteristic feature is that the T-dependence of $(T_1T)^{-1}$ of ^{89}Y[16] and ^{17}O[17], $^{89}(T_1T)^{-1}$ and $^{17}(T_1T)^{-1}$, in the normal state are different from that of ^{63}Cu, $^{63}(T_1T)^{-1}$, although the hyperfine field at O(2,3) sites in the CuO_2 plane and Y site are dominated by the isotropic transferred hyperfine interaction with nearest Cu planar spins. Namely, $^{17,89}(T_1T)^{-1}$ are nearly constant above T_c, while

$^{63}(T_1T)^{-1}$ decreases with increasing temperature above T_c. These findings have attracted interest of many researchers. At the present, the T-dependence of $^{63}(T_1T)^{-1}$ is understood as due to the antiferromagnetic(AF) d-spin fluctuations among Cu spins. While the T-dependence of $^{17,89}(T_1T)^{-1}$ are understood as due to the geometrical cancellation of AF d-spin fluctuations at O and Y sites.[17,18] Hence the staggered component of the spin fluctuations with the wave vector around q=Q at the zone boundary, $(\pi/a, \pi/a, 0)$, is almost filtered at O and Y sites, so that their nuclear spins see only the d-spin fluctuations whose wave vectors are around q=0 at the zone center.

Millis et al[19] analyzed the relaxation data of ^{63}Cu, ^{17}O and ^{89}Y in $YBCO_7$ by using a phenomenological model in which the wave number dependent dynamical susceptibility, $\chi(q,\omega)$, is represented in terms of the random phase approximation, consisting of the q=0 and Q contributions. The main result is that the T-dependence of $(1/T_1)_{AF}$ around q=Q deduced from their analysis has an overall form of $T/(T+T_X)$ with T_X=100K above T_c, associated with the T-dependence of the staggered susceptibility at the zone boundary enhanced by the AF spin fluctuations among Cu spins.

In general, since the Cu relaxation rate should involve the information of the low energy part of $\chi(q, \omega)$ integrated over the whole q-space, the contribution cannot simply be divided into q=0 and Q parts. An important feature for $YBCO_7$ is that the q-dependence of Cu spin fluctuations possesses a rather broad spectrum with a peak at the zone boundary of $Q=(\pi/a, \pi/a, 0)$ and hence is not always dominated only by the q=Q contribution. Therefore it cannot be justified whether or not the analysis for

$YBCO_7$ by Millis et al is correct. And this seems to be related to the fact that neutron diffraction experiments do not succeed yet in observing the inelastic scattering at the zone boundary in contrast to the results of $La_{2-x}Sr_xCuO_4$.[3] It is considered that the Cu relaxation rate of LSCO is largely enhanced in comparison with that of $YBCO_7$, reflecting a large contribution from q=Q. In **Fig.1-1-11**, we illustrate schematically the different q-dependence of Cu spin fluctuations between YBCO and LSCO.[20]

In order to clarify the mechanism for high-Tc superconductivity, we have to know the microscopical feature in the superconducting and normal state in HTSC. An intrinsic T-dependence of Cu relaxation rate arising from the AF spin fluctuations, i.e. the q=Q contribution, has not been clarified yet, and to obtain this information is much better from LSCO than from $YBCO_7$ as mentioned above. In addition, the origins of T_c-variation upon x in LSCO is important in understanding the mechanism for high-T_c superconductivity. In this context, we have carried out a systematic ^{63}Cu NQR and NMR experiments for superconducting $La_{2-x}Sr_xCuO_4$.

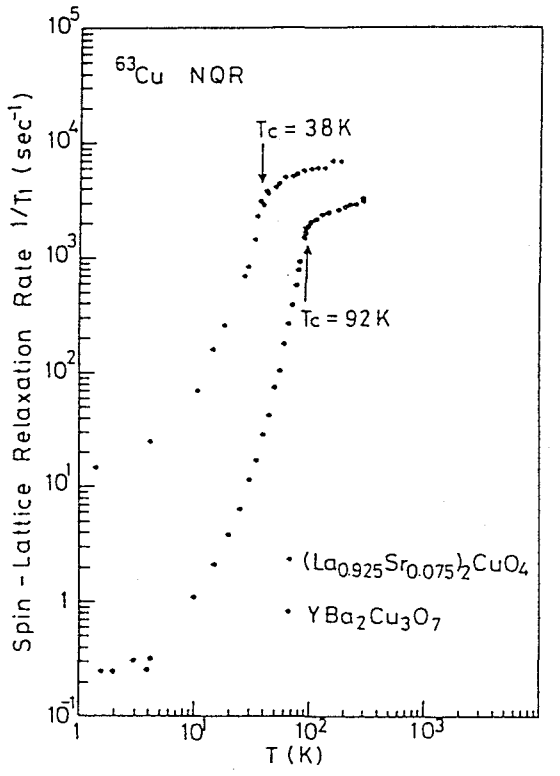

Fig.1-1-9.
T-dependence of $1/T_1$ of ^{63}Cu NQR for x=0.15 in $La_{2-x}Sr_xCuO_4$ and that in $YBa_2Cu_3O_7$.[10]

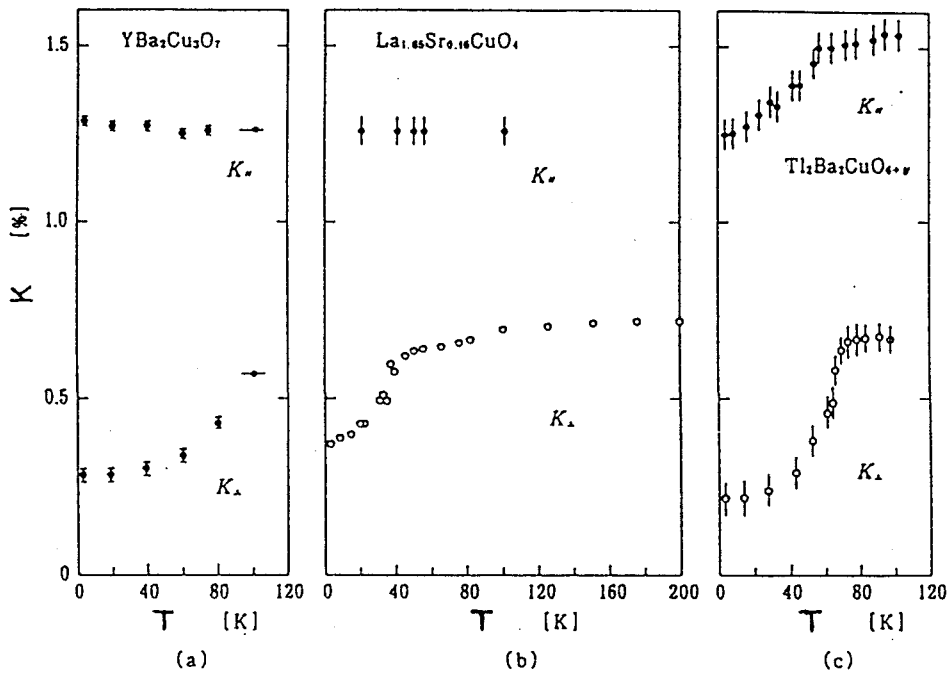

Fig.1-1-10.
T-dependence of Knight shift, K, of ^{63}Cu NMR in $YBa_2Cu_3O_7$,[12] $La_{1.85}Sr_{0.15}CuO_4$ [13,14] and $Tl_2Ba_2CuO_{6+y}$[15]. $K_{\parallel}$ and $K_{\perp}$ indicate the Knight shift parallel and perpendicular to the c-axis, respectively.

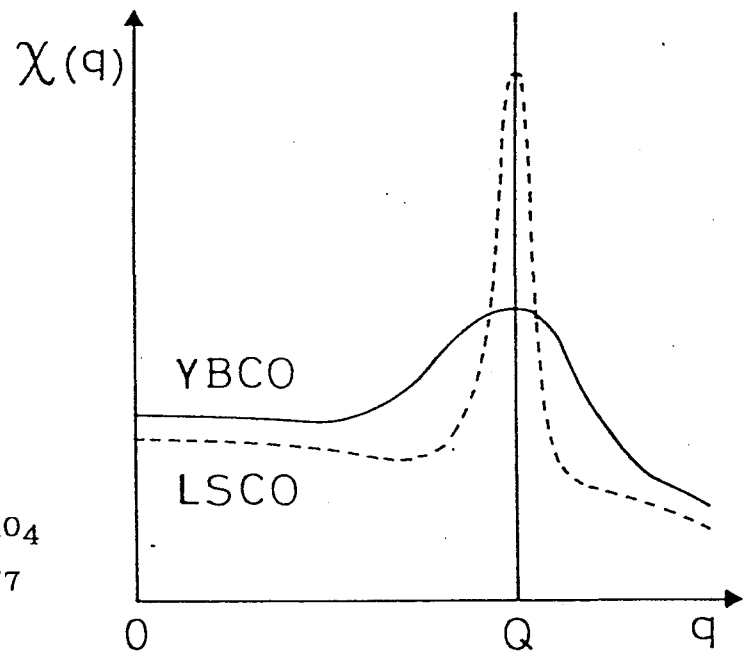

Fig.1-1-11.
Schematic q-dependence of antiferromagnetic spin fluctuations in $La_{2-x}Sr_xCuO_4$ (dashed line) and $YBa_2Cu_3O_7$ (solid line).[20]

1-2. Chevrel Phase Superconductors

The Chevrel phase compounds, $M_mMo_6X_8$ (m=1~ 4, M=Pb, Sn, Tl, Cu, Mn etc and X=S, Se etc),[21] constitute the rhombohedral lattice with the lattice angle, α , of 89° ~ 91° and the lattice constant, a_{rh}, of more than about 6.5Å of large distance compared with the intra cluster atomic distance as shown in **Fig.1-2-1.**[22] $PbMo_6S_8$ [23] and $TlMo_6Se_{7.5}$ [24] exhibit the highest T_c of ~ 12K in series of compounds, while T_c of other compounds ranges from 1K to 6K.[23] The Chevrel compounds do not possess high T_c, but have large upper critical field, H_{c2}, for example, H_{c2}=500~ 600kOe in the case of M=Pb.[23] It has been already reported by Matsumura et al that T-dependence of $1/T_1$ of ^{119}Sn in $SnMo_{6.5}Se_8$ with T_c=2.85K is consistent with a BCS model, having a Hebel and Slichter peak (coherence peak)[25] just below T_c as shown in **Fig.1-2-2.**[26] On the other hand, the $1/T_1$ of ^{205}Tl in $TlMo_6Se_8$ with T_c=9K reported by Nishihara et al had no coherence peak and the T-dependence of $1/T_1$ showed power-law like behavior of $T^{6.9}$ in **Fig.1-2-3.**[27] We measured $1/T_1$ of ^{205}Tl in $TlMo_6Se_{7.5}$ with T_c=12.2K and ^{119}Sn in $Sn_{1.1}Mo_6Se_{7.5}$ with T_c=4.2K once again in order to elucidate the relaxation behavior in strong coupling superconductor. We discuss later the difference between the behavior of $1/T_1$ of Chevrel phase SC and that of High-T_c cuprates SC.

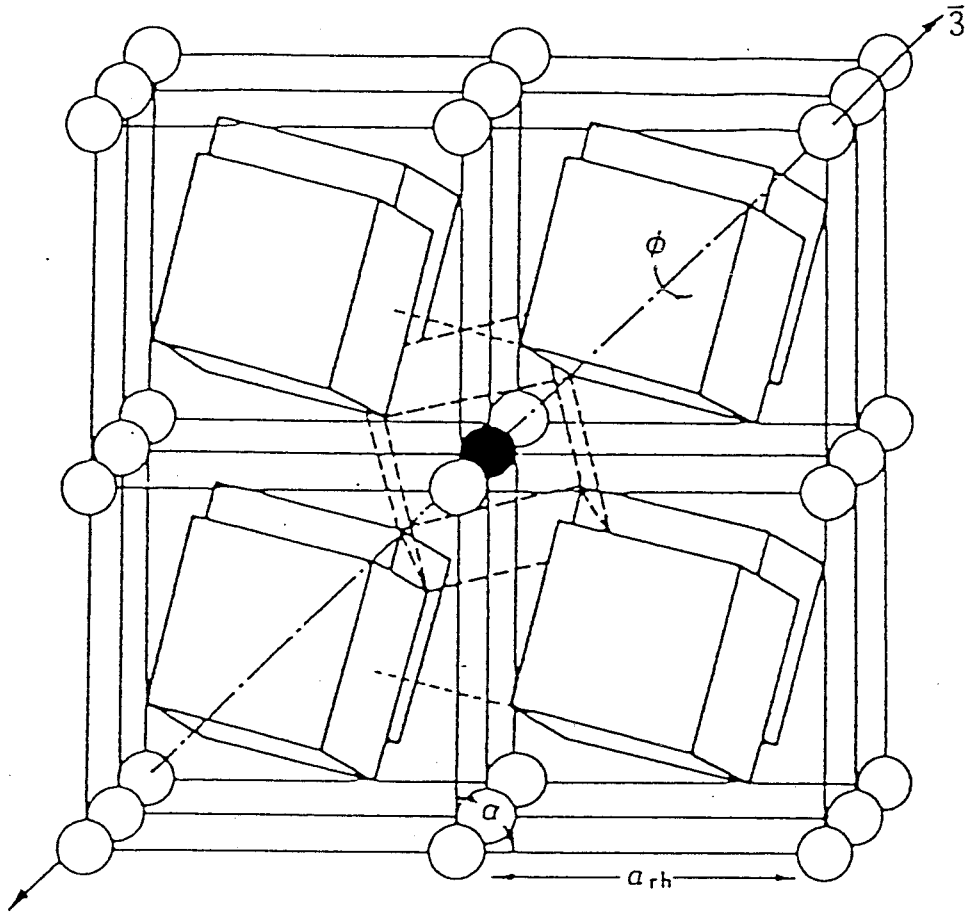

Fig.1-2-1.
Crystal structure of $M_mMo_6X_8$ (m=1~ 4, M=RE, Pb, Tl, Sn etc and X=S, Se etc).[22] Open circles show M ions, and cubes show the blocks of Mo_6X_8, whose corner and center of planes include X and Mo atoms, respectively.

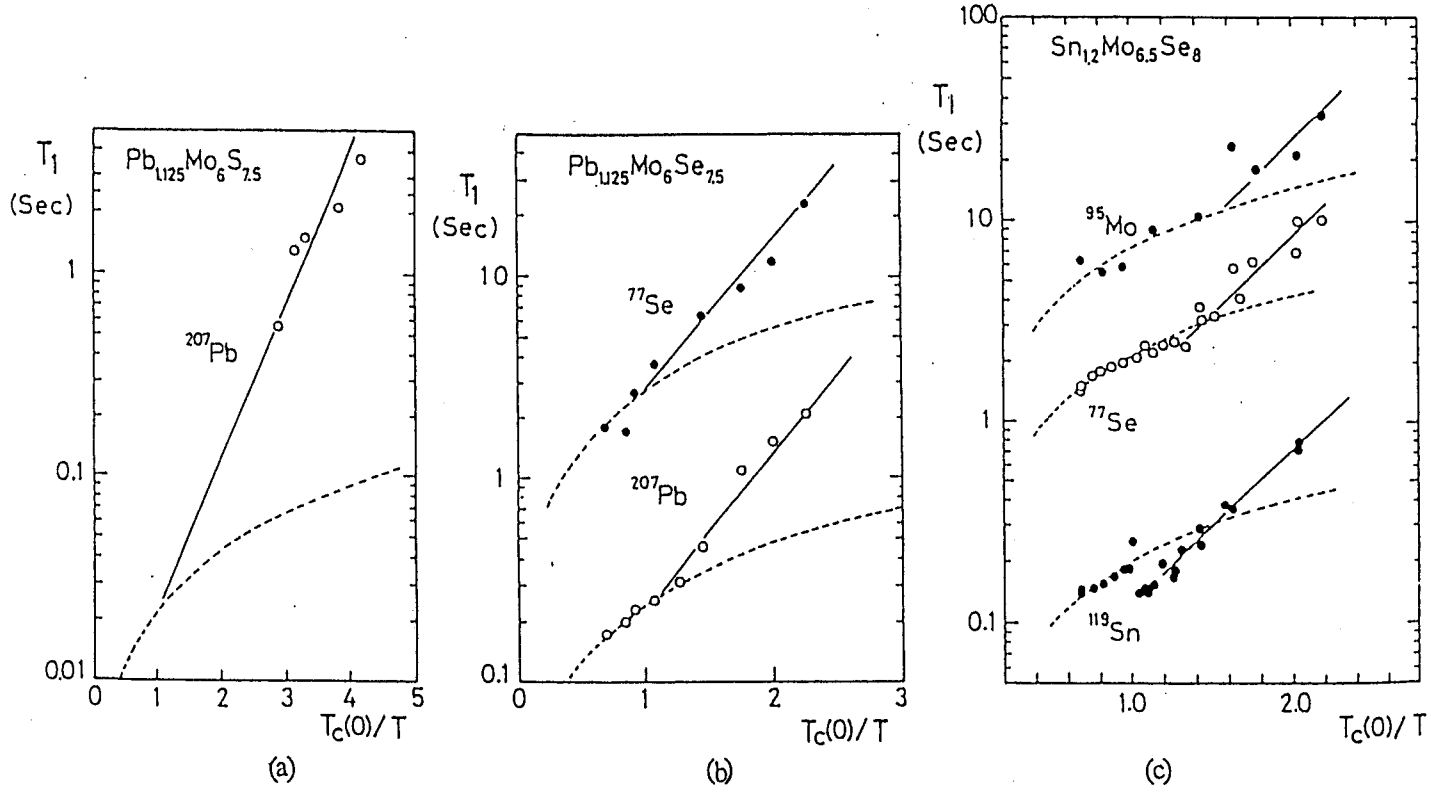

Fig.1-2-2.

(a) Dependence of T_1 for ^{207}Pb on inverse reduced temperature in $Pb_{1.125}Mo_6S_{7.5}$. Solid curve represents the expected temperature dependence when the superconducting energy gap is $3.5\ k_BT_c(0)$. Normal state temperature dependence which is listed in Table I is shown by dashed curve.
(b) Dependence of T_1 for ^{207}Pb and ^{77}Se on inverse reduced temperature in $Pb_{1.125}Mo_6Se_{7.5}$. Solid curve represents the expected dependence when the superconducting energy gap is $3.5\ k_BT_c(0)$. Dashed curve represents the dependence in the normal state which is listed in Table I.
(c) Dependence of T_1 for ^{95}Mo, ^{77}Se, and ^{119}Sn on inverse reduced temperature in $Sn_{1.2}Mo_{6.5}Se_8$. Solid curve represents the exepcted dependence when the superconducting energy gap is $3.5\ k_BT_c(0)$. Dashed curve represents the temperature dependence in the normal state which is listed in Table I. [26]

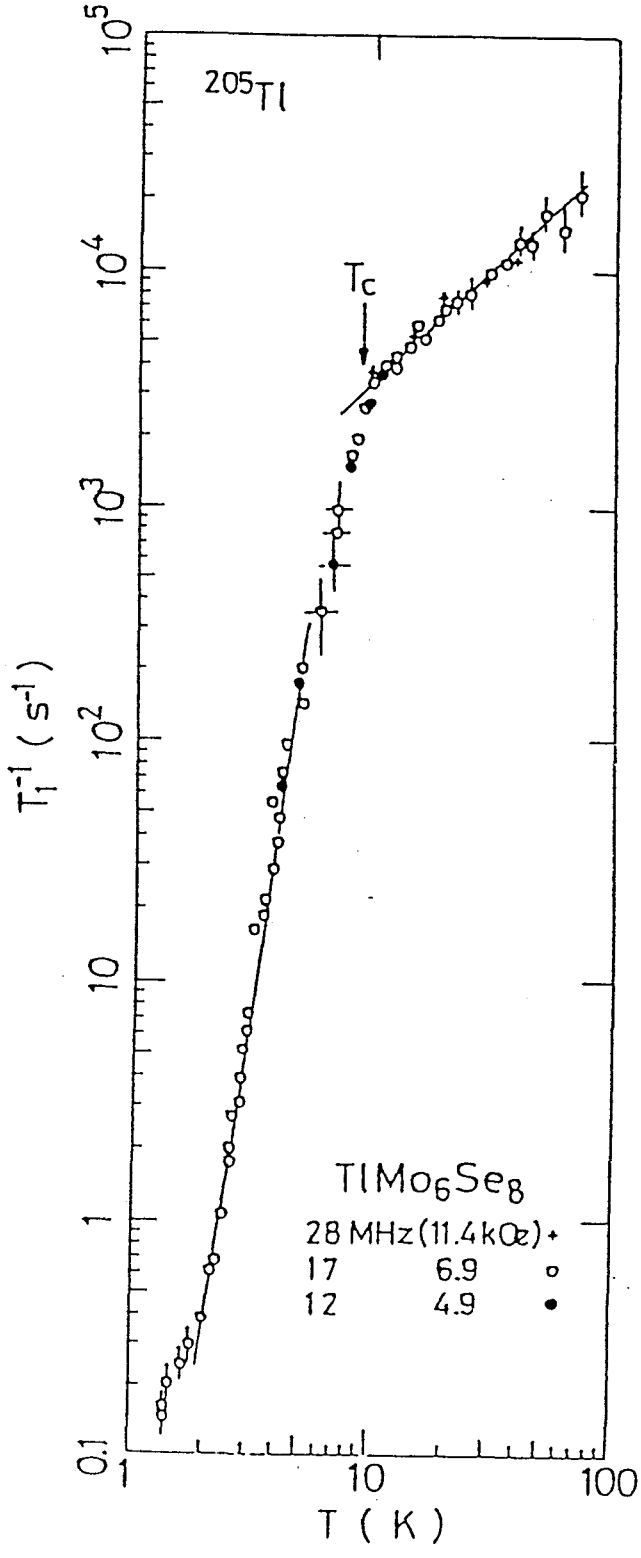

Fig.1-2-3.

T-dependence of $1/T_1$ of ^{205}Tl in $TlMo_6Se_8$ at 12, 17 and 28MHz.[27]

Chapter 2. Introduction to NQR and NMR

In this chapter, we summarize the basic theory for the nuclear magnetic resonance(NMR) and nuclear quadrupole resonance (NQR) techniques, including the T-dependence of the nuclear spin-lattice relaxation time, T_1, and the Knight shift, K, in the normal and superconducing state.

2-1. Hyperfine Interaction[28)]

In general, there are basically two types of hyperfine interactions between nucleus and electron. One is that of nuclear spin with electron spin and orbital angular momentum of electron (hereafter, we call it **magnetic hyperfine interaction**), and the other is between a nuclear electric quadrupole moment and electric field gradient when the nuclear spin is more than 1/2 (**electric quadrupole interaction**).

The hyperfine interaction between the nuclear spin, $\mathbf{I}$, and the electronic spin, $\mathbf{S}$, may be expressed as

$$H = \mathbf{I} \cdot \mathbf{A} \cdot \mathbf{S} \qquad (2\text{-}1)$$

where $\mathbf{A}$ is a hyperfine interaction tensor consisting of such contributions as the Fermi contact ($\rangle$ 0, isotropic), dipole (anisotropic) and core polarization (isotropic) interactions. The **Fermi contact interaction** originated from the direct contact of a nuclear spin with s-electron spins, whose wave function has a finite amplitude at the nuclear site, is written as

$$\frac{8\pi}{3}\gamma_e\gamma_n\hbar^2\mathbf{I}\cdot\mathbf{S}\,\delta(\mathbf{r}) \qquad (2\text{-}2)$$

where γ_e and γ_n are the electro- and nuclear gyromagnetic ratio, respectively, and $\hbar$ is $1/2\pi$ times the Planck constant. The **magnetic dipole interaction** between the electron spin and the nuclear spin is given by

$$-\frac{\gamma_e\gamma_n\hbar^2}{r^3}\left[\mathbf{I}\cdot\mathbf{S}-\frac{3(\mathbf{I}\cdot\mathbf{r})(\mathbf{S}\cdot\mathbf{r})}{r^2}\right] \qquad (2\text{-}3)$$

where **r** is the vector from the nucleus to the electron. The **core polarization interaction**[29] caused via the Fermi contact interaction by the unbalance of the up and down spins of inner s-shells, which is induced by the exchange field of an unpaired spin in outer non-s orbitals, is written as

$$\frac{8\pi}{3}\gamma_e\gamma_n\hbar^2\sum_i\left\{|\phi_i^{\uparrow}(0)|^2-|\phi_i^{\downarrow}(0)|^2\right\}\mathbf{I}\cdot\mathbf{S} \qquad (2\text{-}4)$$

where $\phi_i^{\uparrow,\downarrow}(\mathbf{r})$ are the wave function of the closed s-electrons with the up and down spins, respectively. The hyperfine field induced on a nuclear spin by this interaction is antiparallel to the direction of the magnetization of d- and f-spins and the external magnetic field, i.e. the value of A is negative.

The **orbital hyperfine interaction** between the orbital angular momentum, $\hbar\mathbf{l}$, of electron and the nuclear spin is expressed as

$$\frac{2\gamma_e\gamma_n\hbar^2}{r^3}\mathbf{l}\cdot\mathbf{I}. \qquad (2\text{-}5)$$

The Hamiltonian of **electric quadrupole interaction**, H_Q,

between a nuclear electric quadrupole moment, eQ , and the electric field gradient(EFG), eq , originated from a non-s electron when the nuclear spin, I , is more than 1/2, is given by

$$H_Q = \frac{e^2qQ}{4I(2I-1)} [\, 3I_z^2 - I(I+1)] \ . \qquad (2\text{-}6)$$

Here the quantum axis of the electric field gradient is z-axis, and the asymmetry parameter, η , of the electric field gradient tensor producing an additional contribution is neglected for simplicity.

2-2. Knight Shift, K

In general, the Hamiltonian for the nuclear spins under an external magnetic field, H_{ext}, may be expressed as

$$H = -\gamma_n \hbar I \cdot H_{ext} - \gamma_n \hbar I \cdot H_{loc} + H_Q \qquad (2\text{-}7)$$

where H_{loc} is the internal magnetic field at the nuclear site induced by electrons. The first, second and third terms are originated from the interaction between nuclei and external magnetic field(**Zeeman interaction**), H_Z, the magnetic hyperfine interaction and the electric quadrupole interaction, respectively.

When $H_Z >> H_Q$ under the external magnetic field applied perpendicular to the principal axis of the EFG tensor, the energy level for I=3/2 is shown in **Fig.2-1**. In the case of a nuclear spin at a site with cubic symmetry, i.e. $eq = 0$, a single nuclear magnetic resonance(**NMR**) spectrum is observed as shown in **Fig.2-1(a)**, because of the equal splitting among nuclear energy levels. When the symmetry is not cubic, H_Q exists, resulting in the three resonance lines with the $1/2 \leftrightarrow -1/2$ central transition and $\pm 1/2 \leftrightarrow \pm 3/2$ satellite transitions as shown in **Fig.2-1(b)**. Furthermore, the central line has an additional shift under the H_{ext} perpendicular to the principal axis of the EFG tensor as shown in **Fig.2-1(c)**. On the other hand, when the external magnetic field is applied parallel to the principal axis of the EFG tensor, the central line position is not influenced by the second order effect. When $H_Z=0$, the energy level for I=3/2 is shown in **Fig.2-2**. In this case, a single nuclear quadrupole

resonance(**NQR**) spectrum exists.

In the paramagnetic state, the average value of the spin and orbital angular momentum, $<\mathbf{S}>$ and $<\mathbf{l}>$, parallel to the direction of $\mathbf{H}_{res}$ at the thermal equilibrium appear under H_o. The magnetic susceptibility, χ_o, may be expressed as

$$\chi_o(T) = \chi_{spin}(T) + \chi_{orb} + \chi_{dia} \qquad (2\text{-}8a)$$

when

$$\chi_{spin}(T) = (-g\mu_B <\mathbf{S}> N)/ H_{res} \qquad (2\text{-}8b)$$

and

$$\chi_{orb} = (-\mu_B <\mathbf{l}> N)/ H_{res} \qquad (2\text{-}8c)$$

where χ_{spin}, χ_{orb} and χ_{dia} represent the spin, orbital(Van Vleck) and diamagnetic susceptibility in the unit of one mole (c.g.s. per atom), respectively, and N, g and μ_B indicate the Avogadro number, g-factor(=2 for electron) and Bohr magneton, respectively. On the other hand, the Hamiltonian of **eq.(2-7)** can be expressed as

$$\mathbf{H} = -\gamma_n \hbar\, \mathbf{I} \cdot \mathbf{H}_{res} = -\gamma_n \hbar\, \mathbf{I} \cdot (\mathbf{H}_{ext} + \mathbf{H}_{loc}) \qquad (2\text{-}9a)$$

when

$$\mathbf{H}_{res}=\mathbf{H}_{ext}- \left[\frac{8\pi}{3}\gamma_e \hbar <\mathbf{S}>\delta(\mathbf{r})- \frac{\gamma_e \hbar}{r^3} \left\{ <\mathbf{S}>-\frac{3\mathbf{r}(<\mathbf{S}>\cdot \mathbf{r})}{r^2} \right\} + \frac{2\gamma_e \hbar}{r^3} <\mathbf{l}> \right] \qquad (2\text{-}9b)$$

where $\mathbf{H}_Q$ is neglected for simplicity. The additional term other than $\mathbf{H}_{ext}$ causes a shift of the resonance frequency from

$$\omega_o = \gamma_n \mathbf{H}_{ext} \qquad (2\text{-}10)$$

to a different frequency, ω_{res}. This effect is called the **Knight shift**, K, i.e.

$$K = (\omega_{res} - \omega_o)/\omega_o = (H_{ext} - H_{res})/H_{res}. \quad (2\text{-}11)$$

The Knight shift, K, as well as χ_o may be expressed as

$$K(T) = K_{spin}(T) + K_{orb} + K_{dia} \quad (2\text{-}12)$$

Thus the relation between K and the magnetic susceptibility can be expressed as

$$K_{spin}(T) = \frac{A_{spin}}{N \mu_B} \chi_{spin}(T) \quad (2\text{-}13a)$$

and

$$K_{orb} = \frac{A_{orb}}{N \mu_B} \chi_{orb} \quad (2\text{-}13b)$$

where spin and orb represent the contribution of spin and orbital susceptibility, respectively. Here we neglected the diamagnetic shift, K_{dia}, because it has generally by one order of magnitude smaller than the other ones. Thus the measurements of NMR shifts yield the information on the local magnetic susceptibility. If the T-dependence of χ_o is known, the magnetic hyperfine coupling tensor(hyperfine field), A , can be determined from the slope of K-χ plot by use of **eq.(2-12b)**, because χ_{orb} and χ_{dia} are generally T-independent.[30] In ordinary d-band metals, the isotropic part of A is negative.[30] On the other hand, in HTSC, the interaction between the nuclear spin and the electron spin at the nearest neighbor sites (supertransferred hyperfine interaction) is also important.

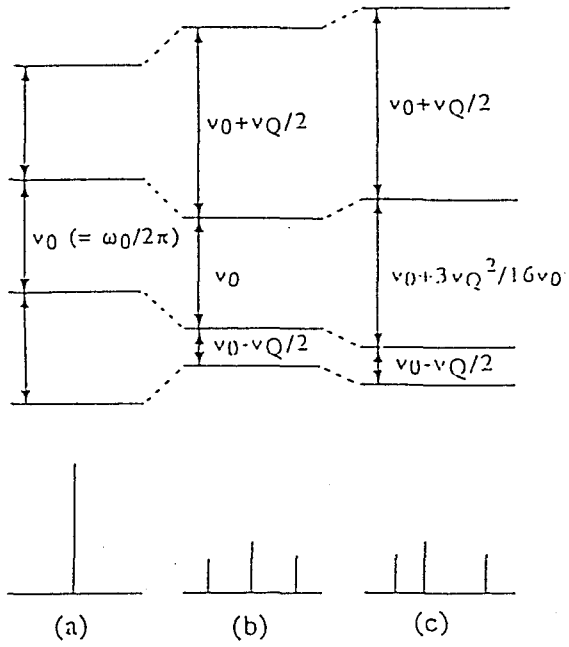

Fig.2-1.
Energy level diagram for a Cu nuclear spin, I =3/2, under the external magnetic field, H_0, perpendicular to the principal axis of the electric field gradient(EFG). (a)Without the electric quadrupole interaction, (b)with first order electric quadrupole interaction, (c)with first and second order electric quadrupole interaction, where $\nu_Q=3e^2qQ/2I(2I-1)\hbar$. When H_0 is applied parallel to the principal axis of EFG, $\nu_Q/2$ and $3\nu_Q^2/16\nu_0$ in (b) and (c) are replaced by ν_Q and 0, respectively. The sketch of expected NMR field swept spectra are shown in the lower panel.

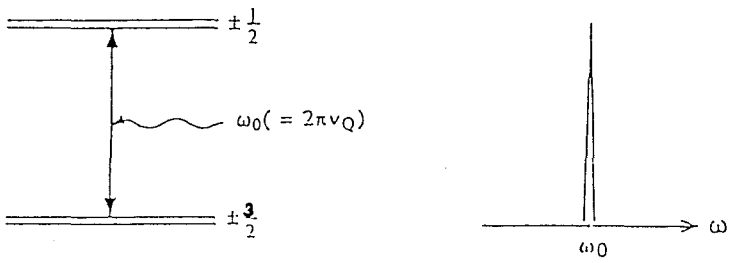

Fig.2-2.
Left; Energy level diagram for I =3/2 under an electric field gradient, eq , (eq >0 and eQ <0 are assumed). Right; Expected NQR spectrum. Here $\hbar\omega_0=(e^2qQ)/2$.

2-3. K in Superconducting State

In BCS state, only the excited quasi-particles contribute to χ_{spin} because the Cooper pairs forming the spin singlet state with up- and down-spins do not contribute to it. The spin susceptibility in the superconducting state, χ_s, is given by

$$\chi_s = -4\mu_B^2 \int_0^\infty N_S(E) \frac{df}{dE} dE \qquad (2\text{-}14)$$

where the density of states in the BCS state, $N_S(E)$, as seen in **Fig.2-3(a)** is expressed as

$$\begin{aligned} N_S(E) &= \frac{N_O E}{(E^2 - \Delta^2)^{1/2}}, \qquad (E \geq \Delta) \\ &= 0, \qquad (E < \Delta) \end{aligned} \qquad (2\text{-}15)$$

at the excited quasi-particles energy, E, in the superconducting state, and N_O and 2Δ are the density of states in the normal state and the energy gap, respectively. Here E is given by

$$E^2 = \varepsilon^2 + \Delta^2, \qquad (2\text{-}16)$$

where ε $(=\varepsilon_k - \varepsilon_F)$ is the energy of a single electron measured from the Fermi energy, ε_F, and the Fermi-Dirac distribution function, f(E), is expressed as

$$f(E) = \frac{1}{\exp(E / k_BT) + 1}. \qquad (2\text{-}17)$$

This result was presented by Yosida,[35] and consistent with the result of the Knight shift of alminum[36] as seen in **Fig.2-4**. For $\Delta(T) >> k_BT$ at low-T($T << T_C$), f(E) is nearly exponential and

rapidly varies for $E \geqq \triangle$. Since only the state near the gap threshold is appreciably populated, K_{spin} decreases exponentially with decreasing temperature as $K_{spin} \sim \exp(-\triangle / k_B T)$ as seen in **Fig.2-5.**

Next when the Cooper pair is in the triplet state, there exist two types of the BW(Balian-Werthamer)[41] state having an isotropic gap, and the ABM(Anderson-Brinkman-Morel)[42] and polar state kaving anisotropic gaps. In the BW state, the Cooper pairs are composed of $(k\uparrow, -k\uparrow)$, $(k\uparrow, -k\downarrow)$ and $(k\downarrow, -k\downarrow)$. In this case, for the Cooper pair with parallel spins, whose direction is easily changed under the magnetic field as well as in the normal state, χ_{spin} is decreased to 1/3 times of the singlet state at T=0K. T-dependence of χ_{spin} in the superconducting state is similar to the BCS state as seen in **Fig.2-5**. In the ABM and polar states,the Cooper pairs are composed of $(k\uparrow, -k\uparrow)$ and$(k\downarrow, -k\downarrow)$. Thus χ_{spin} is not decreased below T_c.

In the spin singlet state having an anisotropic gap, i.e. d-wave state with approximate polar and ABM typs of density of states as in the p-wave state, χ_s are almost proportional to T and T^2 at low-T, respectively, as seen in **Fig.2-6**, because they are proportional to E and E^2, respectively, as mentioned in **section 2-5.**

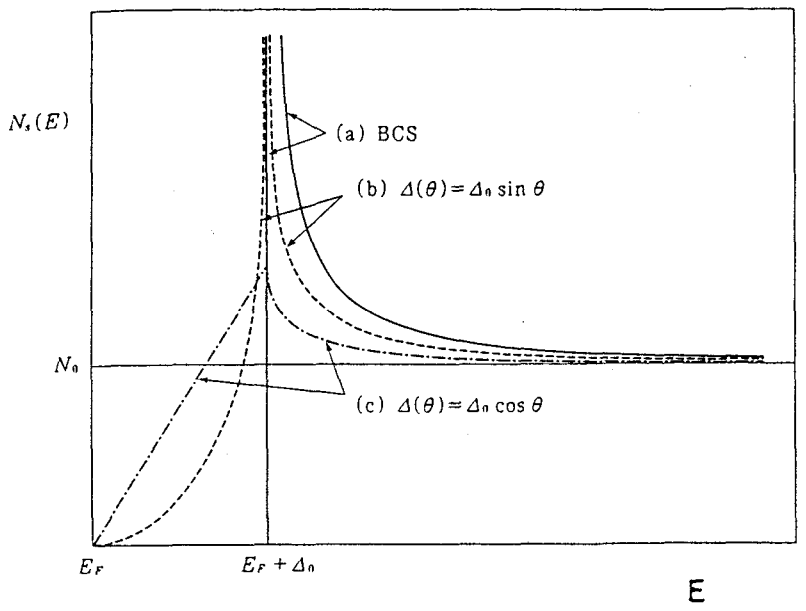

Fig.2-3.
Densities of states for (a) BCS(s-wave) model, (B) ABM(p-wave) model and (c) polar(p-wave) model.

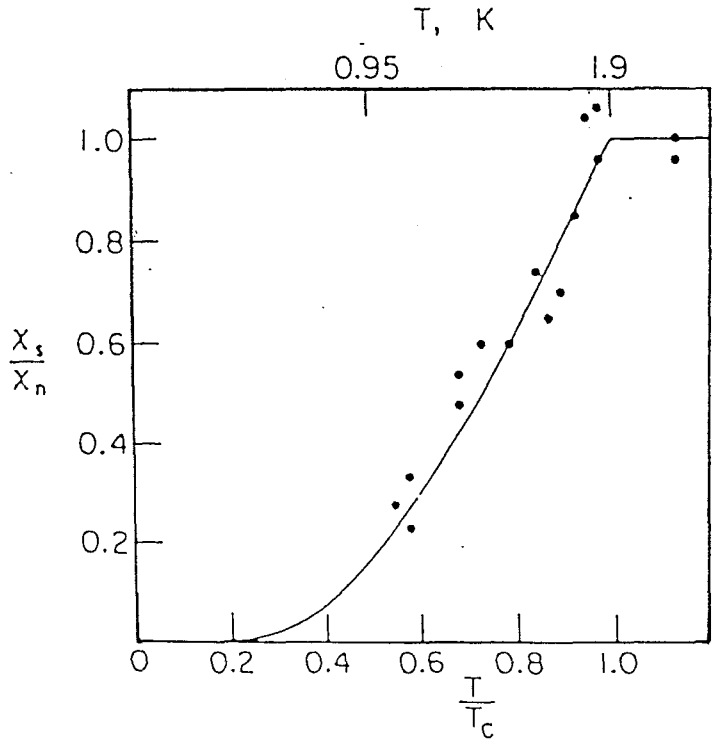

Fig.2-4.
χ_s/χ_n vs T/T_c plot of Al.[36] The solid line is calculated by using of Yosida function.[35]

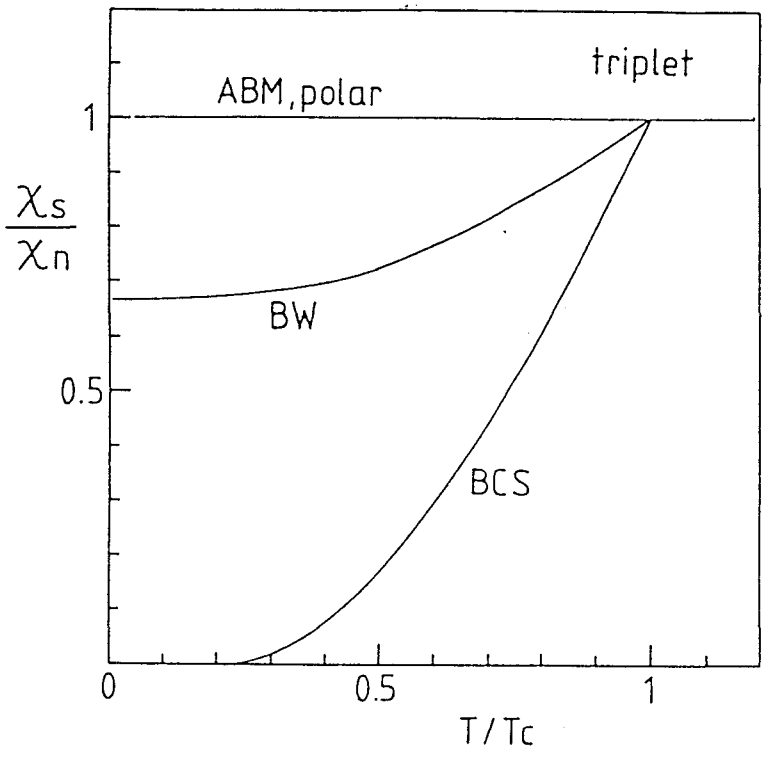

Fig.2-5.
χ_s/χ_n vs T/T_c plot for BCS(s-wave) model, ABM, polar and BW (p-wave) model calculated by using the densities of states in **Fig.2-3** and $2\triangle = 3.52k_BT_c$.

Fig.2-6.
χ_s/χ_n vs T/T_c plot for BCS(s-wave) model and d-wave model tentatively calculated by using the densities of states in **Fig.2-3** and $2\triangle = 3.52k_BT_c$. Here for d-wave model, approximate polar and ABM types of density of states as in the p-wave state are assumed.

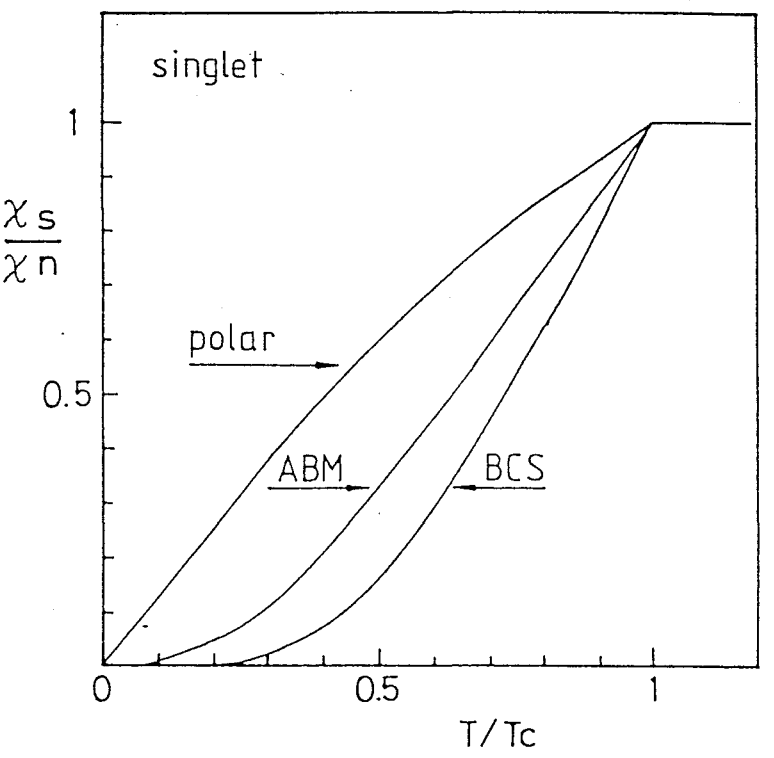

2-4. Nuclear Spin-lattice Relaxation Time, T_1

The population of the nuclear spins at various energy levels at the thermal equilibrium is proportional to the Boltzmann factor, yielding a net nuclear moment, M_o, as shown in **Fig.2-7(a)**. When the upper and lower energy leveles are equally occupied, the nuclear magnetization disappears. Since the nuclear spin system interacts with the thermal bath of the lattice through hyperfine interaction, the initial thermal equilibrium will be recovered. Thus, from the measurement of the time constant of the recovery called the nuclear spin-lattice relaxation time, T_1, we can probe the electronic state.

The time evolution of the nuclear moment after saturation, M(t), can be described by a set of standard rate equations. The equations are readily solved under the specific initial condition to the experiment as shown by Narath.[31,32] When the nuclear spin moment I is 3/2, the magnetization after the saturation pulses, M(t), is expressed as

$$M(t)=M_o\{1-\exp(-3t/T_1)\} \qquad (2\text{-}18a)$$

for the NQR and

$$M(t)=M_o[1-\{0.1\ \exp(-t/T_1)\ +\ 0.9\ \exp(-6t/T_1)\}] \qquad (2\text{-}18b)$$

for the NMR of the central transition, respectively. In these expressions, T_1 is defined as the inverse of twice the transition probability, W, fundamental relaxation rate in accordance with various theoretical treatment, i.e. $1/T_1=2W$.

The general expression of $1/T_1$ presented by Moriya[40] can be written with using the imaginary part of the dynamical spin susceptibility perpendicular to the quantum axis, $\chi_\perp''(q,\omega)$, as

$$1/T_1 = \frac{2\gamma_n^2 k_B T}{(\gamma_e \hbar)^2} \sum_q A_q A_{-q} \frac{\chi_\perp''(q,\omega)}{\omega} , \qquad (2\text{-}19)$$

where k_B, γ_n, γ_e and ω are the Boltzmann constant, nuclear-, electro-gyromagnetic ratios and nuclear Larmor frequency, respectively.

When the interaction among electrons is neglected, $1/T_1$ is expressed as

$$1/T_1 = \frac{\pi}{\hbar} A^2 \int_0^\infty N^2(\varepsilon) f(\varepsilon) \{1-f(\varepsilon)\} d\varepsilon . \qquad (2\text{-}20a)$$

Since $f(\varepsilon)\{1-f(\varepsilon)\}$ is nearly equal to $k_B T\delta(\varepsilon_k-\varepsilon_F)$, the above equation yields

$$1/T_1 = (\pi/\hbar) A^2 N^2(\varepsilon_F) k_B T. \qquad (2\text{-}20b)$$

Thus, $1/T_1$ is proportional to temperature and $N^2(\varepsilon_F)$. Since the Knight shift is also proportional to the density of states, the following relation called the **Korringa relation** holds.[33]

$$T_1 T K^2 = (\gamma_e/\gamma_n)^2 (\hbar/4\pi k_B) = \text{const.} \qquad (2\text{-}21)$$

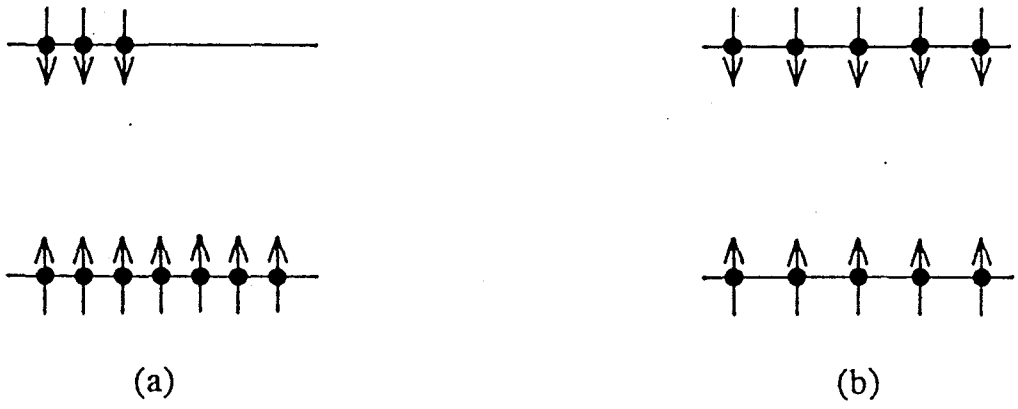

Fig.2-7.
(a) A two level-nuclear spin system in the thermal equilibrium. (b) The state of **saturation**, in which no net nuclear magnetization exists. Note that the figure (a) is extremely exaggerated. In the T-region above 4.2 K, the energy separation between nuclear spin levels is by several orders of magnitude smaller than k_BT. Therefore the nuclear spin system may be treated in a high-T approximation.

2-5. T_1 in Superconducting State[34)]

In the BCS state, the conduction electrons condense into a pairwise occupation of the Bloch state, $| k\uparrow \rangle$, and whose virtual pair, $| -k\downarrow \rangle$. This **coherence effect** puts limitation on scattering processes, and alters the number of excited state electrons available for scattering. In nuclear magnetic relaxation, the perturbation described by the transitional probability for scattering is not time-reversal invariant. The **coherence factor** in the superconducting state found by Hebel and Slichter[25)] multiplies the transition rate in the normal state as

$$C(E,E') = \frac{1}{2}\left[1 + \frac{\Delta^2}{E\,E'}\right] . \qquad (2\text{-}22)$$

Here E and E'(= E + $\hbar\omega$) represent the energy of excited electron for an initial state, $| i\rangle$, and for a final state, $| f\rangle$, respectively. In the result, the appropriate generalization of $1/T_1$ is extended from **eq.(2-20a)** as

$$1/T_1 = \frac{\pi}{\hbar} A^2 \int_{\Delta}^{\infty} \{ N_S^2(E) + M_S^2(E) \}\, f(E)\{1-f(E)\}\, dE \qquad (2\text{-}23)$$

where the **normal** density of states in BCS state, $N_S(E)$, is given by **eq.(2-15)**, and what called the **anormalous** density of states, $M_S(E)$, is given by

$$\begin{aligned} M_S(E) &= \frac{N_0\,\Delta}{(E^2 - \Delta^2)^{1/2}} , \qquad (E \geq \Delta) \\ &= 0 . \qquad (E < \Delta) \end{aligned} \qquad (2\text{-}24)$$

$M_S(E)$ comes from the coherence effect. The integral diverges

logarithmically at E=$\triangle$. When $\triangle$ (T)>>k_BT at low-T(T<<T_c), f(E) is nearly exponential and rapidly varies for E$\geqq\triangle$. Since only the state near the gap threshold is appreciably populated, $1/T_1$ decreases exponentially with decreasing temperature as $1/T_1 \sim \exp(-\triangle/k_BT)$. When $\triangle$ (T)<<k_BT near T_c, Since the states is uniformly populated because of the large f(E), $1/T_1$ has a peak, so called Hebel and Slichter peak or **coherence peak**, increased over the value at T_c. The typical behavior of T-dependence of $1/T_1$ of ^{27}Al in the superconducting state is consistent with that caluculated with using **eq.(2-23)** as seen in **Fig.2-8**.[37]

In the anisotropic condensed state, $N_S(E)$ can be written as

$$N_S(E) = \frac{N_O\ E}{4\ \pi}\int_o^{2\pi}\ \int_o^{\pi}\ \frac{\sin\theta\ d\theta\ d\phi}{\{E^2 - \triangle^2(\theta\ ,\phi\ )\}^{1/2}}\ , \qquad (2\text{-}25)$$

where integral is extended over the spherical region from **eq.(2-15)**. For orbital angular momentum l =0, $\triangle(\theta\ ,\phi\ )=\triangle$ =const., such that the corresponding spectrum has a gap of 2$\triangle$. Since, for l $\neq$ 0, $\triangle(\theta\ ,\phi\ )$ can vanish on poins or lines, a reduction of the density of states near the Fermi level becomes weaker than that for a isotropic superconducting gap.

When the Cooper pair is in the triplet equal-spin pairing, p-wave state, the Cooper pairs are composed of (k$\uparrow$,-k$\uparrow$) and (k$\downarrow$,-k$\downarrow$). In this case, the coherence factor vanishes. For the axial-state(ABM) model for l =1 triplet pairing,

$$\triangle(\theta\ ,\phi\ ) = \triangle\sin\theta\ , \qquad (2\text{-}26)$$

as shown in **Fig.2-9(a)**. Therefore

$$N_S(E) = \frac{N_O E}{4\pi} \int_o^{2\pi} \int_o^{\pi} \frac{\sin\theta \, d\theta \, d\phi}{(E^2 - \Delta^2 \sin^2\theta)^{1/2}}$$

$$= \frac{N_O E}{2\Delta} \ln \left| \frac{E + \Delta}{E - \Delta} \right| , \qquad (2\text{-}27)$$

Thus $1/T_1$ is expressed as

$$1/T_1 = \frac{\pi k_B T A^2 N_O^2}{4\hbar\Delta^2} \int_o^{\infty} E^2 \{\ln \left| \frac{E + \Delta}{E - \Delta} \right| \}^2 (- \frac{df}{dE}) dE \qquad (2\text{-}28)$$

In the low-T limit, where $E/\Delta \rightarrow 0$, $N_S(E) = N_O(E/\Delta)^2$. Thus,

$$1/T_1 \sim T^5 \int (E/T)^4 \exp(- E/k_B T) \, d(E/T) .$$

Therefore $1/T_1$ is proportional to T^5 at low-T. For the polar-state model with $l = 1$ triplet pairing,

$$\Delta(\theta, \phi) = \Delta \cos\theta \qquad (2\text{-}29)$$

as shown in **Fig.2-9(b)**. Therefor,

$$N_S(E) = \frac{N_O E}{4\pi} \int_o^{2\pi} \int_o^{\pi} \frac{\sin\theta \, d\theta \, d\phi}{(E^2 - \Delta^2 \cos^2\theta)^{1/2}}$$

$$= \frac{\pi N_O E}{2\Delta} , \qquad (E < \Delta) \qquad (2\text{-}30)$$

$$= \frac{N_O E}{\Delta} \sin^{-1} \frac{\Delta}{E} . \qquad (E > \Delta)$$

Thus $1/T_1$ is expressed as

$$1/T_1 = \frac{\pi A^2}{\hbar} T^3 \int \frac{N_S^2(E)}{T^2} f(E)\{1 - f(E)\} \, d(\frac{E}{T}) . \qquad (2\text{-}31)$$

Since $f(E)$ is a function of E/T, and $(N_S(E)/T)^2$ proportional to

propotional to T^3 at low-T. The density of states for (b) axial (ABM) state and (c) polar state are shown in **Fig.2-3.**

The order parameter of d-wave pairing $\triangle(\theta, \phi)$ is more complicated than that for p-wave paring, being zero on the lines and poins at the Fermi surface. The order parameter of d-wave pairing in cubic and hexagonal symmetry are, for example,

$$\triangle_c(\theta, \phi) = (\triangle/2)\{(3\cos^2\theta - 1) + i\,(3^{1/2}\sin^2\theta\cos 2\phi)\}$$

and (2-32)

$$\triangle_h(\theta, \phi) = 2\triangle\cos\theta\sin\theta\, e^{i\phi},$$

respectively.[38] When the Cooper pair is d-wave pairing, the pair is singlet. However the coherence factor, $C(\theta\ \phi)$, is vanished because that $\int \triangle(\theta, \phi)\sin\theta\, d\theta\, d\phi = 0$. As well as in the p-wave sate, the divergence of the density of states at $E=\triangle$ is weak, resulting in the weak enhancement of $1/T_1$ just below T_c. The density of states, N_c and N_h, in d-wave pairing are similar to those for p-wave pairing, being proportional to E^2(i.e. $1/T_1 \sim T^5$ at low-T) and E(i.e. $1/T_1 \sim T^3$ at low-T), respectively, as shown in **Fig.2-10.**[39] Thus the power-law like T-dependence of $1/T_1$ is understood for the models with anisotropic gap. If K_{spin} is decreased below T_c, and $1/T_1$ shows the power-law like T-dependence, the d-wave model becomes plausible.

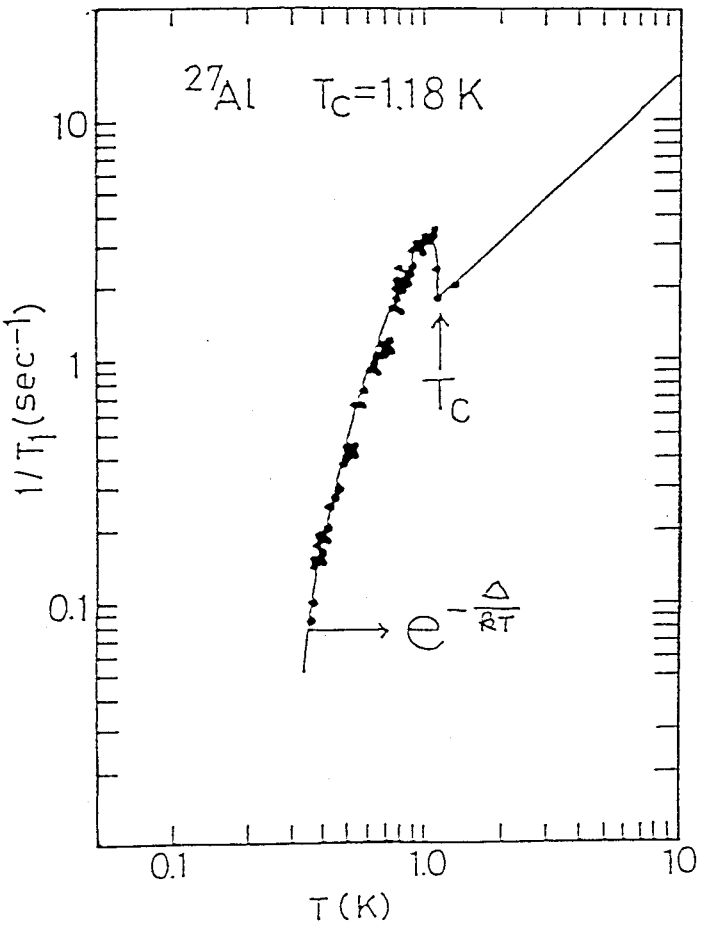

Fig.2-8
T-dependence of $1/T_1$ of Al.[37] The solid line is calculated by using the density of states on BCS model.

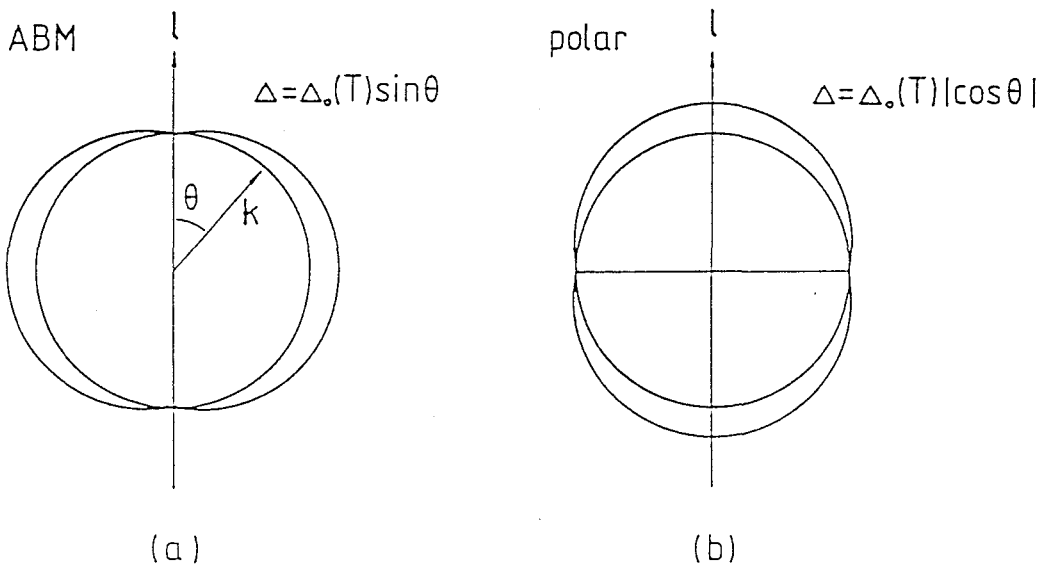

Fig.2-9
Superconducting gap formation for (a) ABM(p-wave) model (b) polar (p-wave) model. l and k are the orbital angular momentum of Cooper pair and the wave vector of electron.

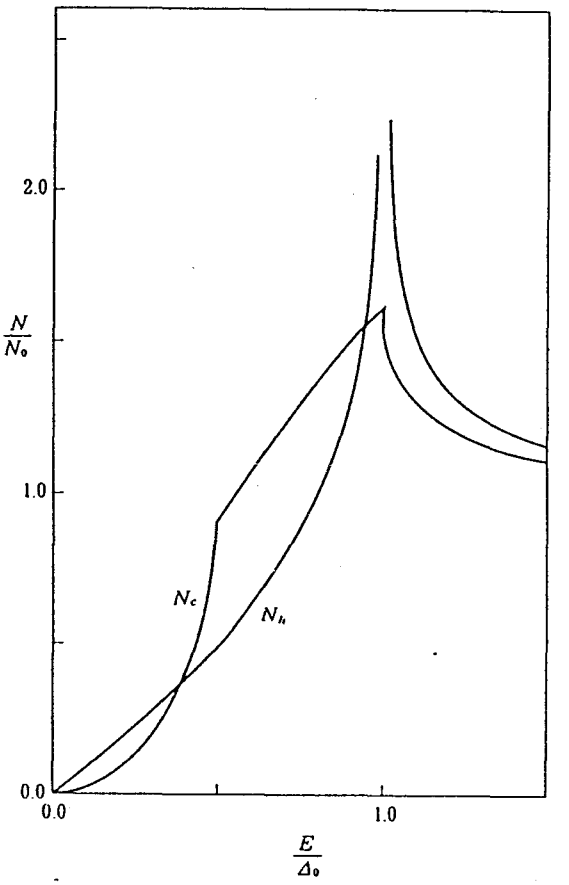

Fig.2-10
Densities of states for d-wave model in cubic (N_c) and hexagonal(N_h) symmetry.[39]

Chapter 3. Experimental Procedure

3-1. Sample Preparation

(1) $La_{2-x}Sr_xCuO_4$

The samples of $La_{2-x}Sr_xCuO_4$ were prepared by the standard solid state reaction as following. Adequate quantities of La_2O_3, $SrCO_3$ and CuO with 99.99% purities were mixed with each other. Powder was pelletized and reacted firstly in air at 900℃ for one day. Then the reacted pellet was ground, pressed into pellet, reacted in air at 1100℃ for two days and annealed at 600℃ for one day. After that the same process was repeated at least once. In addition, the NQR spectrum of Cu at 4.2K and T_c for x=0.24 with repeating five times of the reaction at 1100℃ and those with repeating one time were the same.

The sample was well ground, so that each grain was smaller than 20μ m in diameter, in order to reduce the Meissner shielding effect below T_c. The sample was packed in a cylindrical case made of paper, whose diameter and length are approximately 7mm and 20mm, respectively. The sample case was covered by teflon tape to keep the powder samples free from moisture.

T_c's were determined for each x as 5(x=0.05), 10(0.06), 20(0.075), 24(0.08), 30(0.1), 31(0.12), 36(0.13), 38(0.15), 35(0.17), 29(0.20), 24(0.22) 18(0.24), 10(0.26) and 0K(0.30), respectively, by ac susceptibility measurement. Here T_c is defined as the temperature at which the diamagnetization appears.

(2) Chevrel Compounds

The good samples of Chevrel compounds were made by Ohtani and Nakabori in Okayama University of Science. Sn Chevrel phase compound was prepared as follows. Adequate quantities of Sn, Mo and Se were mixed with each other, sealed into quartz tube in vacuum and reacted firstly at 800℃ for a week. Then the reacted powder was pressed into pellet, sealed into quartz tube in vacuum and finally reacted at 1000℃ for a week. The sample of Tl compound was prepared by solid state reaction following the procedure reported elsewhere,[24] and in addition, the final reaction was made at 520℃ for six weeks. The samples were confirmed to be approximately in a single phase by x-ray measurement. T_c was defined as the temperature where the diamagnetism appears. T_c of Tl and Sn compounds used in our experiment are 12.2K and 4.2K, respectively, the former being consistent with the value reported by Tarascon et al[24]. T_c of our samples are higher than T_c=9K (Tl compound)[27] and T_c=2.85K (Sn compound)[26] used in the previous NMR measurements. It is considered that the volume of impurity phase (for example $MoSe_2$ and Mo_2Se_3 etc) is smaller than previous ones.

3-2. NQR and NMR Measurements

The ^{63}Cu NQR experiment was performed in zero field and the T-region of 1.3~ 300K by using a phase-coherent-pulsed NMR spectrometer. The NQR frequency spectra for LSCO were obtained by measuring the integral of the echo area as a function of frequency point by point at 4.2 and 77K. The sensitivity of the spectrometer was almost constant in the frequency region in this experiment. We did not perform the intensity correction of the spin echo dicay time, T_2, for raw data. We expect that the spectrum is not changed by T_2-correction because the interval between 90° - 180 ° pulses, τ , is short of 12μ sec.

The field-swept ^{63}Cu NMR spectra were obtained by recording the output of a boxcar integrator in the T-region of 1.3~ 260K at frequency of 125.1MHz by using a phase-coherent-pulsed NMR spectrometer. The external magnetic field was applied by use of a superconducting solenoid, whose maximum field is approximately 12T at 4.2K. In order to obtain the sharp resonance line, we used the aligned powder samples along the c-axis, following a method used by Ferrell et al.[43] The powder was well ground smaller than 20μ m in diameter. The resulting sample with an approximate volume fraction of 0.3 was stirred in an organic polymer whose melting point was 50℃ , and after melted, the mixture was solidified by quenching down to 77K in a magnetic field of 11T.

3-3. T_1 Measurement

(1) ^{63}Cu NQR in $La_{2-x}Sr_xCuO_4$

T_1 of ^{63}Cu NQR was measured with the saturation recovery method in zero field and in the T-region of 1.3~ 300K. The echo signal was averaged by using a digital memory, and the intensity was recorded by integrating the echo around its peak. The observed recovery of the nuclear magnetization, M(t), was fitted to the theoretical equations by utilizing a least square method.

For example, the nuclear relaxation behavior for x=0.10, 0.13 and 0.15 is expressed by a unique T_1 above around 40, 60 and 70K, respectively, while below these temperatures, multi-exponential behaviors appear in the relaxation. Typical behaviors for x=0.15 are shown in **Fig.3-1.**[20] Here

$$m(t) = [\,M(\infty) - M(t)]\ /\ M(\infty) = \exp(-3t/T_1)$$

for **eq.(2-18a)** is plotted against t, where M(t) is the nuclear magnetization at time, t, after the saturating pulses. The distribution of T_1 in this system is considered to be due to an inevitable effect caused by the random mixture of La and Sr. When the relaxation behavior is not simple exponential, there remains an ambiguity in determining T_1. At low-T, the long component of T_1 is more reliably determined because of the improvement of signal to noise ratio. In order to see the overall T-dependence of T_1 over the wide T-region,. we adopt the value tentatively obtained from the slope where m(t) decreases from 100 to 37% (down to 1/e) of the initial value(so called T_{1S}), from 30 to 10%

(so called T_1) and from 10 to 5%(so called T_{1L}), respectively.

(2) ^{205}Tl and ^{119}Sn NMR in Chevrel Compounds

T_1 of ^{119}Sn in $Sn_{1.1}Mo_6Se_{7.5}$ was measured at the frequency of 9.8MHz in the magnetic field of 6.1kOe in the T-region of 1.3~ 12K by using a phase-coherent-pulsed NMR spectrometer. T_1 of ^{205}Tl in $TlMo_6Se_{7.5}$ was measured at 8.7 and 17MHz in 3.5 and 6.9kOe, respectively, in the T-region of 1.5~ 80K. The nuclear relaxation behavior for ^{119}Sn is expressed by a unique T_1 over whole T-region. However, for those of ^{205}Tl, multi-exponential behaviors appear below around 3K. The detail will be discussed in **Chapter 4.**

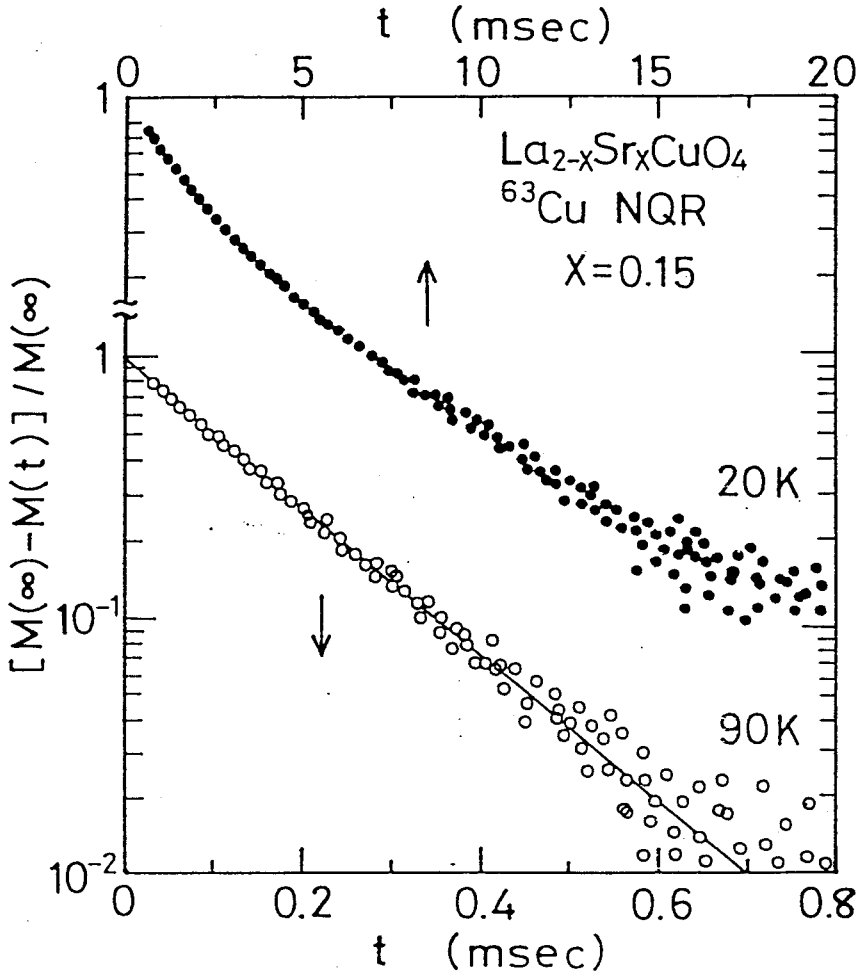

Fig.3-1.
Relaxation curves of the nuclear magnetization of ^{63}Cu NQR at 20 and 90K for x=0.15 in $La_{2-x}Sr_xCuO_4$.[20] Here m(t) = [M(∞)-M(t)] /M(∞) are plotted against time, t, after the saturating pulses, where M(t) is the nuclear magnetization at t. There appears an appreciable distribution of T_1 below T_c.

Chapter 4. Experimental Results

4-1. Cu NQR Spectrum in $La_{2-x}Sr_xCuO_4$

Figure 4-1-1 shows the Cu NQR spectra at 4.2K for x=0.10~ 0.30 in $La_{2-x}Sr_xCuO_4$. Cu has two isotopes ^{63}Cu and ^{65}Cu with the nuclear spin I=3/2. The ratios of their natural abundances, $^{63}A/^{65}A$, and their quadrupole moments, $^{63}Q/^{65}Q$, are 2.235 and 1.081, respectively. For x=0.10, the ratios of intensities, $^{63}Int./^{65}Int.$, and the resonance frequencies, $^{63}\nu_Q/^{65}\nu_Q$, are consistent with $^{63}A/^{65}A$ and $^{63}Q/^{65}Q$, respectively. Therefore the frequency on the central peaks of each spectrum corresponds directly to the NQR frequency, ν_Q, for ^{63}Cu. The frequency on the left side peaks corresponds to ν_Q for ^{65}Cu.

Fig.4-1-2 shows the central ^{63}Cu NQR spectra at 77K for x=0.075~ 0.15.[20] As seen in **Fig.4-1-1 and -2**, the full width at half maximum of the intensity, FWHM, for each spectrum having almost the same value of about 2.2MHz is not remarkably changed against the Sr content and the temperature at 4.2 and 77K, which is by one order of magnitude larger than about 0.22MHz for $YBa_2Cu_3O_7$ [72]. This large width is expected to be due to the microscopic distribution of Sr content in LSCO. A reliable estimation for the T-dependence of ν_Q is difficult because of the large width and the poor signal to noise ratio. The T-variation of ν_Q for x=0.10~ 0.15 is expected to be less than 0.2MHz between 4.2 and 77K.

As seen in **Fig.4-1-1**, there exists another ^{63}Cu NQR line on the right side.[44,45] The ^{63}Cu NQR line for set B does not exist for x=0.10. The intensity of set B is increased upon x from

around x=0.125 (i.e. 1/8) as shown in **Fig.4-1-1**. As seen in **Fig.1-1-1**, the Cu site has eight nearest neighbor La or Sr ions in the present system. thus, for x=0.125, one La ion in eight nearest neighbor La sites around Cu site is substituted by a Sr ion.

ν_Q for ^{63}Cu is shown against Sr content, x, in **Fig.4-1-3**. ν_Q for ^{63}Cu of set A is increased linearly from 33.9 to 38MHz with increasing x from 0.075 to 0.30 at 4.2 and 77K. On the other hand, ν_Q for ^{63}Cu of set B is not increased largely upon x. In non-superconducting samples with x more than 0.30 transformed from the orthorhombic to the tetragonal structure, only the NQR line corresponding to set B exists,[45] therefore the structure for Cu with the NQR line of set B may be the tetragonal like structure.

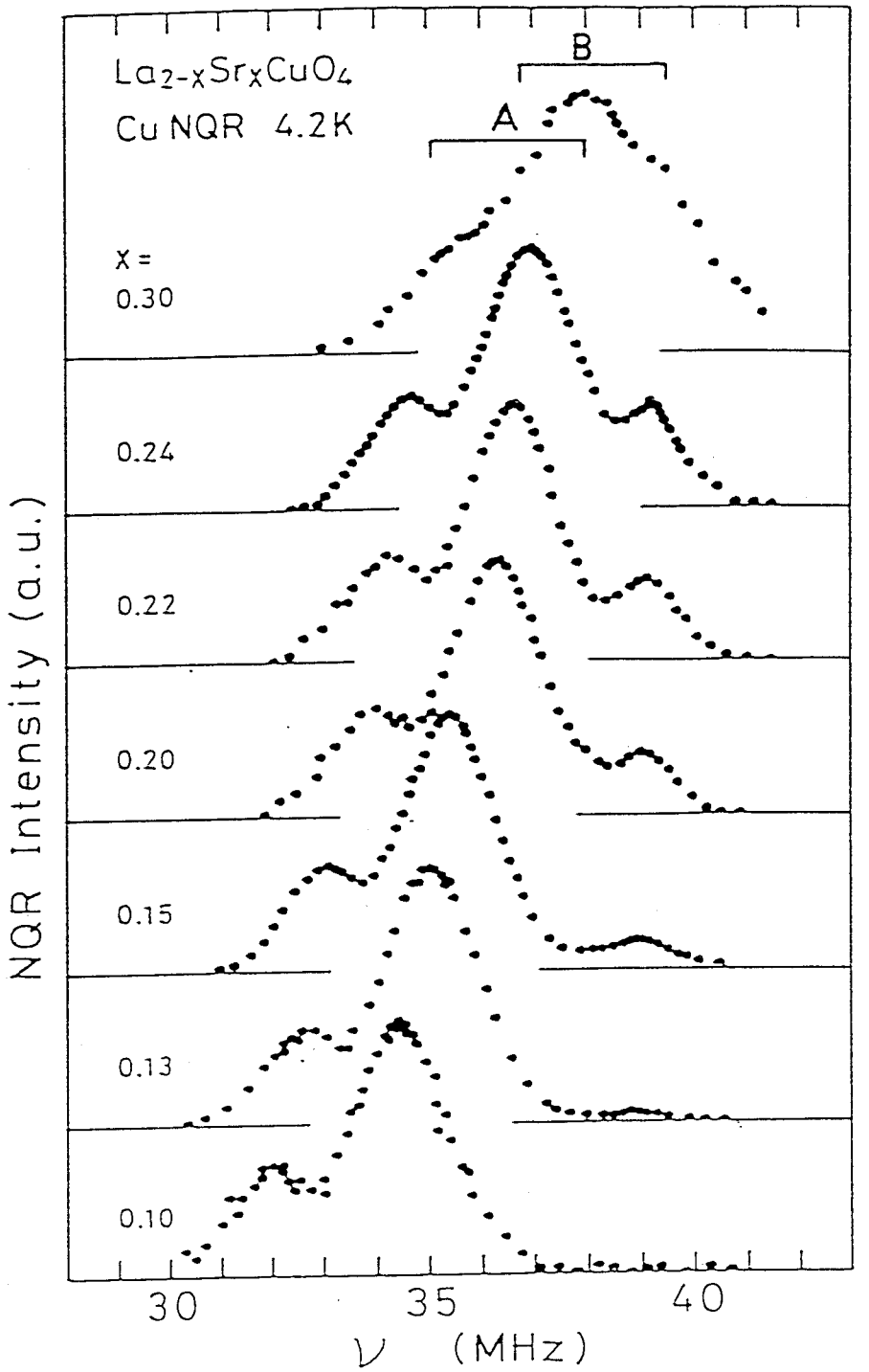

Fig.4-1-1.
NQR spectra of Cu for x=0.10~ 0.30 in $La_{2-x}Sr_xCuO_4$ at 4.2K in zero field.

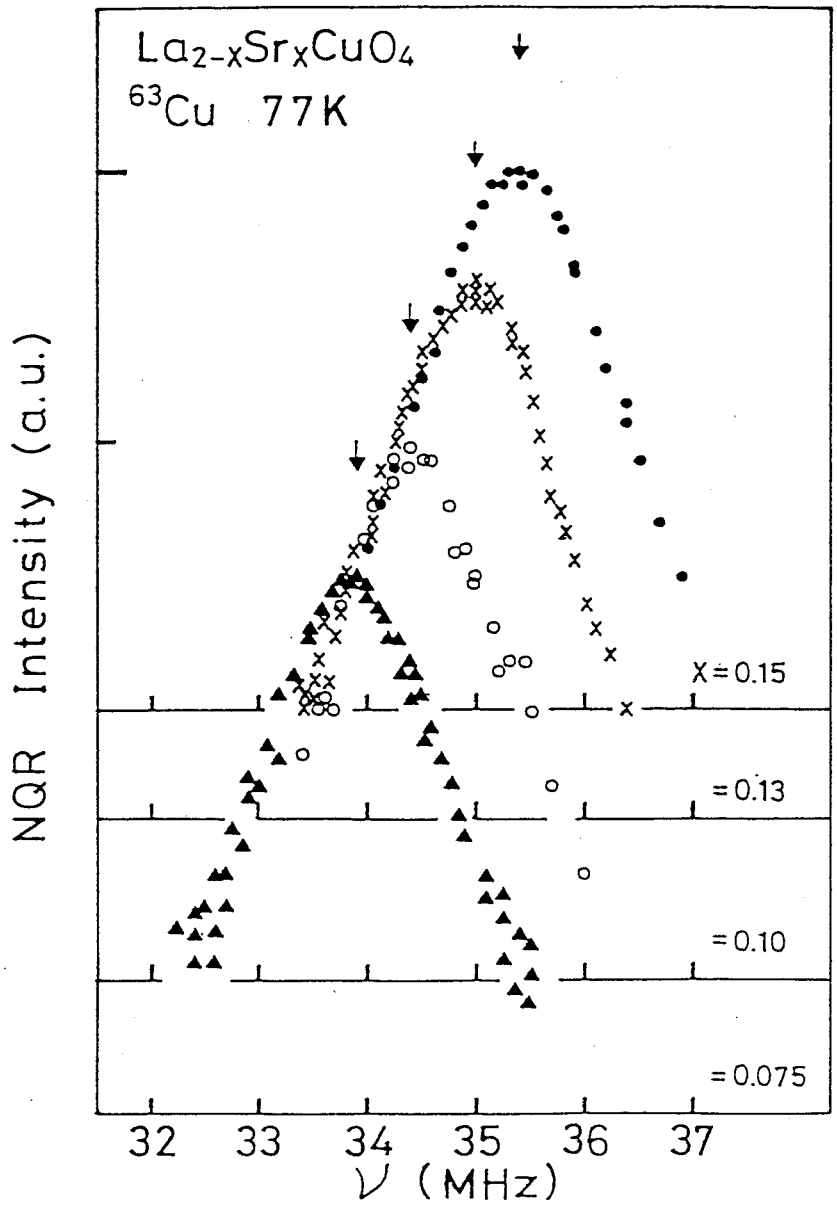

Fig.4-1-2.
NQR spectra of ^{63}Cu for x=0.075(▲), 0.10(○), 0.13(×) and 0.15 (●) in $La_{2-x}Sr_xCuO_4$ at 77K in zero field.[20]

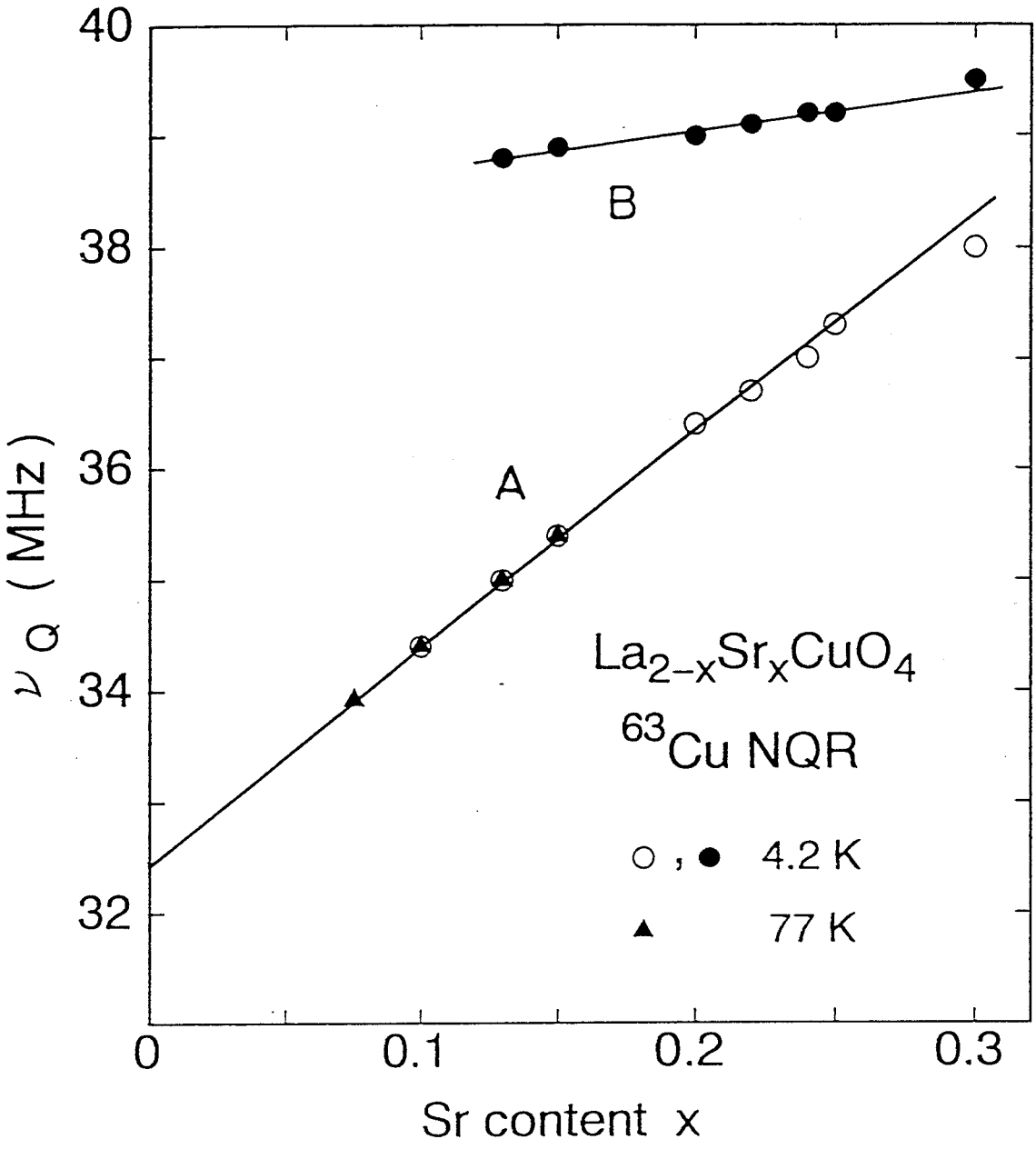

Fig.4-1-3.
Sr content dependence of the NQR frequency, ν_Q, of ^{63}Cu in $La_{2-x}Sr_xCuO_4$ at 4.2 and 77K in zero field.

4-2. T_1 of ^{63}Cu NQR in $La_{2-x}Sr_xCuO_4$ in Normal State

T_1 was mainly measured at the frequency for ^{63}Cu of set A (central peak of each spectrum) as shown in **Fig.4-1-1**. **Fig.4-2-1** shows an overall T-dependence of $1/T_1$ of ^{63}Cu for x=0.075~ 0.24, together with the data of YBCO (T_c=92K).[20,46,51,57] $1/T_1$ for x=0.075 could only be measured above 77K because of the poor signal to noise ratio due to a quite short spin echo decay time, T_2, below 77K. As seen in the figure, $1/T_1$ is significantly enhanced and then the T-dependence becomes weaker with decreasing Sr content and tends to be saturated with increasing temperature. Below around 100K, $1/T_1$ begins to decrease appreciably and approaches a linear T-dependence near T_c, i.e. T_1T=constant.

So far, there have been many efforts to explain the unusual Cu relaxation behavior associated with the development of AF spin correlation.[19,47~49] However, it is still now difficult to argue which proposal is best at present. A most important point to be stressed is that $(T_1T)^{-1}$ is related to the staggered susceptibility, $\chi_Q(T)$, at the zone boundary, $Q=(\pi/a, \pi/a)$, in the square lattice in the framework of a model based on either strong[19,50] or weak[48] correlation limit. Both models assume commonly a presence of a large enhancement of the q-dependent susceptibility at the zone boundary.

In order to see the systematic variation of $(T_1T)^{-1}$ related to $\chi_Q(T)$ against hole concentration, the T-dependence of $(T_1T)^{-1}$ is shown in **Fig.4-2-2**.[20,46,51] $(T_1T)^{-1}$ with an extremely enhanced value than that for the **normal** Fermi liquid [$(T_1T)^{-1}$~ $1sec^{-1}K^{-1}$] increases with decreasing temperature and approaches almost a constant value in the T-region near T_c. **Fig.4-2-3** shows

m(t) plotted against tT.[20] The points fall approximately on a curve within an experimental scattering although m(t) is not simple exponential. This indicates that all the components of T_1 follow T_1T=const. relation in the narrow T-region of 40~ 55K for x=0.15 and 32~ 43K for x=0.10.

As seen in **Fig.4-2-2**, the strong T-dependence of $(T_1T)^{-1}$ in higher T-region reminds us of the Curie-Weiss law of the susceptibility. As a matter of fact, we have experimentally a relation of

$$T_1T = (T + \theta) / A\,C, \tag{4-1}$$

as shown in **Fig.4-2-4** [20,46,51] and hence

$$(T_1T)^{-1} = A\,C / (T + \theta). \tag{4-2}$$

where A is proportional to the square of the hyperfine field A_{hf} and the gyromagnetic ratio $^{63}\gamma_N$ for ^{63}Cu. It should be noted that A_{hf}^2 is described by the term of $(A_\perp - 4B)^2$ since Cu spin fluctuations in LSCO is antiferromagnetically coupled among four nearest neighbor Cu spins. Here $A_\perp$ and B are the on-site hyperfine field perpendicular to the c-axis and the isotropic supertransferred hyperfine field, respectively. We suppose that this T-dependence is associated with the Curie-Weiss law of the staggered susceptibility, $\chi_Q(T)$, namely

$$\chi_Q(T) = C / (T + \theta)\,. \tag{4-3}$$

This behavior is also seen in another HTSC as show in **Fig.4-2-5**.

20,46,51,68)

The remarkable feature is that the Weiss temperature, θ , is linearly extrapolated to 0K for x=0.05 with decreasing Sr content as shown in **Fig.4-2-6**, in which T_c and the Neel temperature, T_N, are also shown.[20,46,51] In contrast to the linear increase of θ with increasing Sr content, the slope C, increases slightly. In addition, the nuclear relaxation behavior for $La_{2-x}Sr_xCuO_4$ expressed by a multi-exponential caused by the distribution of T_1 occurs below around the Weiss temperature, θ .[46,57]

Here, we compare our result with the theory. Recently, Moriya et al. have extended the SCR theory of a weakly or nearly AF metal to the two-dimensional system. The T-linear increase of the resistivity has been interpreted reasonably.[48] In particular, it is surprising that the T-dependence of T_1T in **Fig.4-2-4**, which is inversely proportional to $\chi_Q(T)$, is quite similar to the calculated results of $1/\chi_Q(T)$.

On the other hand, it has been proposed that $1/T_1$ of Cu in high-T_c materials such as $YBa_2Cu_3O_7$, $YBa_2Cu_3O_{6.5}$, $LaBa_2Cu_3O_{6.9}$ and $La_{1.85}Sr_{0.15}CuO_4$ are better fitted by a form of $1/T_1 = a + bT$ in the higher T-region than around 150K.[11] Furthermore, the second term, bT, for $YBa_2Cu_3O_7$ has quantitatively been estimated by using the value of $(T_1T)^{-1}$ for ^{17}O, [17] which is supposed to reflect mainly the d-spin fluctuations around the zone center (q=0) due to the geometrical cancellation of AF spin correlation.[11,18,19] However differently from the fit of $1/T_1 = a + bT$ proposed by Imai,[11] we have found the experimental relation of $(T_1T)^{-1} = AC/(T+\theta.)$ for whole x in $La_{2-x}Sr_xCuO_4$ as seen in **Fig.4-2-4**. As a matter of fact, we have confirmed that $1/T_1$ for the compounds with x=0.15 reported by Imai is well

fitted by a formula of $C/(T+\theta)$ with $\theta \sim 100K$ as well. Here the different θ from our value may be attributed to the slight different Sr content from our sample. Thus, as far as the relaxation behavior in LSCO is concerned, it is extracted from a experimental point of view that $(T_1T)^{-1}$ obeys a Curie-Weiss law like T-dependence , i.e. $C/(T+\theta)$, deviates from this relation below θ and approaches to a nearly constant value. In addition, we tried to estimate a q=0 contribution to the relaxation rate in LSCO, $^{63}(T_1T)_0^{-1}$. Although it is not clear whether or not there is a physical justification in a procedure to divide $1/T_1$ into two contributions from q=0 and q=Q for LSCO, by using $(T_1T)^{-1}$ of ^{17}O for CuO_2 plane in $La_{1.85}Sr_{0.15}CuO_4$,[52] $^{63}(T_1T)_0^{-1}$ was estimated to be $1.3sec^{-1}K^{-1}$ as well as in the case of YBCO. With decreasing Sr content, $^{63}(T_1T)_0^{-1}$ is expected to decrease further because the measured spin susceptibility, $\chi(q=0)$, which is proportional to $^{63}(T_1T)_0^{-1}$ reduces. As compared with the observed values of $^{63}(T_1T)^{-1}$ in **Fig.4-2-2**, $^{63}(T_1T)_0^{-1}$ is by one order of magnitude smaller than those of $^{63}(T_1T)^{-1}$ for LSCO. As the result, the T-dependence of $^{63}(T_1T)^{-1}$ - $^{63}(T_1T)^{-1}$ is not largly changed. Apparently, it is evident that $(T_1T)^{-1}$ of ^{63}Cu in $La_{2-x}Sr_xCuO_4$ in the vicinity of the magnetic phase boundary is largely dominated by the spin fluctuations around the zone boundary, q=Q.

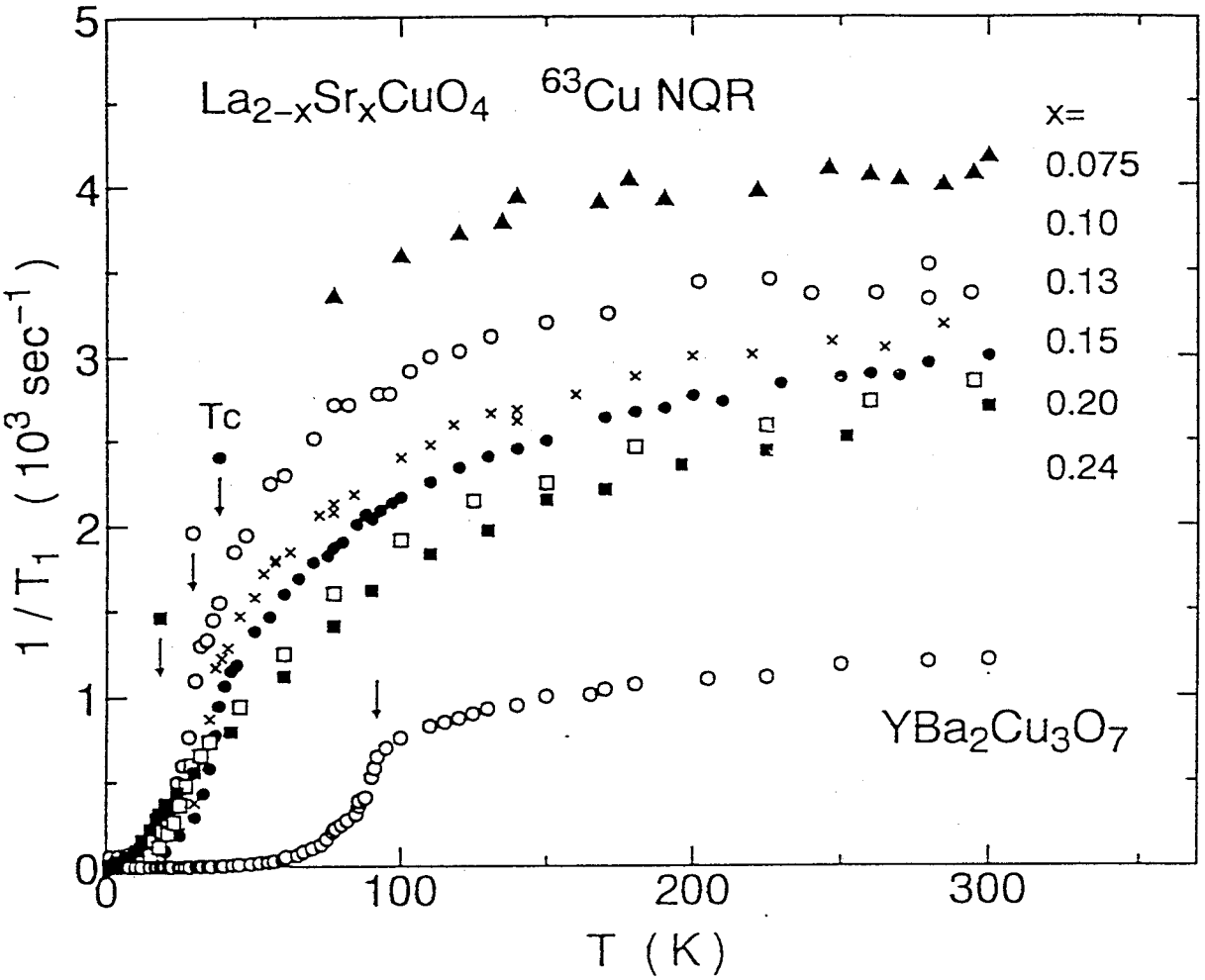

Fig.4-2-1.
T-dependence of $1/T_1(=2W)$ of ^{63}Cu for x=0.075(▲), 0.10(○), 0.13(×), 0.15(●), 0.20(□) and 0.24(■) in $La_{2-x}Sr_xCuO_4$ plotted in a linear scale together with the result of $YBa_2Cu_3O_7$ (○). 20,46,51,57)

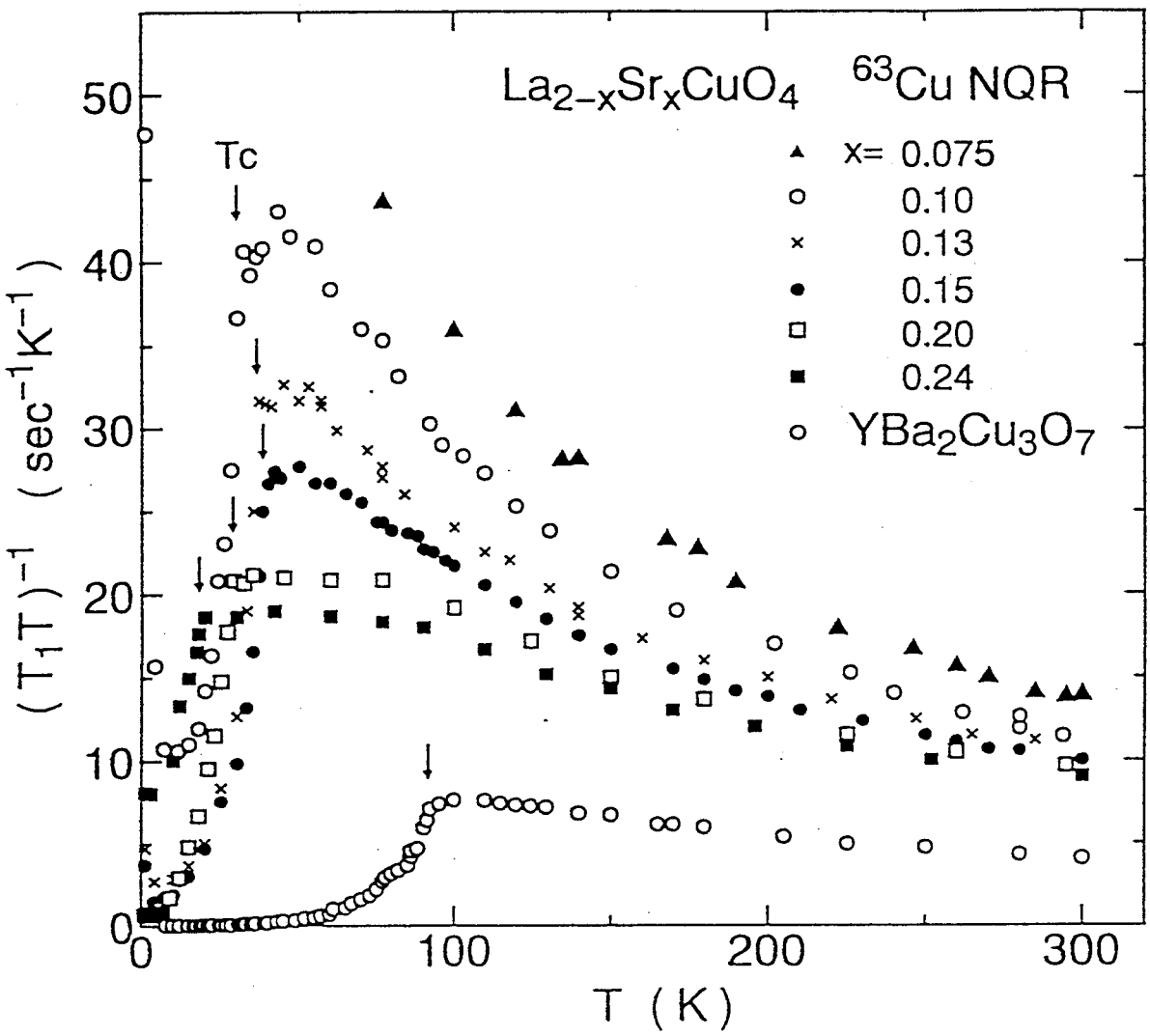

Fig.4-2-2.
T-dependence of $(T_1T)^{-1}$(=2W/T) of ^{63}Cu for x=0.075(▲), 0.10(○), 0.13(×), 0.15(●), 0.20(□) and 0.24(■) in $La_{2-x}Sr_xCuO_4$ plotted in a linear scale together with that of $YBa_2Cu_3O_7$(○).[20,46,51]

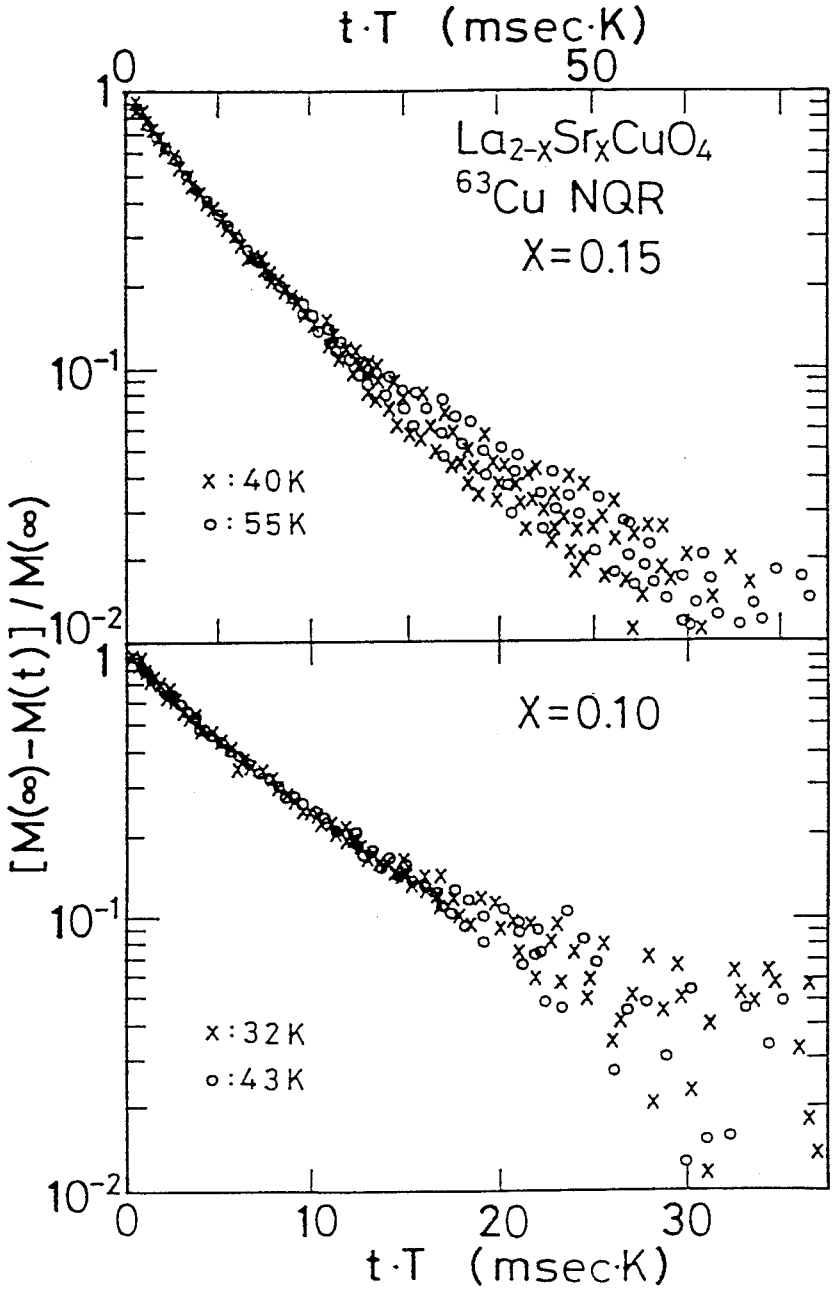

Fig.4-2-3.
Relaxation curves of the nuclear magnetization, m(t), vs the product of time, t, and temperature, T, at 40 and 55K for x=0.15, and those at 32 and 43K for x=0.10 in $La_{2-x}Sr_xCuO_4$, respectively.[20] The points fall approximately on a curve within an experimental scattering. This indicates that all the components of T_1 follow T_1T=const. relation in the narrow T-region above T_c for both compounds.

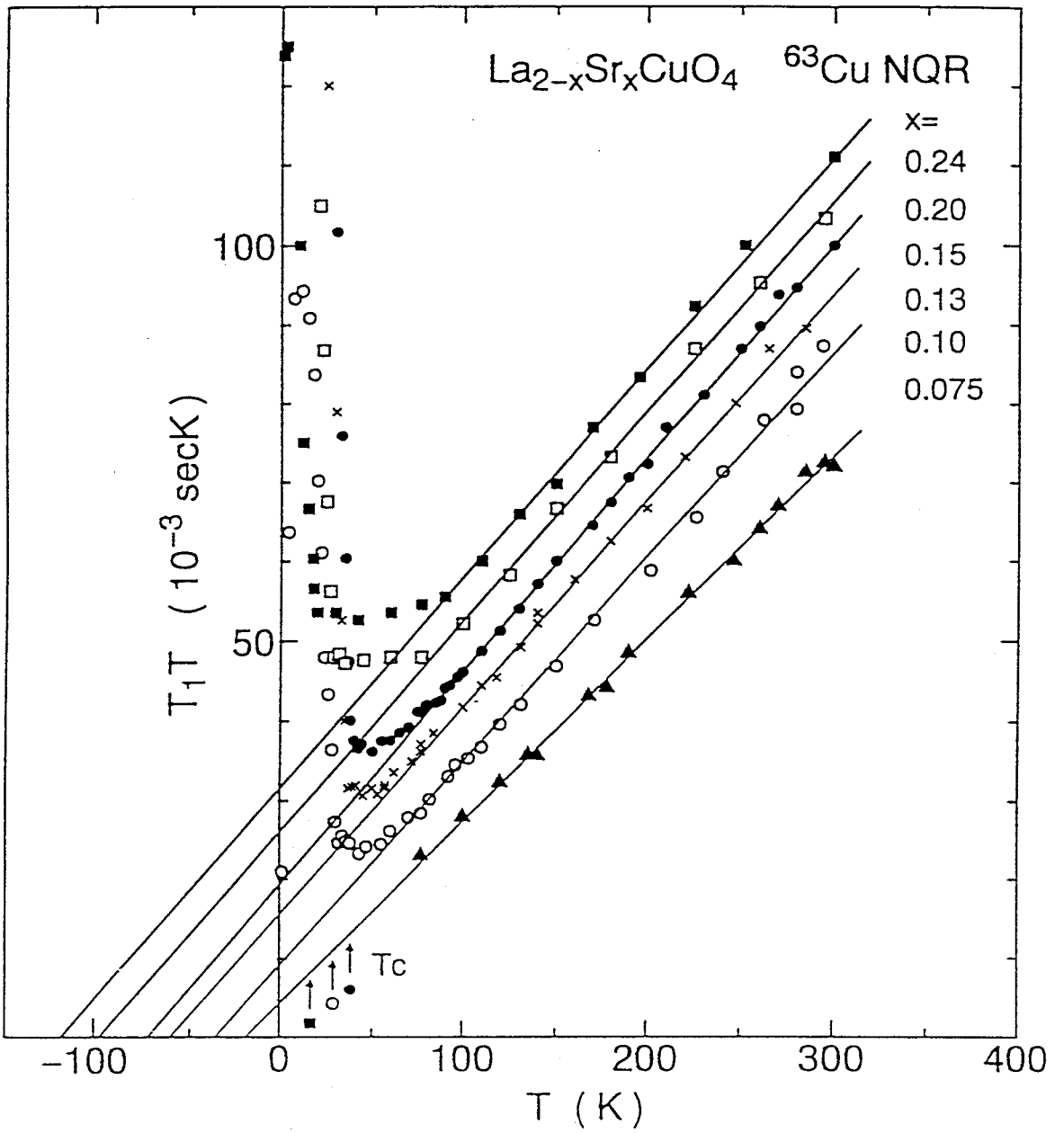

Fig.4-2-4.

T-dependence of $T_1T(=T/2W)$ of ^{63}Cu for x=0.075(▲), 0.10(○), 0.13(×), 0.15(●), 0.20(□) and 0.24(■) in $La_{2-x}Sr_xCuO_4$. [20,46,51] A relation of $(T_1T)=(T+\theta)/AC$ (see the text) is deduced experimentally for each compound with different θ.

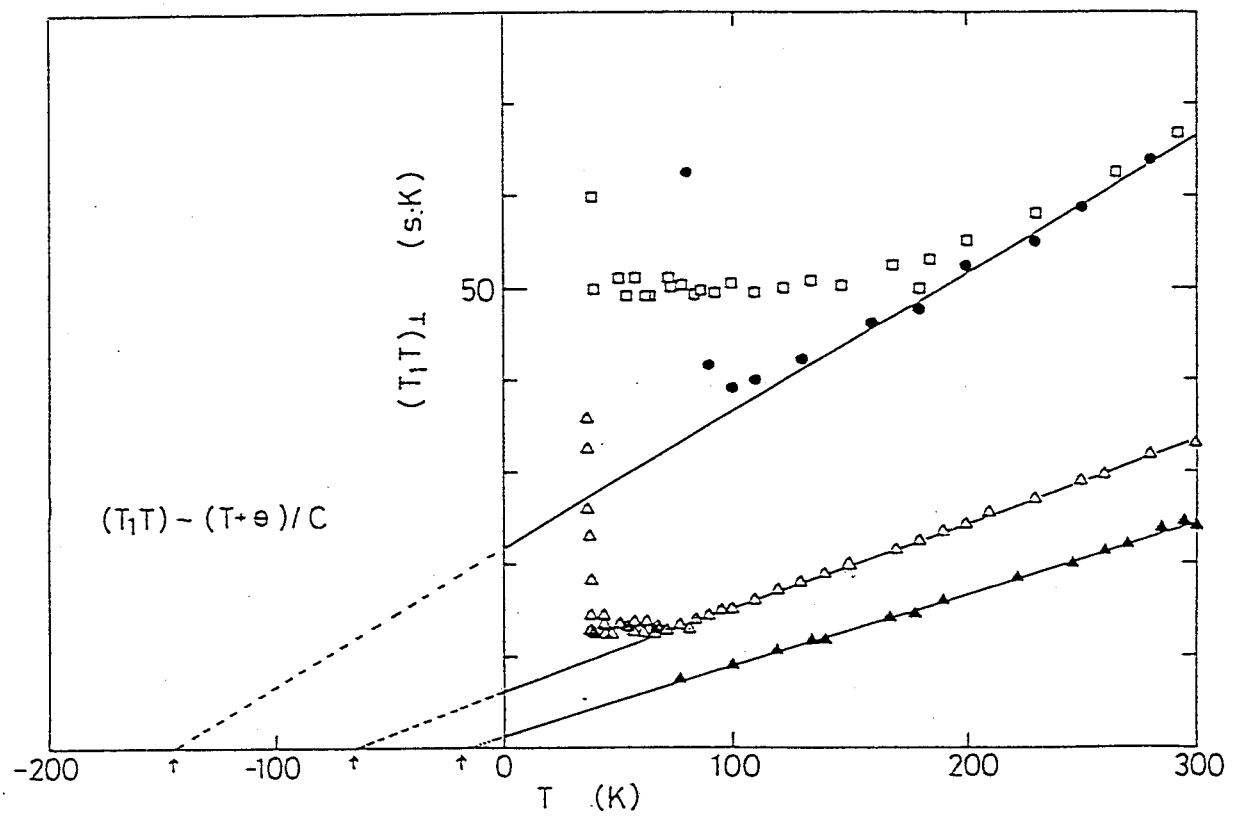

Fig.4-2-5.

T-dependence of $(T_1T)_\perp$ (=T/2W) of ^{63}Cu for x=0.075(▲) and 0.15 (△) in $La_{2-x}Sr_xCuO_4$, $YBCO_7$(●) and Tl(2201)(□).[20,46,51,68] A relation of $(T_1T)=(T+\theta)/AC$ with different θ is also deduced experimentally for another HTSC. Here $(T_1T)_\perp$ is the T_1T perpendicular to the c-axis estimated by use of the hyperfine field.

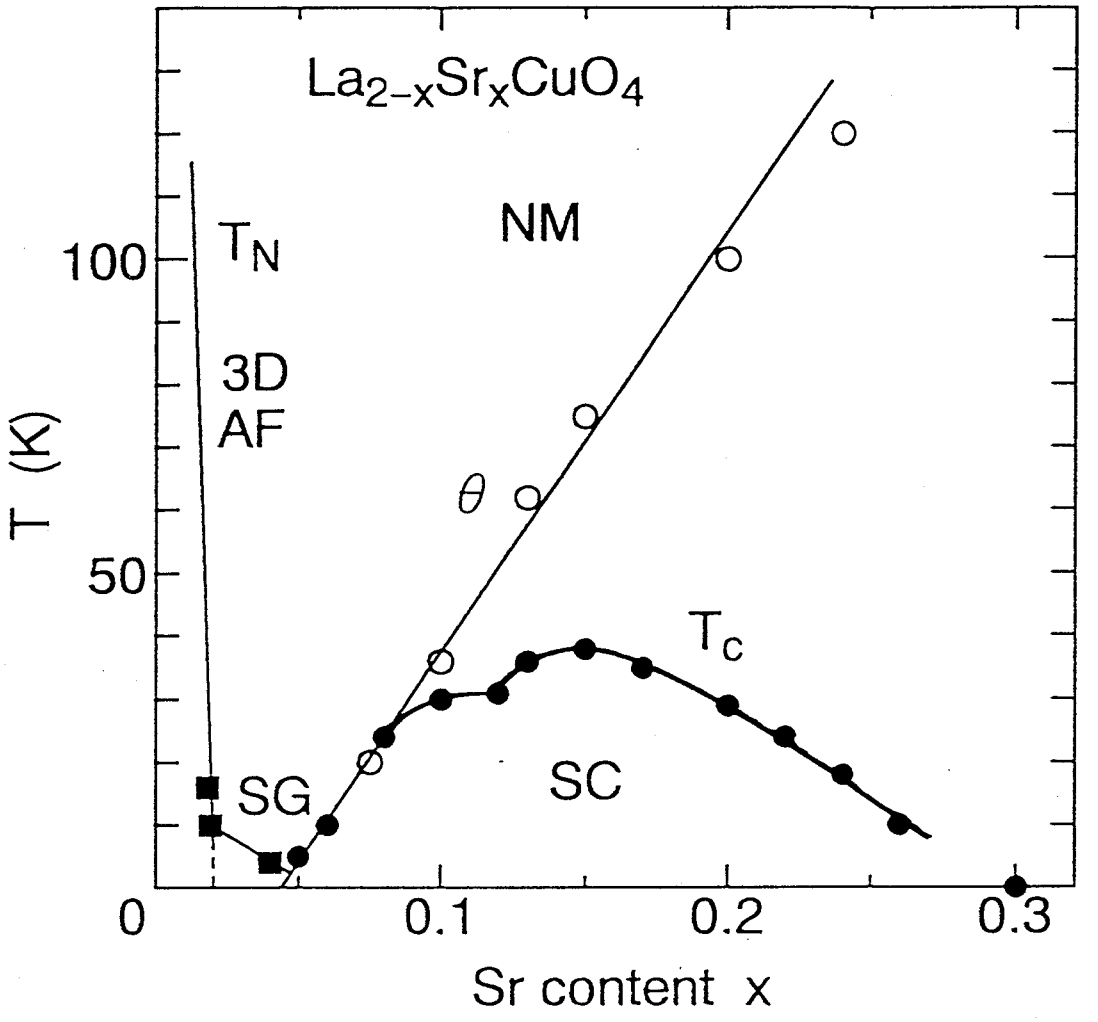

Fig.4-2-6.
Sr content dependence of T_N(■), T_c(●) and θ (○).[20,46,51] θ is extracted by fitting the data to (T+θ)/AC in Fig.4-2-6. A solid line is a guide to the eye, and θ becomes almost zero near the magnetic phase boundary around x=0.05.

4-3. T_1 of ^{63}Cu NQR in $La_{2-x}Sr_xCuO_4$ in Superconducting State

Next, we show the results of the T-dependence of T_1 in superconducting state.

(1) Lightly Doped Region for $x \leq 0.15$

$1/T_1(=2W)$ of ^{63}Cu for x=0.075(◇), 0.10(□) and 0.15(●) in $La_{2-x}Sr_xCuO_4$ is plotted in **Fig.4-3-1**.[20,46,57] T_{1S} and T_{1L} are also shown in the figure by marks △, ▲ and ▽, ▼, respectively, to show the region of distribution of T_1 below T_c. As a comparison, the result for $YBa_2Cu_3O_7$(○)[55] is also shown. $1/T_1$ of ^{63}Cu in LSCO is considerably larger than that in YBCO both above and below T_c. Although the distribution of T_1 increases with decreasing temperature below T_c, all the components of $1/T_1$ are confirmed to decrease below T_c, which indicates that there is no normal part in the sample and no significant distribution of T_c.

In order to emphasize the characteristic feature below T_c, the T-dependence of $1/T_1$ normalized by the value at T_c for x=0.10(□) and 0.15(●) in $La_{2-x}Sr_xCuO_4$ and $YBa_2Cu_3O_7$(○)[55] is plotted against T/T_c in **Fig.4-3-2**.[20] As seen in the figure, the behavior of rapid reduction of $1/T_1$ from T_c down to $0.8T_c$ is independent of Sr content and T_c. This reduction behavior is a common feature not only observed in the Cu relaxation of CuO_2 plane[13] as shown in **Fig.4-3-3** but also in the relaxation of ^{17}O[17] and ^{89}Y[16] in YBCO. Accordingly, it is evident that the same mechanism works in the relaxation process just below T_c which cannot be interpreted by the conventional BCS model.[25]

Here it should be emphasized that the terminology of BCS model is used in a usual sense that the isotropic energy gap is opened at the Fermi level below T_c, which causes the enhancement of $1/T_1$ just below T_c.

In **Fig.4-3-2**, with further decreasing temperature, $1/T_1$ of LSCO deviates from a steep decrease and tends to be saturated at lower temperature. The saturated value increases with decreasing Sr content, which cannot be attributed to trivial impurities. The saturated parts could be caused by a localized nature of Cu d-spins with decreasing hole content.[20,46,57]

(2) Over Doped Region for $x \geqq 0.15$

Figure 4-3-4 shows the T-dependence of $1/T_1(=2W)$ of ^{63}Cu for $x=0.15$(●), 0.20(□), 0.22(△) and 0.24(■) in $La_{2-x}Sr_xCuO_4$ [46,57] together with that of $YBa_2Cu_3O_7$(○)[55] in zero field.[46,57] In the normal state, the T-region where T_1T=const. relation holds above T_c extends toward over doped region.[46,56,57] In order to emphasize the characteristic feature below T_c as well as the lightly doped region, the T-dependence of $1/T_1$ normalized by the value at T_c is plotted against T/T_c in **Fig.4-3-5**. Here marks are as same as those in **Fig.4-3-4**. In the superconducting state, the rapid decrease of $1/T_1$ below T_c has not only been observed in the lightly doped Sr content region of $x \leqq 0.15$, but also in the over doped region of $x=0.20 \sim 0.24$ in $La_{2-x}Sr_xCuO_4$. In addition, all the components of T_1 decrease rapidly below T_c over whole Sr content region.[57] With further decreasing temperature, $1/T_1$ in over doped region deviates from a steep decrease and tends to be proportional to temperature at

lower temperature as Sr content is increased from x=0.20 to 0.24. Actually, the relaxation curves of the nuclear magnetization, m(t), plotted against the product of time, t, and temperature, T, for x=0.22 and 0.24 in the T-region of 1.3~ 4.2K and 1.3~ 7K, respectively, fall approximately on a curve within an experimental scattering as shown in **Fig.4-3-6**. This indicates that all the components of T_1 follow T_1T=const. relation in these T-region. This situation is seen for the relaxation curves of m(t) of ^{63}Cu for set B as shown in **Fig.4-1-1** for x=0.24 plotted against the product of t and T in the T-region of 1.3~ 4.2K as shown in **Fig.4-3-7**. There is a doubt that the NQR line of set B is not from superconducting part, therefore it may be expected that $1/T_1$ is not decreased below T_c. $1/T_1$ of ^{63}Cu for set B for x=0.24 is decreased below T_c, and the T-dependence, having by about 1/2 times smaller value than that of ^{63}Cu for set A, is almost the same as that of ^{63}Cu for set A. Thus Cu for set B is also in superconducting state. The details will be discussed in **section 5-3**.

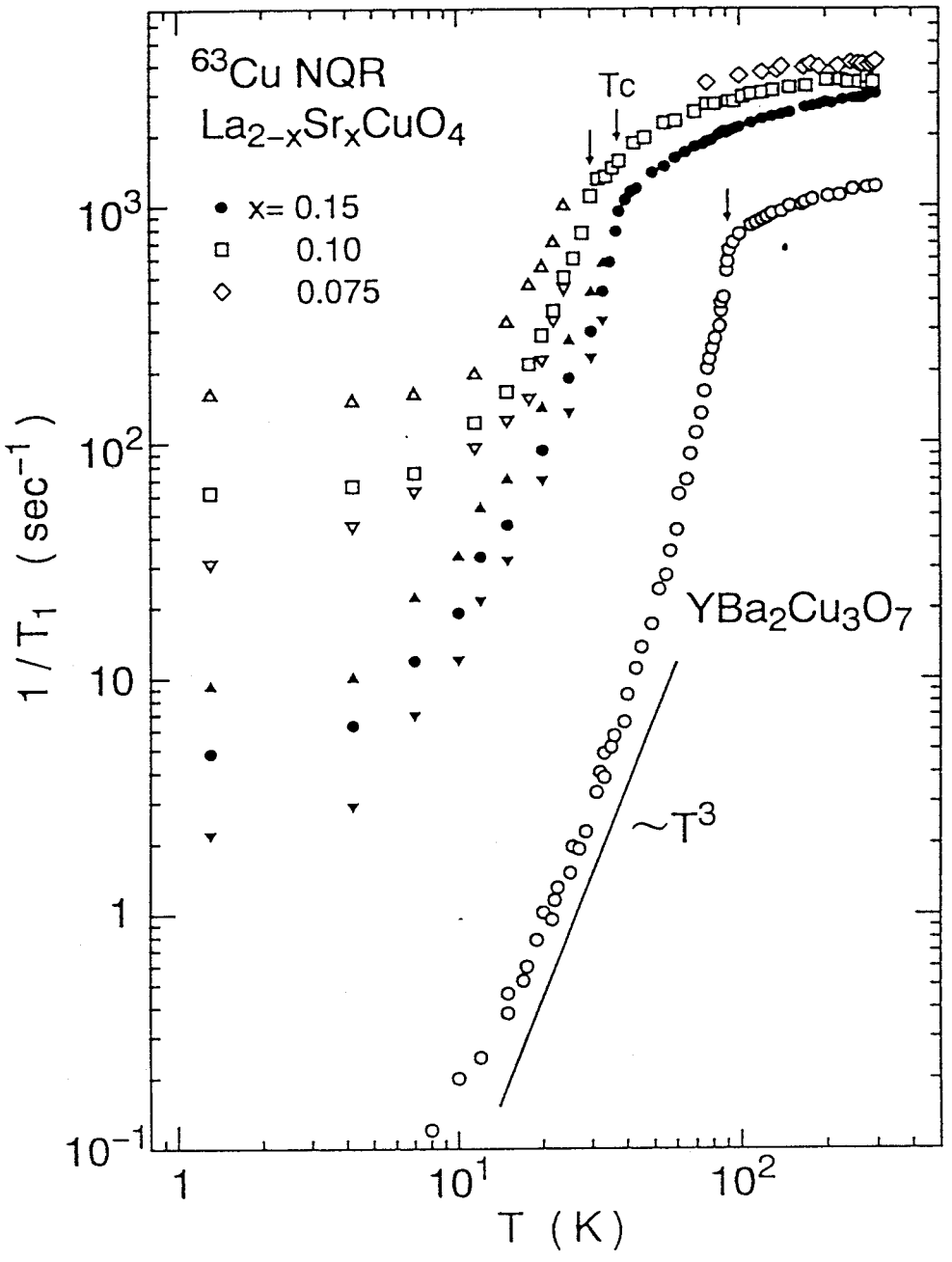

Fig.4-3-1.

T-dependence of $1/T_1$(=2W) of ^{63}Cu for x=0.075(◇), 0.10(□) and 0.15(●) in $La_{2-x}Sr_xCuO_4$ and that of $YBa_2Cu_3O_7$(○)[55] with T_c=20, 30, 38 and 92K, respectively.[20,46,57] ○ and ● circles for LSCO represent $1/T_1$ evaluated from the slope where m(t)=[M(∞)-M(t)]/M(∞) decreases from 30 to 10 % of the initial value. △, ▲ and ▽, ▼ indicate $1/T_1$ obtained from the slope where m(t) decreases from 100 to 37% and from 10 to 5%, respectively, i.e. T_{1S} and T_{1L}. Here M(t) is the nuclear magnetization at time, t, after the saturating pulses.

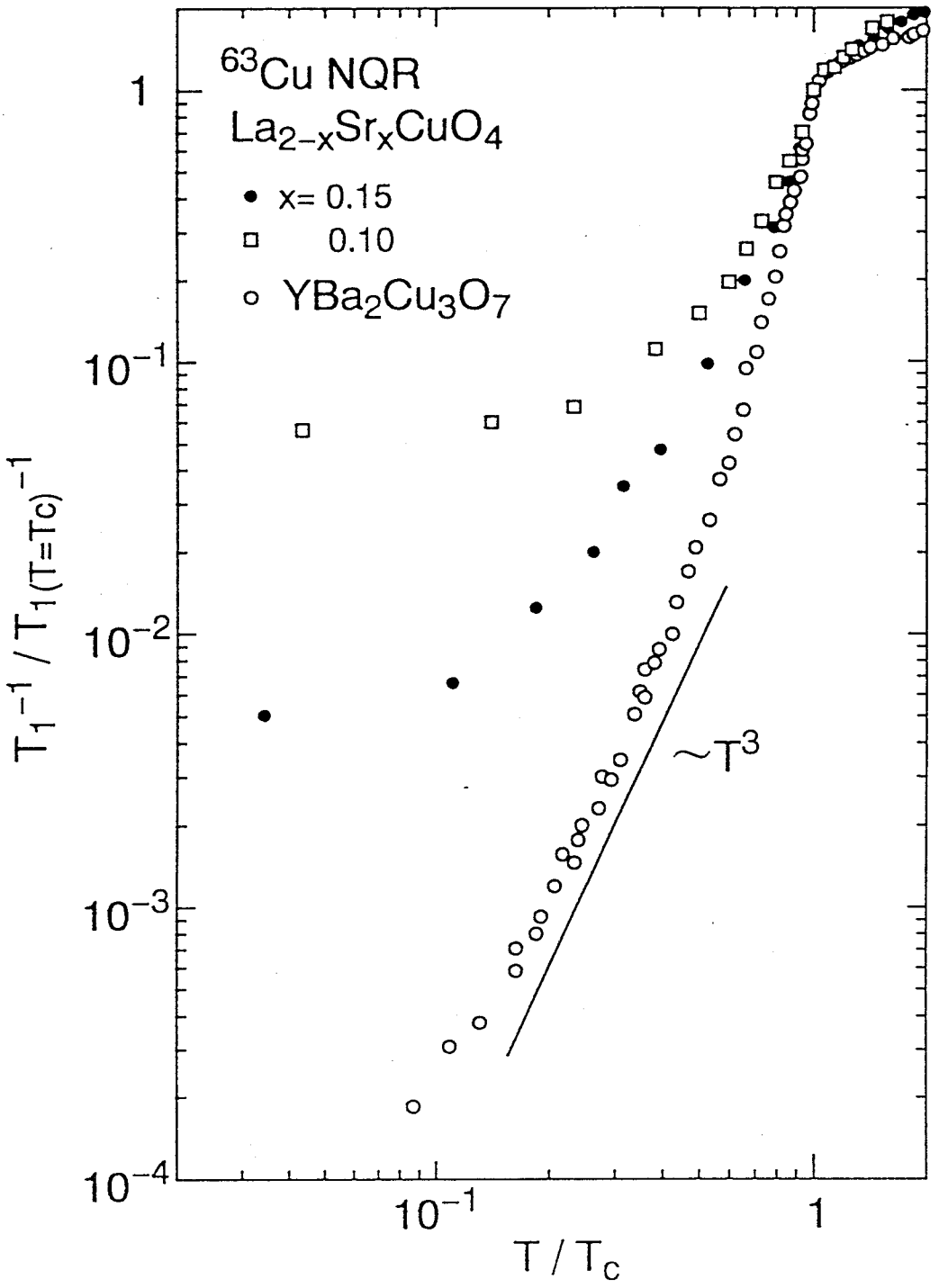

Fig.4-3-2.
The normalized T-dependnece of $1/T_1$, i.e. $T_1^{-1}/T_{1(T=Tc)}^{-1}$, of ^{63}Cu is plotted against T/T_c.[20,55] The marks of T_1 for various compounds are the same as those in **Fig.4-3-1.**

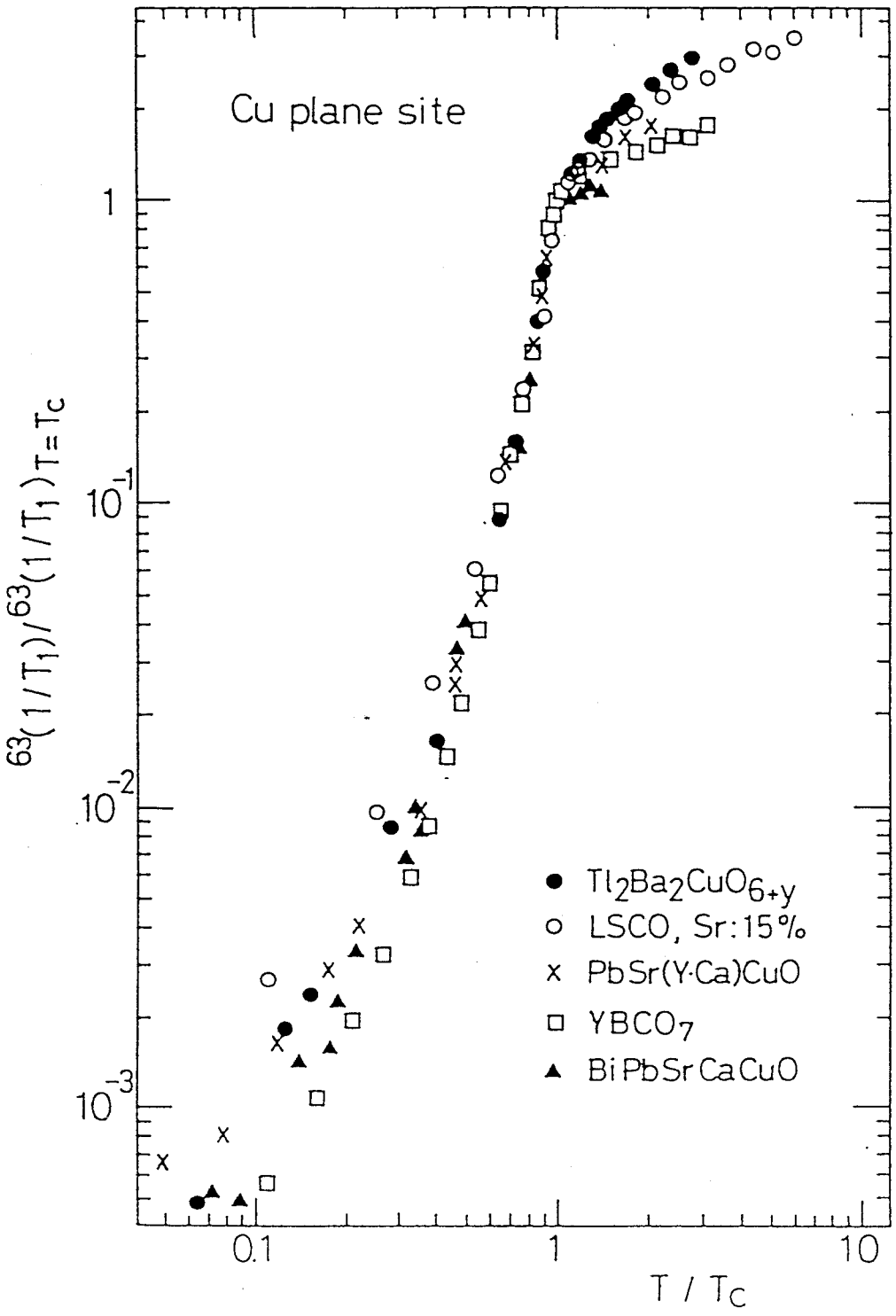

Fig.4-3-3.
The normalized T-dependnece of $1/T_1$, i.e. $T_1^{-1}/T_{1(T=Tc)}^{-1}$, of ^{63}Cu in various high-T_c compounds is plotted against T/T_c.[13)]

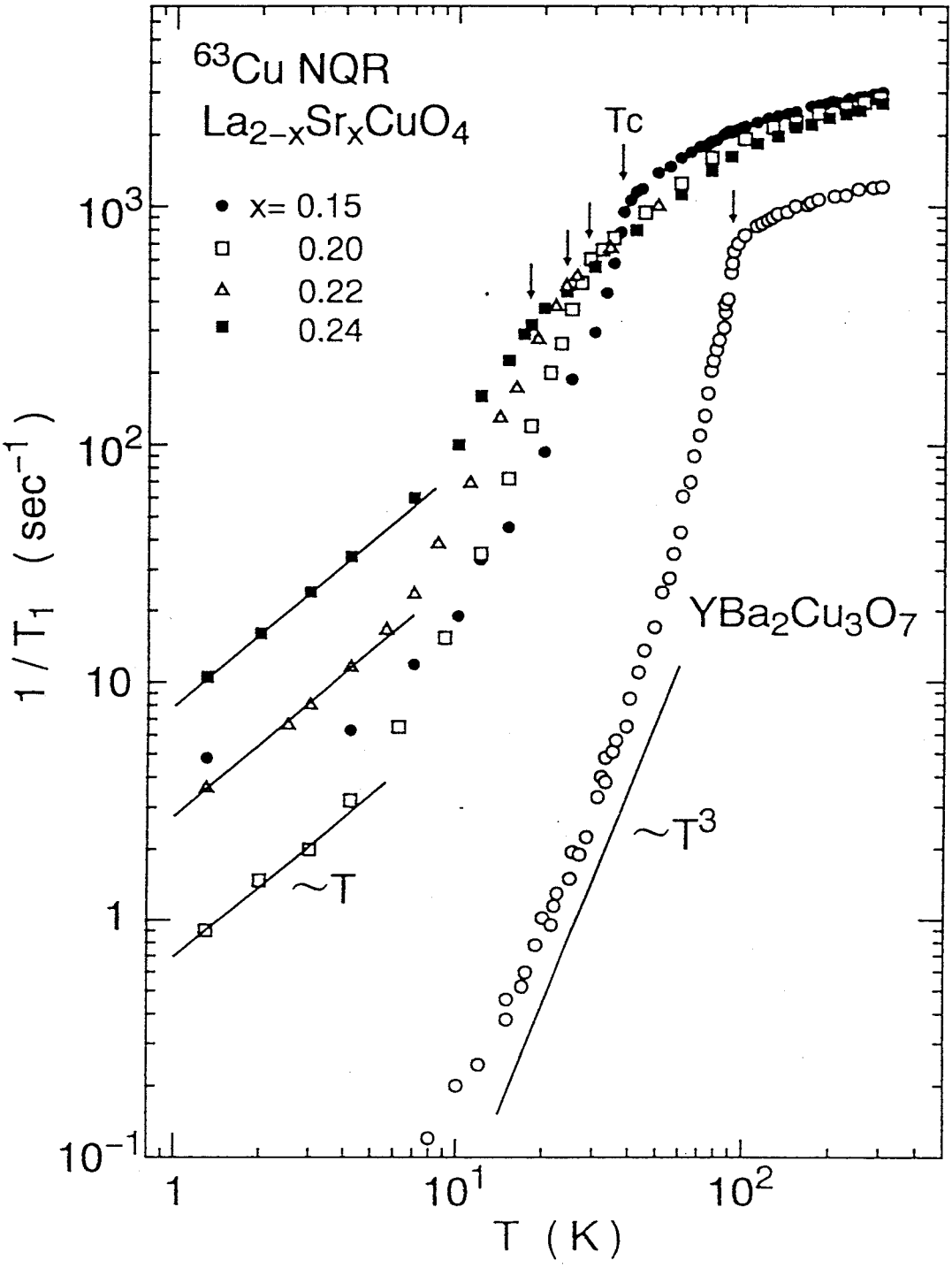

Fig.4-3-4.
T-dependence of $1/T_1$(=2W) of ^{63}Cu for x=0.15~ 0.24 in $La_{2-x}Sr_xCuO_4$ and that of $YBa_2Cu_3O_7$(○)[55] in zero field.[46,57] $1/T_1$ decreases rapidly as in the lightly doped region below x=0.15 and tends to be proportional to temperature at lower Temperature as Sr content is increased from x=0.20 to 0.24.

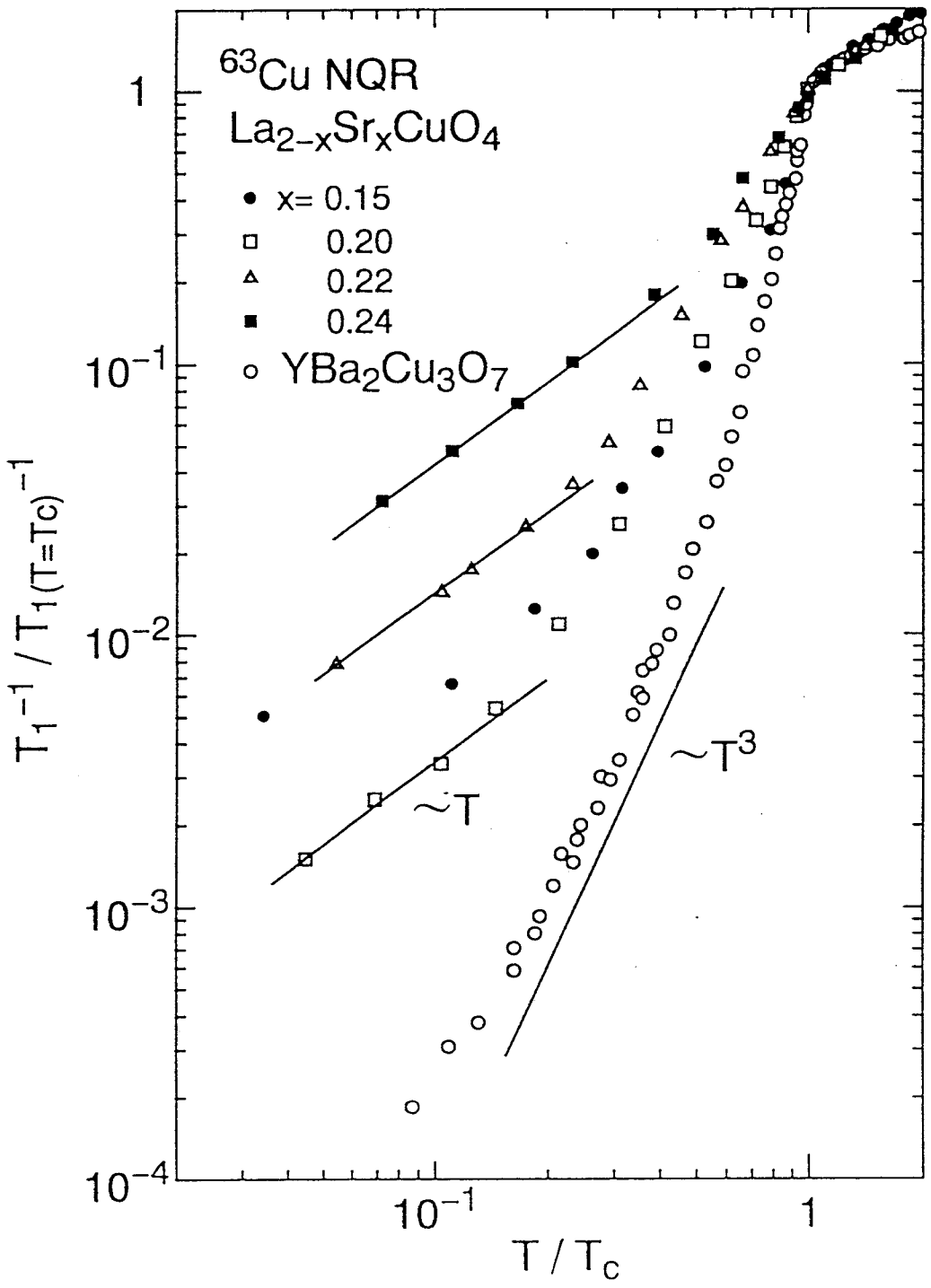

Fig.4-3-5.
The normalized T-dependnece of $1/T_1(2W)$, i.e. $T_1^{-1}/T_{1(T=Tc)}^{-1}$, of ^{63}Cu for x=0.15~0.24 in $La_{2-x}Sr_xCuO_4$ and that of $YBa_2Cu_3O_7$ (○)[55] in zero field is plotted against T/T_c.[46,57] The marks of T_1 for various compounds are the same as those in **Fig.4-3-4.**

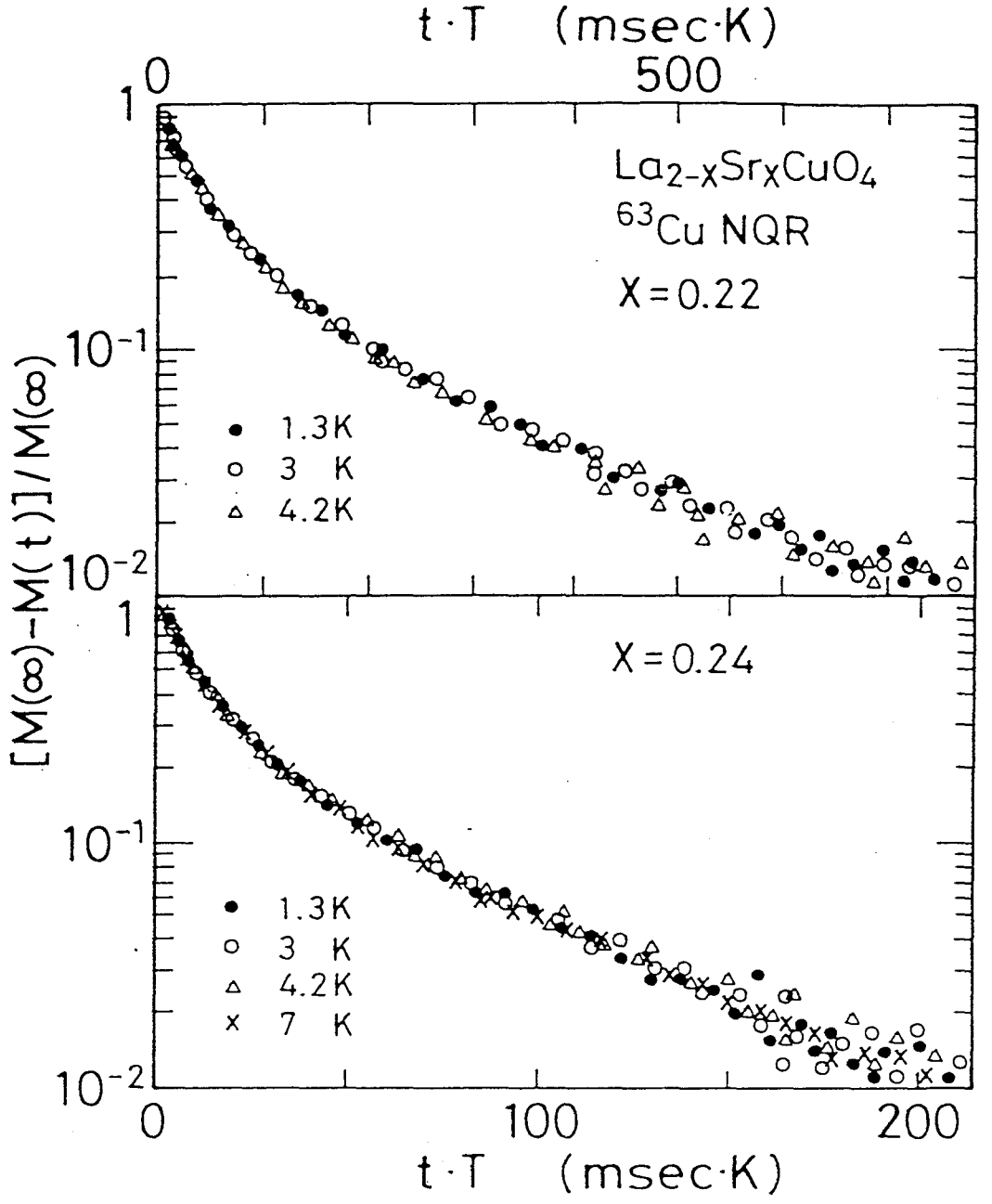

Fig.4-3-6.

Relaxation curves of the nuclear magnetization, $m(t)=[M(\infty)-M(t)]/M(\infty)$, of ^{63}Cu in the T-region of 1.3~ 4.2K for x=0.22 and of 1.3~ 7K for x=0.24 plotted against the product of time, t, and temperature, T. The data fall approximately on a curve within an experimental scattering. This indicates that all the components of T_1 follow T_1T=const. relation for both compounds in these T-region.

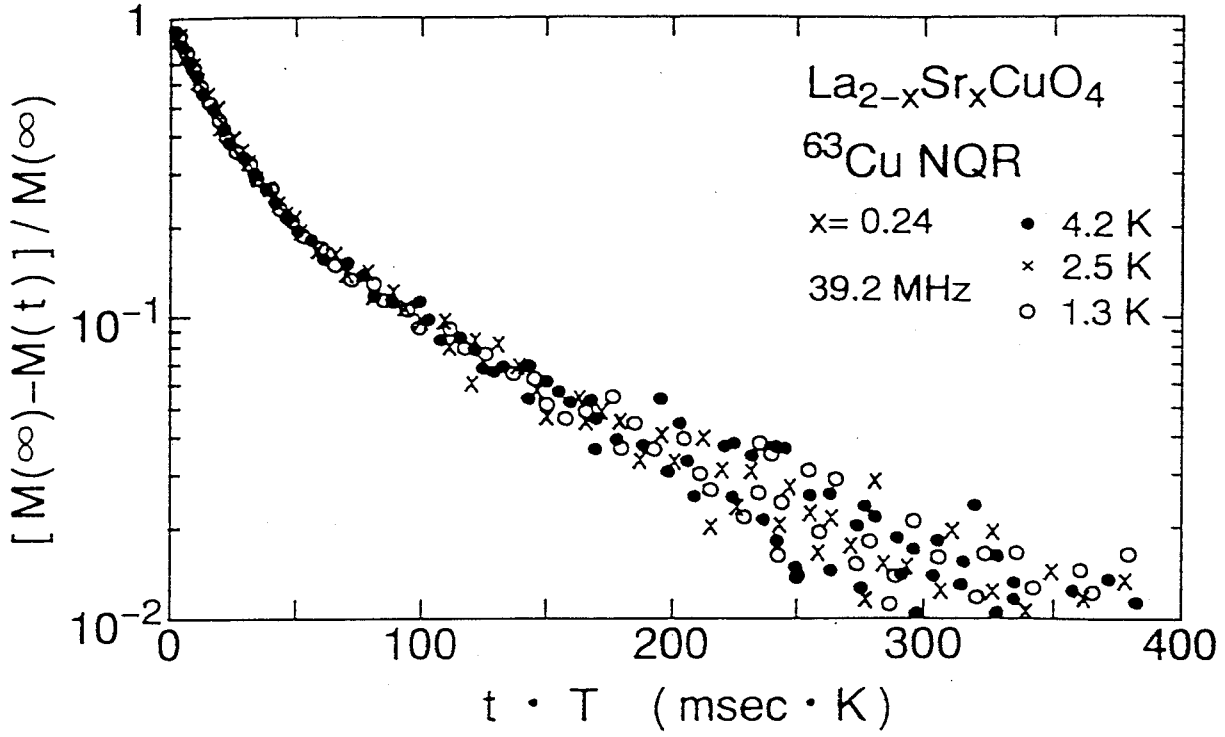

Fig.4-3-7.
Relaxation curves of the nuclear magnetization, m(t)=[M(∞)-M(t)]/M(∞), of ^{63}Cu for set B as shown in **Fig.4-1-1** in the T-region of 1.3~ 4.2K for x=0.24, plotted against the product of time, t, and temperature, T. The data fall approximately on a curve within an experimental scattering. This indicates that all the components of T_1 follow T_1T=const. relation in these T-region.

4-4. ^{63}Cu NMR in $La_{2-x}Sr_xCuO_4$

Fig.4-4-1 shows the central transition NMR spectra of ^{63}Cu for x=0.24 in $La_{2-x}Sr_xCuO_4$ at 4.2 and 20K and at the frequency of 125.1MHz with the c-axis perpendicular to the magnetic field, $c \perp H$.[57] The peak position of the spectrum in the superconducting state at 4.2K is clearly shifted as a whole from that in the normal state at 20K. The full width at half maximum of the intensity, FWHM, is almost T-independent with a value of 1.7kOe. All the components of T_1 are also decreased rapidly below T_c as mentioned in **section 4-3**. These results show that most of the Cu sites in CuO_2 layer undergo a superconducting transition just below T_c, owing to the random distribution of Sr and La as seen in the distribution of T_1. This situation is seen over whole Sr content.

The principal axis of the electric field gradient at a Cu site is almost parallel to the crystal c-axis because of the dx^2-y^2 character of the wave function. In order to determine the quadrupolar and Knight shift separately, we took series of spectra at several different frequencies in the region of 95.1~125.1MHz. According to the second order perturbation theory, the resonance frequency, ω_o, for the central transition spectrum with $H \perp c$ is given by

$$\omega_o = (1+K)\ \gamma_N H_{res} + \frac{\nu_Q^2\ [I(I+1)-3/4]}{16(1+K)\ \gamma_N H_{res}} + \triangle'\omega\ , \qquad (4\text{-}8)$$

where the first term involves the Knight shift, the second term is the second order shift of the quadrupolar interaction, and the last term is the small correction from the higher order effects

of the quadrupole interaction. $\gamma_N/2\pi$ and nuclear spin, I, are 1.1285kHz/Oe and 3/2 for ^{63}Cu, respectively. $\Delta'\omega$ is a very small quantity ($\Delta'\omega/\omega_o < 2\times 10^{-4}$), because the applied field is very large as compared to ν_Q, therefore we can ignore the term of $\Delta'\omega/\omega_o$. Thus we expect a linear relation between $(\omega_o-\gamma_N H_{res})/(\gamma_N H_{res})$ and $(\gamma_N H_{res})^{-2}$ as

$$\frac{\omega_o-\gamma_N H_{res}}{\gamma_N H_{res}} = K + \frac{3\nu_Q^2}{16(1+K)(\gamma_N H_{res})^2}. \qquad (4\text{-}9)$$

This relation is confirmed experimentally as seen in **Fig.4-4-2**. Actually, the ν_Q's extracted from the slope of solid lines in the figure have 37.2(NQR=37), 35.9(36.4), 34.9(35.4) and 34.2(34.4)MHz for x=0.24, 0.20, 0.15 and 0.10, respectively, being almost consistent to the results of NQR experiments. The intercepts of these lines give the Knight shift.

Fig.4-4-3 shows the T-dependence of the Knight shift parallel to the c-axis, $K_{\parallel}$, for x=0.1(▼), 0.15(□), 0.20(▽) and 0.24(■) and perpendicular to the c-axis, $K_{\perp}$, for x=0.1(▲), 0.15(○), 0.20(△) and 0.24(●) of ^{63}Cu in $La_{2-x}Sr_xCuO_4$, respectively.[57] $K_{\parallel}$ is x- and T-independent with almost the same value of 1.2%, being almost the same value for $YBCO_7$,[12] dominated by the orbital Knight shift. This value is almost the same value for Tl(2201)[15] at low-T. In the normal state, $K_{\perp}$ reveals a weak T-dependence and is increased upon x as a whole, testifying the increase of the uniform susceptibility, χ_o, at the zone center, q=0. $K_{\perp}$ for whole x are markedly decreased below T_c. The Knight shift in the over doped region is enhanced largely with increasing x from 0.15 to 0.24 at low-T far below T_c. Since the orbital shift of $K_{\perp}$ has almost the same value over

whole x and the diamagnetic shift of $K_{\perp}$ is less than -0.03% at 4.2K in the magnetic field of 11T as shown from the proton NMR in $YBCO_7$,[52] a residual Knight shift is ascribed to the spin shift.

Fig.4-4-4 shows the nuclear magnetization, m(t), of ^{63}Cu under $c \perp H$ at 1.4 and 4.2K for x=0.24 and 0.20, plotted against the product of time, t, and temperature, T. m(t) falls on a curve within the experimental errors, which means that all the components of T_1 hold T_1T=const. as well as NQR results. Thus the behavior of T_1T=const. and the presence of a residual spin shift make an evidence that a finite density of state is left even in the superconducting state, which means that the system is in a gapless superconducting regime. The detailed analysis in the over doped region will be presented in **section 5-3**.

The full width at half maximum of the intensity, FWHM, of ^{63}Cu NMR is shown in **Fig.4-4-5**. The FWHM for x=0.10 increase at low-T in the superconducting state, also suggesting a localized nature of Cu d-spins at low-T in the lightly doped region as well as T_1=const. like behavior as shown in **section 4-3**. Here, ▲ (▼), ○ , △ (▽) and ● (■) represent the value of FWHM with $c \perp H$($c \parallel H$) for x=0.10, 0.15, 0.20 and 0.24, respectively.

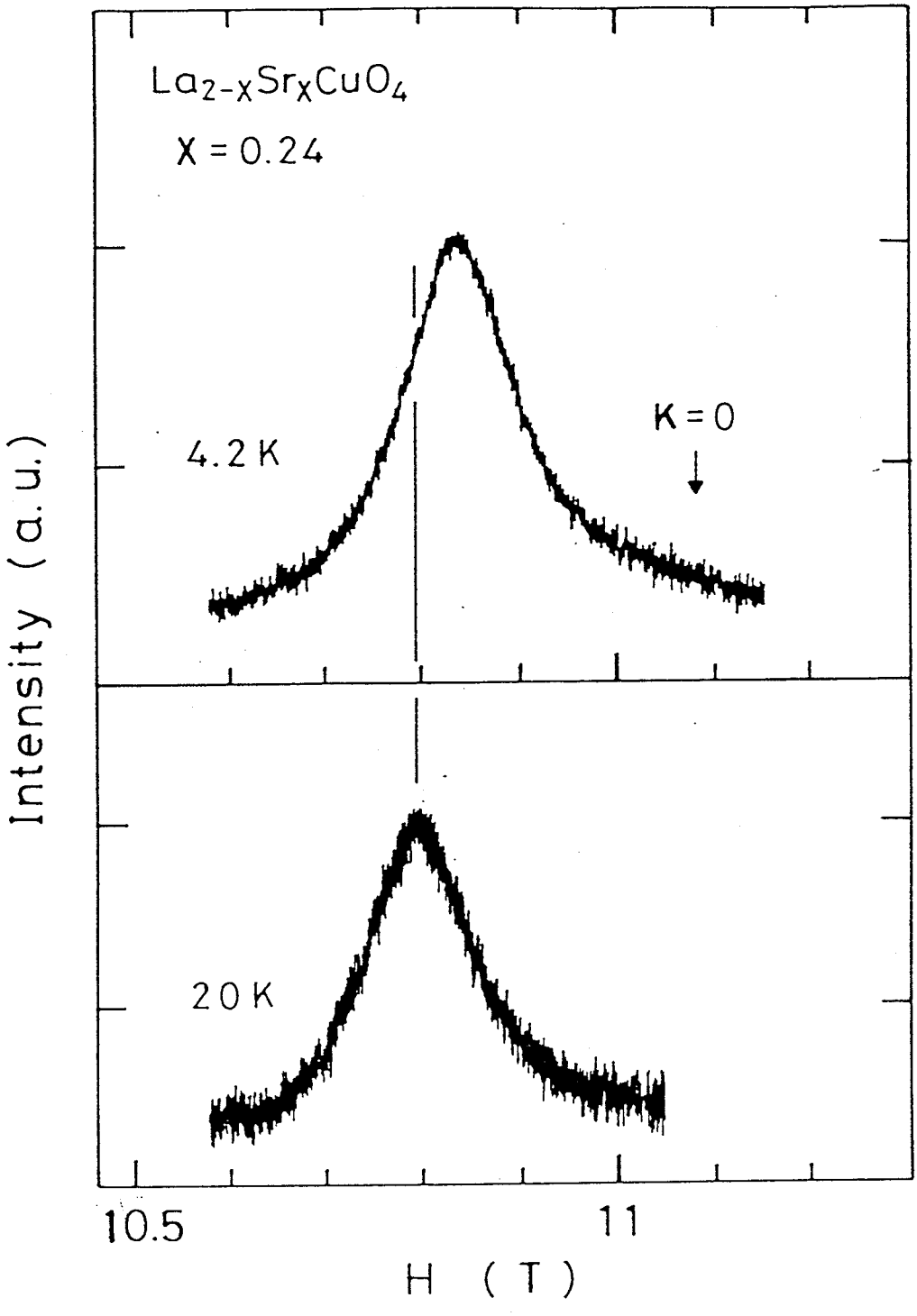

Fig.4-4-1.
The field swept ^{63}Cu NMR spectra for x=0.24 in $La_{2-x}Sr_xCuO_4$ with the external field perpendicular to the c-axis at 125.1MHz at 4.2 and 20K.[57] Here a repetition time between two pulses is 50msec.

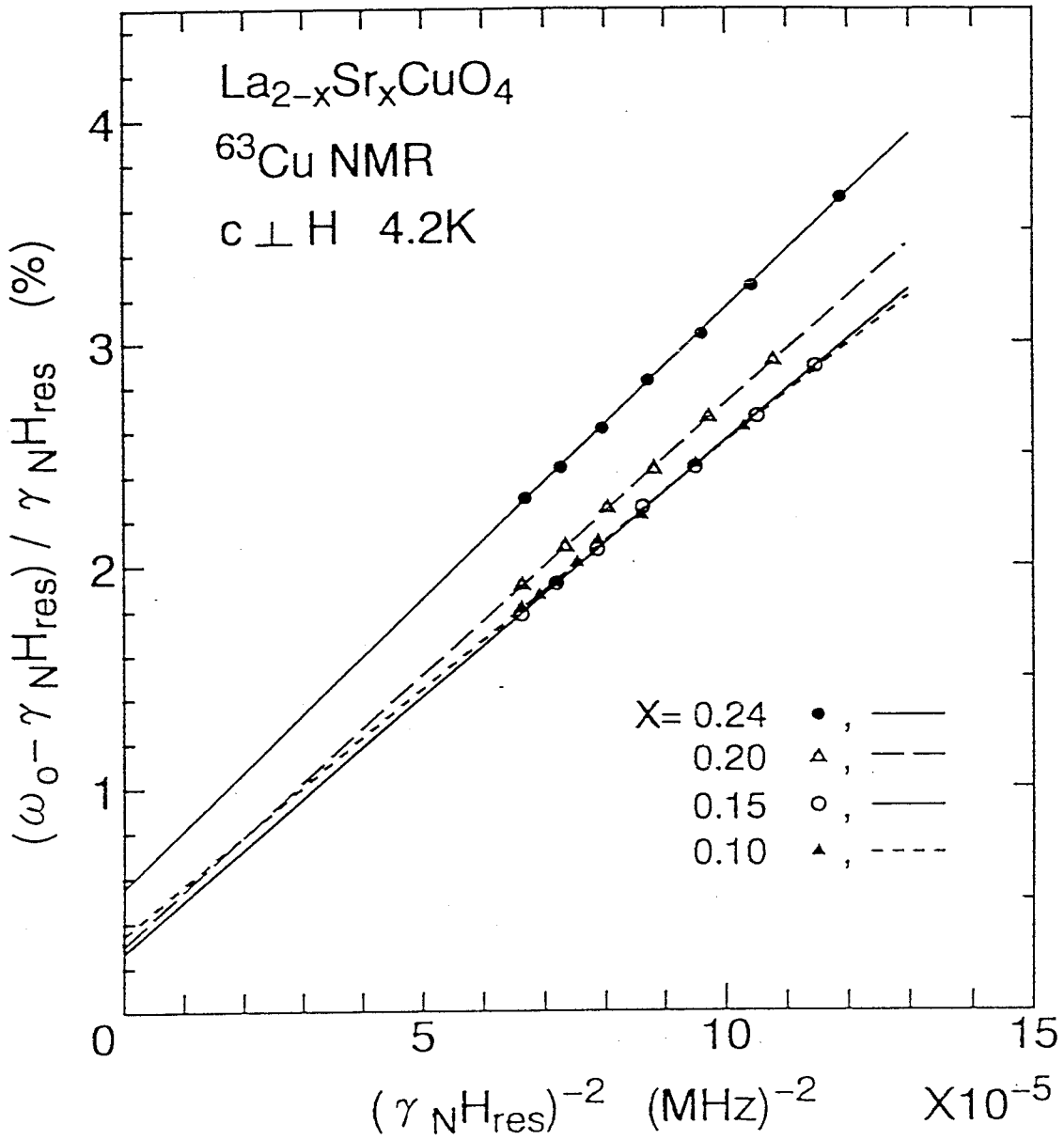

Fig.4-4-2.
(ω o-γ N Hres)/γ N Hres vs (γ N·Hres)$^{-2}$ plot in the Sr content region of x=0.10~ 0.24 in $La_{2-x}Sr_xCuO_4$.[57] From this figure, K and ν Q for each x are obtained.

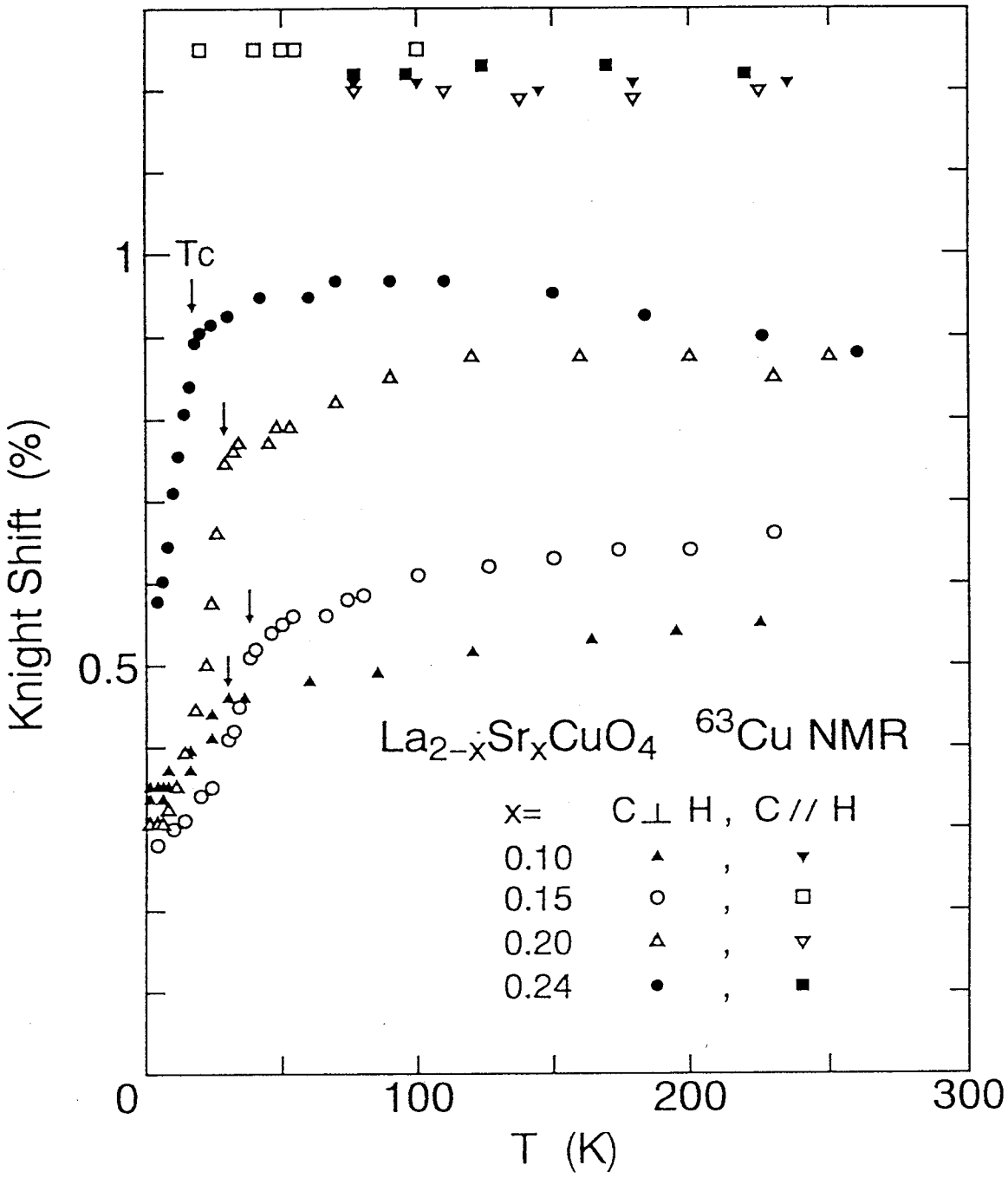

Fig.4-4-3.

T-dependence of Knight shift of ^{63}Cu in the Sr content region of x=0.10~ 0.24 in $La_{2-x}Sr_xCuO_4$.[57] Here ▼ , □ , ▽ and ■ represent the Knight shift parallel to the c-axis, $K_{\parallel}$. ▲ , ○ , △ and ● represent the Knight shift perpendicular to the c-axis, $K_{\perp}$.

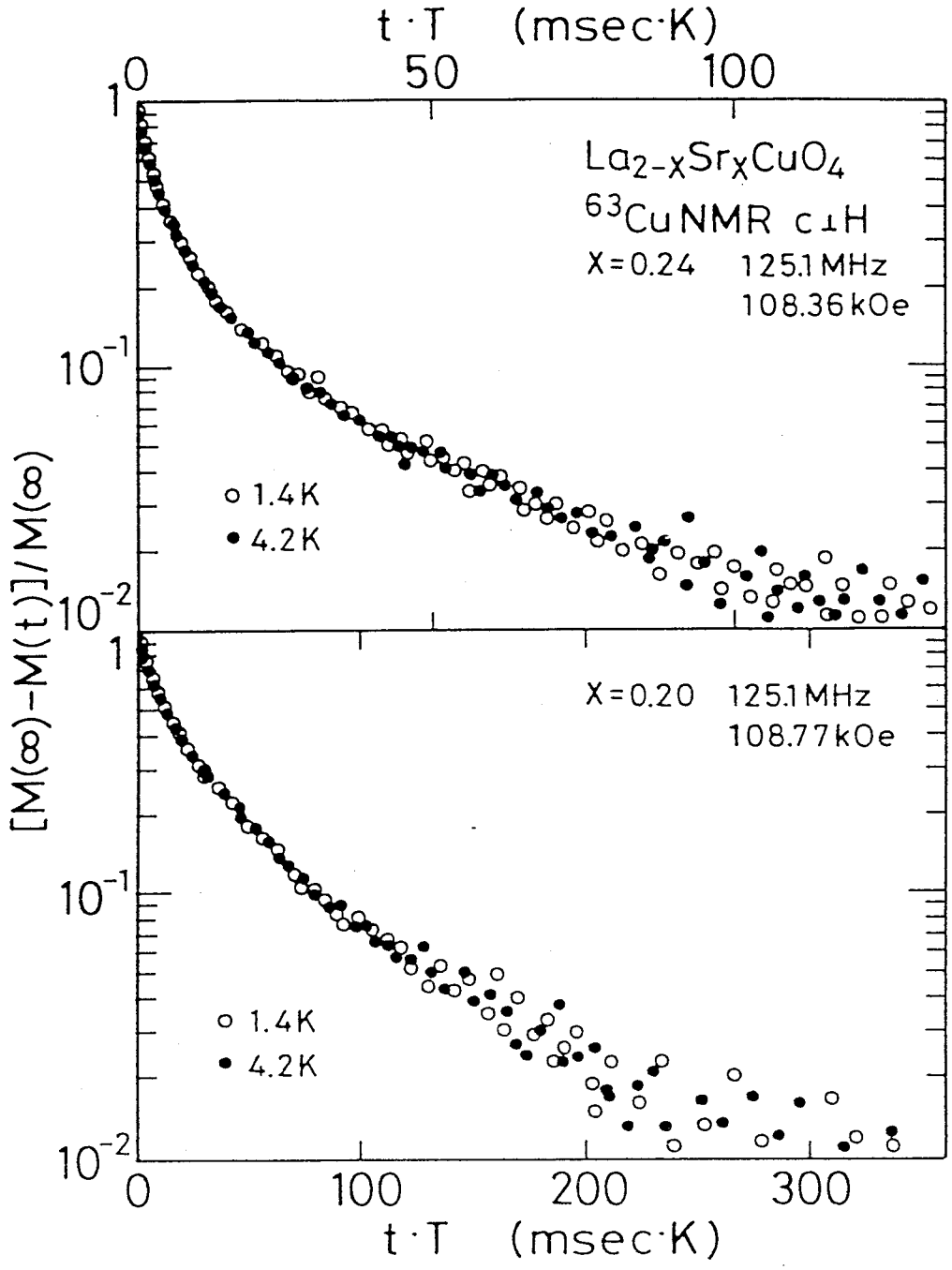

Fig.4-4-4.

Nuclear magnetization, m(t), of ^{63}Cu for x=0.24 and 0.20 with c⊥H at 1.4 and 4.2K, plotted against the product of time, t, and temperature, T. m(t) falls on a single curve within the experimental scattering. This indicates that all the components of T_1 hold T_1T=const. as well as NQR results.

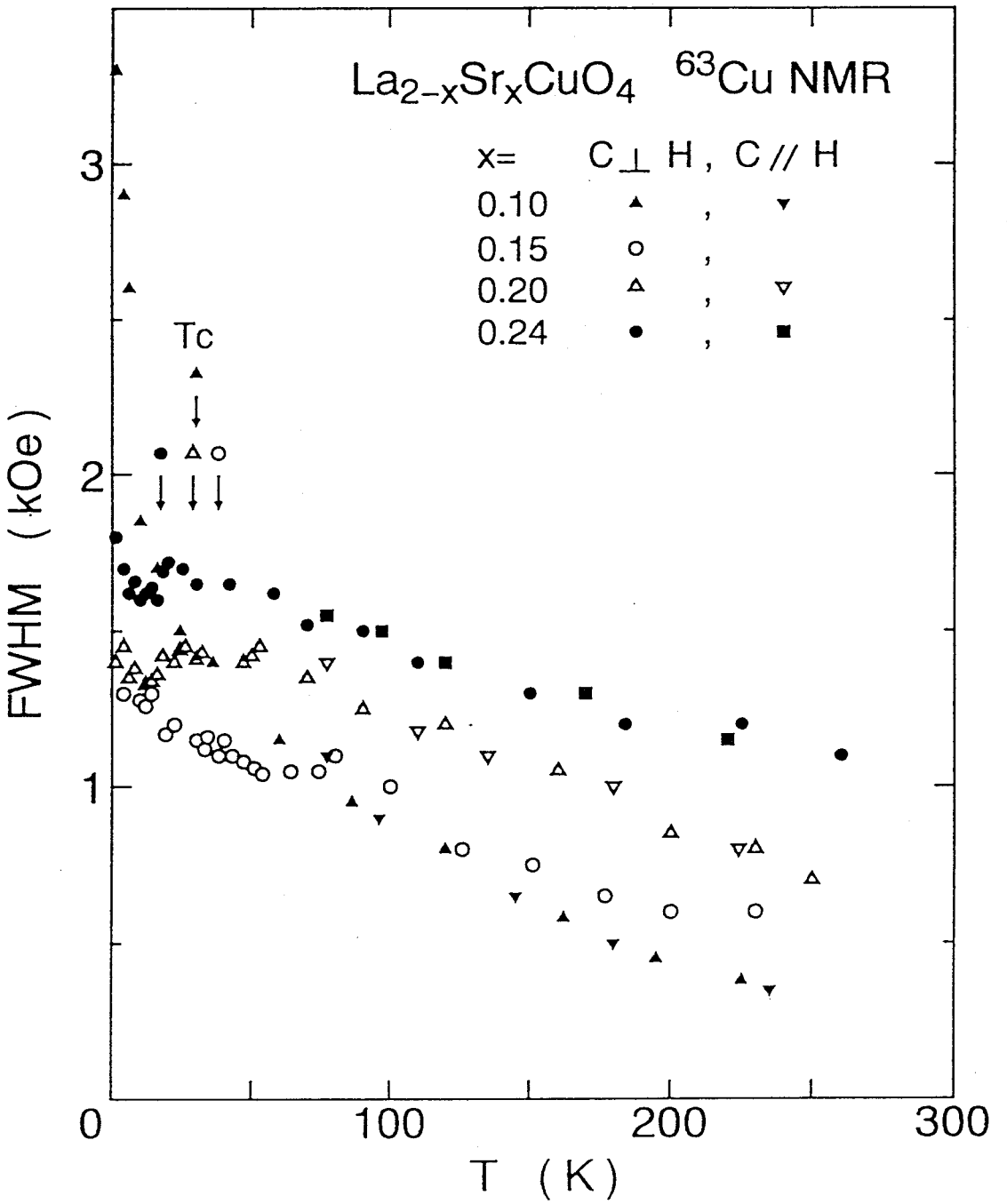

Fig.4-4-5.
Full width at half maximum of the intensity, FWHM, of ^{63}Cu NMR. ▲ (▼), ○, △ (▽) and ● (■) represent the value with c⊥H(c∥H) for x=0.10, 0.15, 0.20 and 0.24, respectively.

4-5. ^{205}Tl and ^{119}Sn NMR in Chevrel Phase Superconductors $TlMo_6Se_{7.5}$ and $Sn_{1.1}Mo_6Se_{7.5}$

T_1 of ^{119}Sn with a nuclear spin of 1/2 in $Sn_{1.1}Mo_6Se_{7.5}$ was precisely determined in the T-region of 1.3~ 12K from a single exponential behavior of

$$m(t) = [M(\infty)-M(t)]/M(\infty) = \exp(-t/T_1)$$

where M(t) is the nuclear magnetization at time, t, after the saturating pulses. In **Fig.4-5-1**, the T-dependence of $^{119}(1/T_1)$ at 9.8MHz(▲) in 6.1kOe in the normal state shows the Korringa law like behavior with T_1T=0.41secK, being almost the same value of T_1T=0.58secK reported by Matsumura et al[26),55)] In the superconducting state, $^{119}(1/T_1)$ shows the coherence peak just below T_c and decreases exponentially with further decreasing temperature from about 3K($0.8T_c$) down to 1.3K($0.37T_c$). Here T_c=3.5K is defined by a.c. susceptibility measurement in the magnetic field of 6.1kOe. Although we have not measured the magnetic field dependence of $^{119}(1/T_1)$, the coherence peak of $^{119}(1/T_1)$ is expected to increase with decreasing field.

The T-dependence of $1/T_1$ of ^{205}Tl with a nuclear spin of I=1/2 in $TlMo_6Se_{7.5}$ at 17MHz(●) and 8.7MHz(×) in 3.5kOe and 6.9kOe, respectively, are shown in **Fig.4-5-1**.[55)] $^{205}(1/T_1)$ also shows the Korringa law like behavior with $T_1T=2.94\times 10^{-3}$secK in the normal state. This value is the same as that reported by Nishihara et al[27)]. In the superconducting state, the prominent feature is that $^{205}(1/T_1)$ has no coherence peak just below T_c and decreases exponentially over four orders of magnitude from

10K($0.8T_c$) down to 2K($0.15T_c$) for the data at 8.7MHz(×) in 3.5kOe. Since the decrease of T_c in 6.9kOe was less than 0.2K from T_c=12.2K in zero magnetic field, we suppose $T_c(H)$ in $H \leqq$ 6.9kOe is nearly equal to T_c in zero field. No magnetic field dependence of $^{205}(1/T_1)$ was observed from 13.5K above T_c down to 2.5K. Thus the lack of the coherence peak of $^{205}(1/T_1)$ is not due to the magnetic field. When a nuclear magnetic relaxation is due to the interaction between a nuclear electric quadrupole moment and the electric field gradient produced by conduction electrons, the transition rate for scattering is time-reversal invariant. Therefore the second term in the coherence factor has a negative value, resulting in the depression of the coherence peak as seen for the $1/T_1$ of ^{181}Ta in Ta_3Sn measured by Wada and Asayama.[58] However ^{205}Tl has I=1/2, therefore it is not in this situation. Below around 2.5K, $^{205}(1/T_1)$ tends to saturate with increasing the field from 3.5 to 6.9KOe, accompanied by a deviation from a simple exponential decay of m(t). Thus the intrinsic relaxation behavior begins to be masked by the presence of the vortices in the mixed state at considerably low-T. This result of exponential decrease of $^{205}(1/T_1)$ is different from the result reported by Nishihara et al[27] that the T-dependence of $^{205}(1/T_1)$ obeys the power law like T-dependence of $T^{6.9}$.

It is considered that the exponential decrease of $^{119}(1/T_1)$ and $^{205}(1/T_1)$ below T_c is associated with the presence of the isotropic superconducting energy gap. So far, in **Fig.4-5-2**, $^{119}(T_1)$ and $^{205}(T_1)$ are plotted against $T_c(H)/T$.[55] $^{205}(T_1)$ and $^{119}(T_1)$ varies as $\exp(\Delta/k_BT)$, i.e. $T_1=\exp(\Delta/k_BT)$, with an isotropic energy gap(s-wave gap) of $2\Delta=4.5$ and $3.6k_BT_c$, respectively. Therefore even though the coherence peak is

depressed, the s-wave picture is evidenced by the exponential decrease of $1/T_1$ below T_c. Here the value of $2\triangle = 3.6k_BT_c$ of $^{119}(T_1)$ is almost the same as the value of $2\triangle = 3.5k_BT_c$ of the previous one reported by Matsumura et al[26] and is nearly equal to $2\triangle = 3.52k_BT_c$ for the weak coupling(BCS) SC. $2\triangle = 4.5k_BT_c$ of $^{205}(1/T_1)$ corresponds to the larger value as for the strong coupling SC. The detailed discussion will be presented in **section 5-1.**

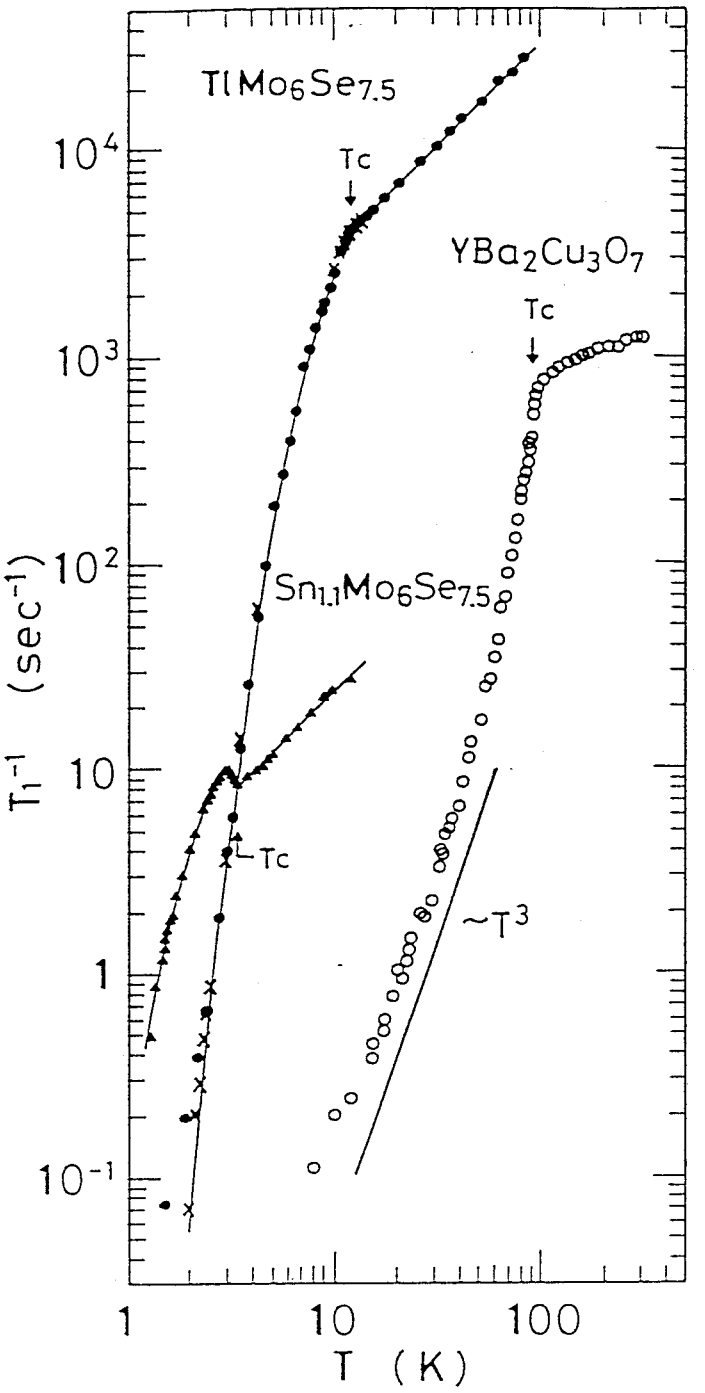

Fig.4-5-1.

T-dependence of $1/T_1$ of ^{205}Tl in $TlMo_6Se_{7.5}$ in the external field of H=3.5kOe(×) and 6.9kOe(●), that of ^{119}Sn in $Sn_{1.1}Mo_6Se_{7.5}$ in H=6.1kOe(▲) and that of ^{63}Cu in $YBa_2Cu_3O_7$(○)[63~ 66] in zero field.[55] Solid lines above and below T_c for $^{205}(1/T_1)$ data represent the Korringa law like behavior with $T_1T=2.94\times 10^{-3}$secK and the exponetial behavior of $\exp(-\Delta /k_BT)$ with $2\Delta =4.5k_BT_c$, respectively. And for $^{119}(1/T_1)$, those are $T_1T=0.41$secK and $2\Delta =3.6k_BT_c$.

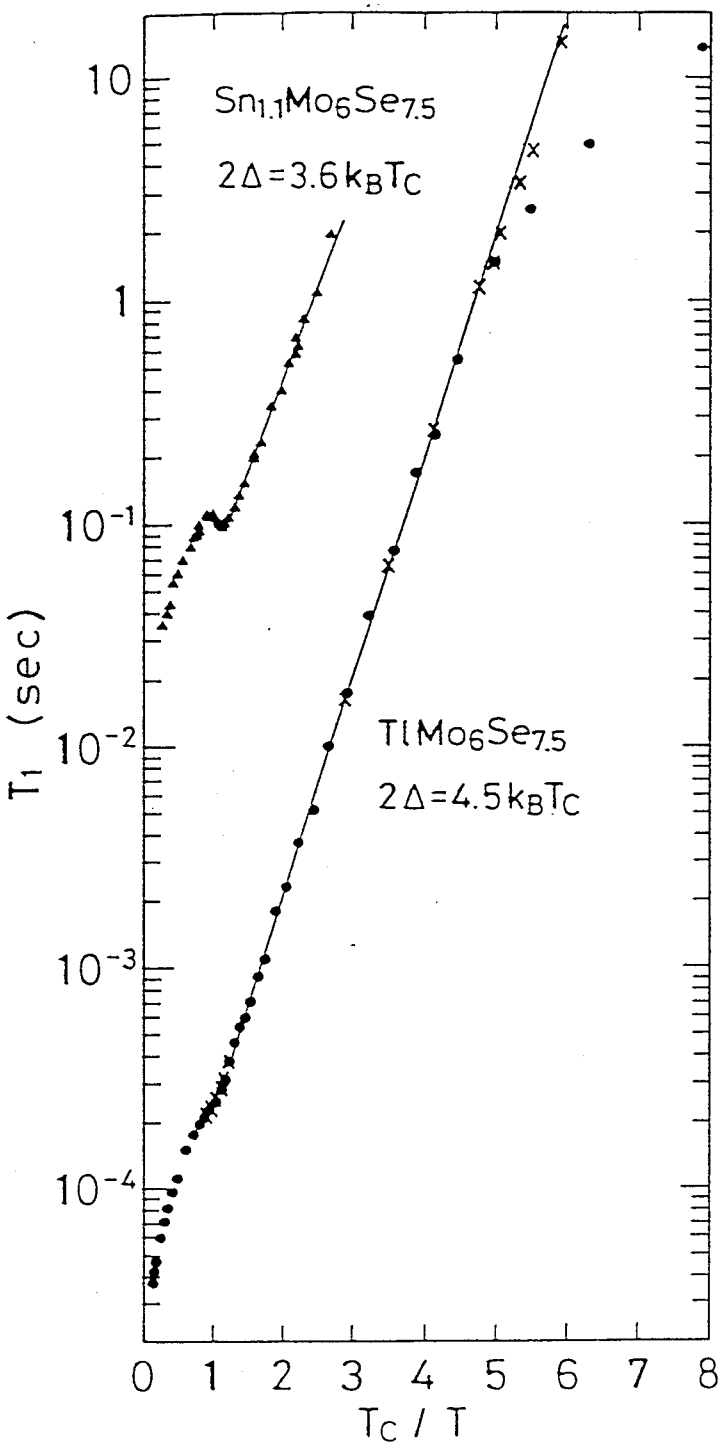

Fig.4-5-2.

T_1 versus T_c/T plot for $TlMo_6Se_{7.5}$(●) and $Sn_{1.1}Mo_6Se_{7.5}$(▲).[55] The solid line for $TlMo_6Se_{7.5}$ is a best fit to the form of $T_1=\exp[(\Delta/k_BT_c)(T_c/T)]$ with $2\Delta=4.5k_BT_c$, which is larger than $2\Delta=3.6k_BT_c$ for Sn compound. Note that the exponential behavior of T_1 in $TlMo_6Se_{7.5}$ is varied in a large T-region of $0.2T_c$(2.5K) and $0.8T_c$(10K) without the coherence peak just below T_c.

Chapter 5. Discussion

5-1. Comparison between High Temperature Superconductors and Chevrel Phase Superconductors

Allen and Rainer have shown that the numerical solution of the Eliashberg equations based on an s-wave model with a strong electron-phonon coupling, which is almost the same as that the quasiparticle life time effect pointed out by Dolgov et al[59] and Coffey[60], leading to suppress the coherence peak of $1/T_1$.[61] They tried to explain the behavior of $1/T_1$ of High-T_c cuprates SC by using this model. We plotted the T_1 data of $TlMo_6Se_{7.5}$(●) and $Sn_{1.1}Mo_6Se_{7.5}$(○) in **Fig.5-1-1** quoted from **Fig.2** in **ref.61**.[55] Here

$$(1/T_{1S}T)/(1/T_{1N}T) = T_{1N}/T_{1S}$$

is plotted against T/T_c. $1/T_{1N}T$ is the value in the normal state. The upper and lower curves are the calculations based on Eliashberg theory with the electron-phonon coupling constant λ = 1.66 and 3.2 estimated by using the hypothetical phonon spectrum of $\alpha^2F(\omega)$ and the Coulomb coupling constant μ^*=0.095 and 0.1, respectively. Accordingly, each value of λ used in the calculation should be not definitively taken as discussed in **ref.61**. In the figure, the coherence peak is depressed from the upper curve to down curve when λ is increased from 1.66 to 3.2, and at the same time, in this model, the energy gap as compared with the BCS value of $2\Delta = 3.52k_BT_c$ is enhanced with increasing λ . This similar behavior of $1/T_1$ is seen in those of Chevrel

phase compounds, thus it is considered that with increasing λ, the coherence peak is depressed from the $^{119}(T_{1N}/T_{1S})$ curve with $2\Delta = 3.6k_BT_c$ and $T_c = 3.5K$ to the $^{205}(T_{1N}/T_{1S})$ curve with $2\Delta = 4.5k_BT_c$ and $T_c = 12.2K$. On the other hand, (T_{1N}/T_{1S}) for ^{63}Cu NMR (□)[17] and ^{17}O NMR(×)[17] in the CuO_2 plane of $YBa_2Cu_3O_7$ seems to be close to the down curve with $\lambda = 3.2$ in the narrow region from $T/T_c = 0.9$(T=83K) to $T/T_c = 0.55$ (T=51K). However, the value of (T_{1N}/T_{1S}) measured by ^{63}Cu NQR(△) in **zero field** in $YBCO_7$ [63~66] is smaller than these values, and the strong reduction of $1/T_1$ just below T_c cannot be reproduced by the phonon-damping model even when compared carefully with the calculation with a strong coupling limit with $\lambda = 3.2$ as seen in **Fig.5-1-1**.

As an example, the T-dependence of $^{63}(1/T_1)$ of ^{63}Cu(○) in $YBa_2Cu_3O_7$ [63~66] in **zero field** is shown in **Fig.4-5-1** where the data down to 10K determined from a simple exponential decay of the nuclear magnetization, m(t), are presented. The behavior of rapid decrease of $1/T_1$ with no coherence peak is commonly shared in most of high-T_c materials as seen in **Fig.4-3-3**,[13] independent of the doping rate and the enhancement of the AF spin correlation causing the marked change of the normal state properties.[67,68] It is worth noting that $1/T_1$ of ^{17}O [17] also possesses a similar T-dependence to that of ^{63}Cu even though the AF spin correlation is filtered at oxygen site due to the geometrical cancellation.[17~19,47,62,69] $^{63}(1/T_1)$ in $YBa_2Cu_3O_7$ has a T^3 like T-dependence in the T-region between $\sim 0.16T_c$(15K) and $\sim 0.5T_c$(45K),[63~66] which is enough to argue whether or not an isotropic energy gap is present as seen in the result of $TlMo_6Se_{7.5}$(● and ×).[55] $1/T_1$ of Chevrel compounds shows the exponential decrease with decreasing temperature, even though the coherence peak of $1/T_1$ is

depressed due to the phonon damping effect smearing out the density of states near T_c. Thus this behavior is different from both of the rapid decrease of $^{63}(1/T_1)(\bigcirc)$ just below T_c and a T^3 like T-dependence in the T-region between $\sim 0.5T_c$ and $\sim 0.16T_c$ as seen in **Fig.4-5-1**.[55] The strong damping effect due to the electron-phonon coupling is indeed realized in the result of series of Chevrel phase SC, but cannot interpret the result in high-T_c cuprates even from a qualitative point of view. Thus it is considered that an anisotropic **d-wave model** with gap zeros of line at the Fermi surface as argued in heavy fermion SC,[70] which can also explain the impurity effect[71] at low-T and the results as mentioned in this thesis, is the most promising in interpreting the NMR results of High-T_c cuprates SC.

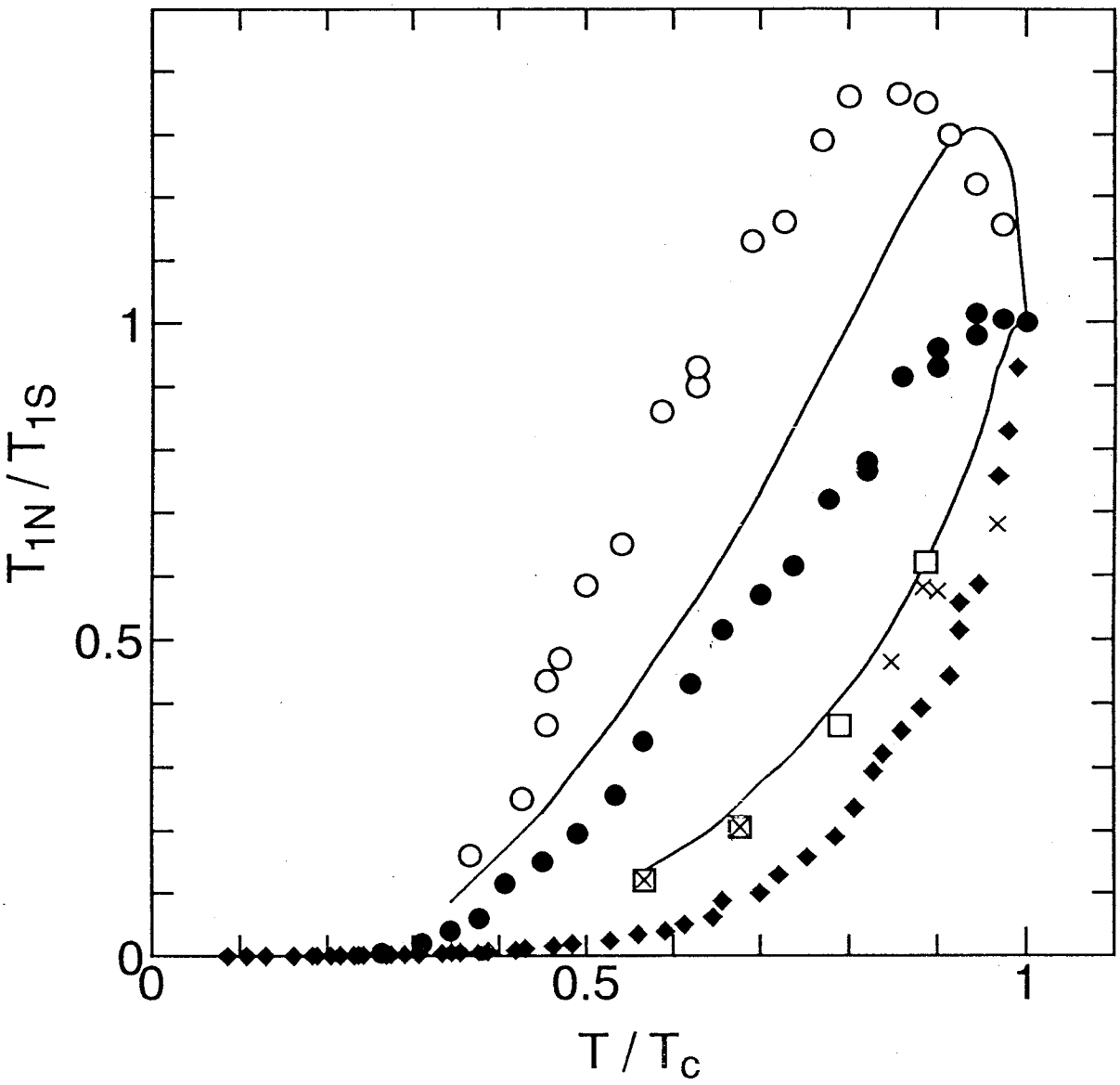

Fig.5-1-1.

Nuclear spin relaxation $(1/T_{1S}T)/(1/T_{1N}T) = T_{1N}/T_{1S}$ versus temperature T/T_c of ^{205}Tl in $TlMo_6Se_{7.5}$(●) and that of ^{119}Sn in $Sn_{1.1}Mo_6Se_{7.5}$(○) in a linear scale.[55] The upper and lower curves quoted from **Fig.2** in **ref.61** are the calculations based on Eliashberg theory with the electron-phonon coupling constant λ =1.66 and 3.2 estimated by using the hypothetical phonon spectrum of $\alpha^2F(\omega)$ and the Coulomb coupling constant μ^*=0.095 and 0.1, respectively. The marks of ◆, □ and × are the data of $1/T_1$ for ^{63}Cu NQR,[63~66] ^{63}Cu NMR[17] and ^{17}O NMR[17] in the CuO_2 plane of $YBa_2Cu_3O_7$, respectively.

5-2. Normal State in $La_{2-x}Sr_xCuO_4$

We measured T_1 of ^{63}Cu in the Sr content region of x=0.075~0.24 in $La_{2-x}Sr_xCuO_4$.[20,46,51,57] We have found that the relaxation rate, $1/T_1$, is markedly enhanced over a wide T-region above T_c with decreasing Sr content. This testifies the increase of χ_Q with decreasing x. $(T_1T)^{-1}$ follows a characteristic T-dependence of $C/(T+\theta)$ associated with the Curie-Weiss law of $\chi_Q(T)$ above θ K and then approaches a constant value in a narrow T-region above T_c. The remarkable feature is that the Weiss temperature, θ, is reduced from 120K to 20K with the decrease of the Sr content from x=0.24 to 0.075, being almost zero near the magnetic phase boundary around x=0.05. There is a notable interrelation between T_c and θ, namely both decrease with decreasing Sr content, with T_c=0K at θ=0K.

The Cu relaxation result is well interpreted by the SCR theory of spin fluctuations in a nearly AF two dimensional metal.[48] So far, there have been lots of theoretical approaches from the strong correlation limit as a possible model for HTSC such as the t-J model.[49] In contrast to these, it should be noted that the SCR theory is an approach from a weak correlation limit.

Recently, Kohno and Yamada derived rigorous expressions for the specific heat, spin susceptibility, the nuclear spin-lattice relaxation time, T_1, and T^2 term of electrical resistivity by a microscopic treatment consisting of d- and p-electrons based on a Fermi liquid picture.[50] Assuming large AF spin fluctuations and using our experimental finding that $(T_1T)^{-1}$ follows the Curie-Weiss law of $C/(T+\theta)$, they derived an expression of the

resistivity as

$$R \sim \chi_Q(T)\, T^2 \sim T^2/(T + \theta). \qquad (5\text{-}1)$$

From this result, we see that the resistivity is proportional to T^2 with the coefficient enhanced by the $\chi_Q(T)$ at low-T far below θ and approaches **T-linear** like T-dependence at high-T far above θ. This appears to be the simplest interpretation for T-linear resistivity. For LSCO, since θ is almost comparable to T_c in the lightly doped region, it is expected that T-linear resistivity is observed in the wide T-region above T_c, which is in accord with the experiment. The experimental results such as the T-dependence of $1/T_1$ and the resistivity, which were considered to be unconventional, are well understood from the approaches based on the Fermi liquid picture in which the large AF spin fluctuations is taken into consideration.

In the normal state, the Knight shift perpendicular to the c-axis, $K_\perp$, reveals a weak T-dependence and is increased with increasing x as a whole.[57] The enhancement of $K_\perp$ upon x at low-T above T_c testifies the increase of the uniform susceptibility, χ_o, due to the decrease of χ_Q upon x as shown for $1/T_1$. Recently, Oda et al have implied that d.c.χ for LSCO cosists of the T-independent term, χ_o, the spin susceptibility of Cu, χ_{spin}, and Curie term increased with increasing x appearing above x=0.18, C/T, as shown for LBCO in **Fig.5-2-1.**[76] This T-dependence of χ_{spin} extracted from the measured susceptibility is similar to the T-dependence of $K_\perp$. They have considered that the Curie term comes from the localized Cu atoms, which destroys superconductivity. However, for $K_\perp$, the remarkable increase of

the width of NMR spectrum at low-T due to the Curie term is not seen in the over doped region. Thus we consider that the causes of decrease of T_c is not due to the localized Cu atoms arising the Curie term.

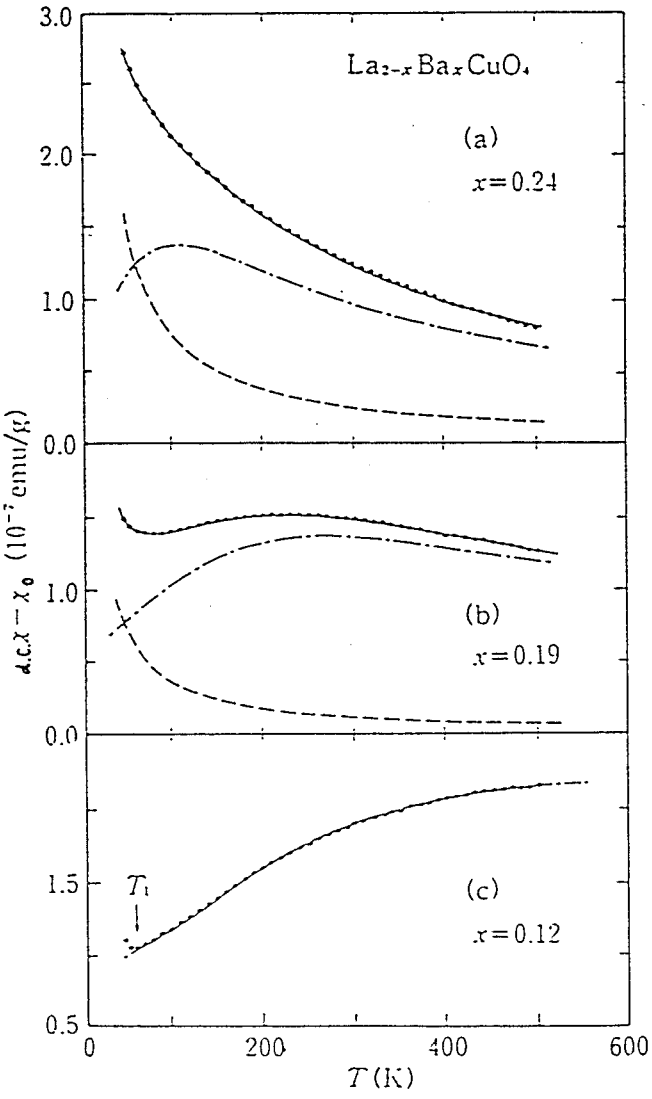

Fig.5-2-1.
T-dependence of d.c.χ for $La_{2-x}Ba_xCuO_4$.[76] The spin susceptibility of Cu, χ spin, (dash-dotted line) is obtained by a subtraction from d.c.χ (solid line) of the T-independent term, χ_0, and Curie term, C/T, (broken line).

5-3. Superconducting State in $La_{2-x}Sr_xCuO_4$

In the superconducting state, $1/T_1$ of Cu in LSCO reveals a rapid decrease down to $0.8T_c$ without an enhancement just below T_c, being independent of Sr content and Weiss temperature, θ .[20,46,57] The rapid reduction of $1/T_1$ below T_c is known to be independent of the strength of the external field, the number of CuO_2 plane and the atomic site, Cu,[13] O[17] and Y[16] in several high-T_c materials. In contrary to this, $1/T_1$ at low-T exhibits a different behavior in case by case. So far, the Knight shift perpendicular to the c-axis, $K_\perp$, is reduced below T_c in whole x-region as well as the results of $1/T_1$, verifying the presence of superconducting phases with an intermediate T_c lower than the maximum T_c of 38K from a microscopic point of view.[57]

We show below that both of the T-dependence of T_1 and Knight shift below T_c for x=0.24 and 0.20 in the over doped region can be interpreted by an application of a gapless d-wave model.[57] The steep decrease just below T_c and the power-law like T-dependence at low-T of $1/T_1$ in HTSC cannot be interpreted by an s-wave model, whatever the quasiparticle damping is taken into account, as mentioned in **section 5-1**. Since $1/T_1$ of Cu in LSCO is decreased rapidly without enhancement just below T_c, and a T_1T=const. relation and a residual spin Knight shift are seen at low-T far below T_c in the over doped region, we consider that a d-wave model is valid for understanding the T-dependence. The s-wave model with considerably large value of the residual density of states as seen for x=0.24(T_c=18K) at low-T leads to T_c of almost 0K.

We used the model argued in Zn-doped $YBa_2Cu_3O_7$ [72] for the

T-dependence of Knight shift and T_1, in which the gap zeros of lines at the Fermi surface originating from d-wave pairing and the residual density of states at the Fermi level associated with a pair breaking effect are taken into account. Actually, in order to interpret the physical quantities at low-T in heavy fermion superconductors(HFSC), this type of treatement by non-magnetic impurity was first made by Schmitt-Rink, Miyake and Varma[71] and Hirschfeld et al[73] in terms of the unitarity limit. We adopt here density of states based on a d-wave model with a gap function of approximately polar state, $C(\theta, \phi) = \Delta \cos\theta$, for simplicity as shown in **Fig.5-3-1**.[72] The functional forms are given by

$$N_S(E) = (\pi\, rN_O)/2 = N_{res} \qquad (E<r\Delta),$$

$$N_S(E) = (\pi\, N_O E)/(2\Delta) \qquad (r\Delta<E<\Delta), \qquad (5\text{-}2)$$

$$N_S(E) = (N_O E/\Delta)\, \sin^{-1}(\Delta/E) \qquad (\Delta<E),$$

where $r=(2N_{res})/(\pi\, N_O)$. Here, the extent of the gapless is introduced only by a parameter, N_{res}. We try to interpret the results of K and T_1 of Cu in the over doped region of LSCO by use of this model.

Fig.5-3-2 shows the T-dependence of K_S/K_{Tc} for x=0.24(●) and 0.20(○) plotted against T/T_c where the spin part of $K_\perp$, K_S, estimated by assuming the orbital part of $K_\perp$, K_{orb}=0.24%, is normalized by the value at.T_c. The solid lines are the calculation with $2\Delta = 4.5k_BT_c$ and r=0.32 (N_{res}/N_O=0.5) for x=0.24, and with $2\Delta = 8k_BT_c$ and r=0.083 (N_{res}/N_O=0.13) for x=0.20,

respectively. Here the assumption of K_{orb}=0.24% in LSCO is supported by the facts that the Knight shift parallel to the c-axis, $K_{||}$, for $YBCO_7$ [12] and LSCO in whole Sr content region is almost T-independent with the same value of about 1.2%, dominated by the orbital susceptibility. $K_{||}$ for Tl(2201)[15] at low-T has the same value of 1.2% as seen in **Fig.1-1-10**. In addition, the residual shift of $K_{\perp}$ dominated by the orbital susceptibility at low-T for $YBCO_7$ [12] and Tl(2201)[15] have the same value of 0.24%. As seen in **Fig.5-3-2**, K_S/K_{Tc} for x=0.24 and 0.20 are well fitted by the lines with N_{res}/N_O=0.5 and 0.13 and 2Δ =4.5 and $8k_BT_c$, respectively. If the Knight shift can be interpreted by the gapless d-wave model, the results of T_1 should also be fitted by use of the same parameters as those for the Knight shift. Then we have tried to calculate T_1.

The normalized $1/T_1T$ by the value at T_c, i.e.

$$R/R_{Tc} = (1/T_1T) / (1/T_1T)_{Tc} ,$$

of ^{63}Cu for x=0.24 is plotted against T/T_c in **Fig.5-3-3**. Here ▲ (△), ● (○) and ▼ (▽) represent T_{1s}, T_1 and T_{1L} for set A (set B) as mentioned in **section 4-1**, respectively. As seen in **Fig.5-3-3**, $1/T_1$ of Cu for two different sets is interpreted by the same gapless d-wave parameters as those for the Knight shift, and the Cu site for set B with tetragonal like structure is in the superconducting state. In addition, the value of $1/T_1$ of Cu for set B is almost 1/2 times smaller than that for set A in the normal state for x=0.24, testifying to the suppression of χ_Q for the Cu Site with tetragonal like structure.

Fig.5-3-4 shows the normalized $1/T_1T$ by the value at T_c,

$R/R_{Tc}=(1/T_1T)/(1/T_1T)_{Tc}$, of ^{63}Cu for x=0.20 is plotted against T/T_c. Here △ , □ and ▽ represent T_{1S}, T_1 and T_{1L} for set A as mentioned in **section 4-1**, respectively. The solid lines are the calculation by use of the same parameters as those of the Knight shift for x=0.20 as shown in **Fig.5-3-2**. We consider that T_1 for x=0.20 is also well interpreted by this model as well as for x=0.24, although there exists an experimental error for both of T_1 and Knight shift measurements.

Fig.5-3-5 shows N_{res}/N_o(○) and Tc(●) plotted against Sr content, x. In the over doped region, T_c is decreased upon N_{res}/N_o. As seen in **Fig.5-3-6**, the tendency of decreasing of T_c/T_{co} upon N_{res}/N_o in the over doped region of LSCO(●) is almost the same as calculation based on the non-magnetic impurity scattering in the unitarity limit by Schmitt-Rink, Miyake and Varma,[74] having not rapid reduction upon increasing N_{res}/N_o. Here, ● , ○ represent the data for the LSCO in the over doped region and the Zn-doped $YBCO_7$, [72] respectively. Here T_{co} for LSCO and $YBCO_7$ are assumed as T_{co}=38 and 92K, respectively.

On the other hand, recently, Takagi et al[75] have claimed that the superconductivity disappears in the over doped region associated with an orthorhombic to tetragonal structural phase transition near x=0.2 and the bulk superconducting phase is confined to a much narrower composition region than believed[6,7]. However, it is not settled whether or not the orthorhombic and tetragonal phases in over doped region exhibit superconductivity with lower-T_c as reported in the earlier works.[5,7] Our NMR and NQR results have supported.both phases(orthorhombic and tetragonal) are superconducting from a microscopic point of view. We have considered that the origin of the gapless

superconductivity is due to the pair breaking occurred by the structural instability from the orthorhombic to tetragonal upon hole doping, and T_c is decreased by the pair braking effect and the suppression of AF spin fluctuations in the over doped region.

On the other hand, in the lightly doped region, $1/T_1$ for Cu NQR follows T_1=const. relation, caused by a localized nature of Cu d-spins at low-T.[20,46,57] On the results of the full width at half maximum of the intensity, FWHM, for ^{63}Cu NMR as shown in **section 4-4-6**, the FWHM for x=0.10 has almost twice value of those for another x at low-T in the superconducting state, also suggesting the exsistence of a localized nature. So far, $(T_1T)^{-1}$ in the normal state follows a characteristic T-dependence of $C/(T+\theta)$ associated with the Curie-Weiss law of the staggered susceptibility, $\chi_Q(T)$, at the zone boundary, $Q=(\pi/a, \pi/a)$ due to the development of AF spin correlation.[20,46,51] The Weiss temperature, θ, decreases linearly with decreasing Sr content. The Sr content extrapolated to θ =0K corresponds just to x=0.05 that is the boundary between the superconductivity and the static magnetic ordering.[20,46,51] The results as mentioned above implies that the AF spin fluctuations at considerably low frequency, i. e. $\omega \sim 0$, is increased with decreased hole content near the magnetic phase boundary. Thus we consider that T_c is decreased in the lightly doped region with decreasing hole content and its mobility.

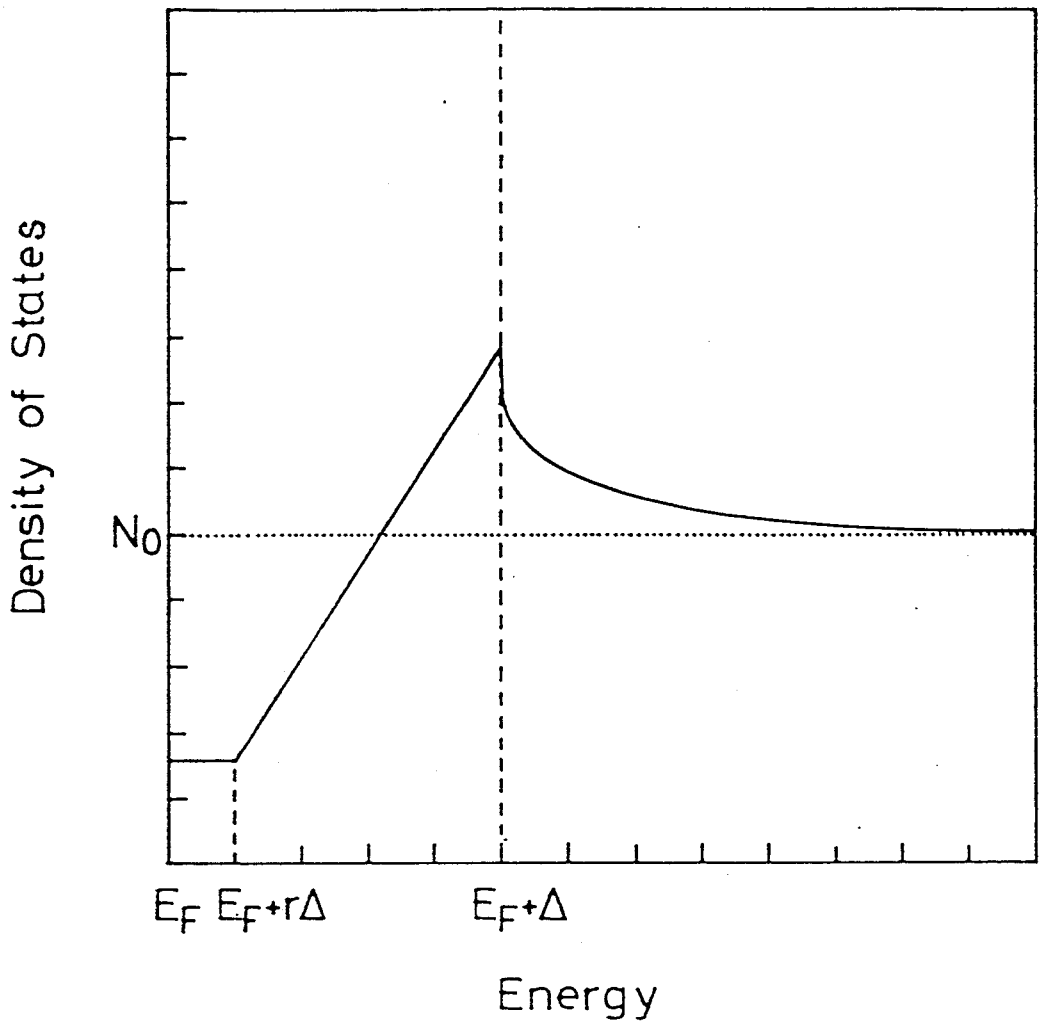

Fig.5-3-1.
Model density of states in which the gap zeros of lines at the Fermi surface originating from d-wave pairing and the residual density of states at the Fermi level associated with a pair breaking effect are taken into account.[72] The functional forms are given by

$$N_S(E) = (\pi\, rN_0)/2 = N_{res} \qquad (E<r\Delta),$$
$$N_S(E) = (\pi\, N_0 E)/(2\Delta) \qquad (r\Delta<E<\Delta),$$
$$N_S(E) = (N_0 E/\Delta)\, \sin^{-1}(\Delta/E) \qquad (\Delta<E),$$

where $r=(2N_{res})/(\pi\, N_0)$.

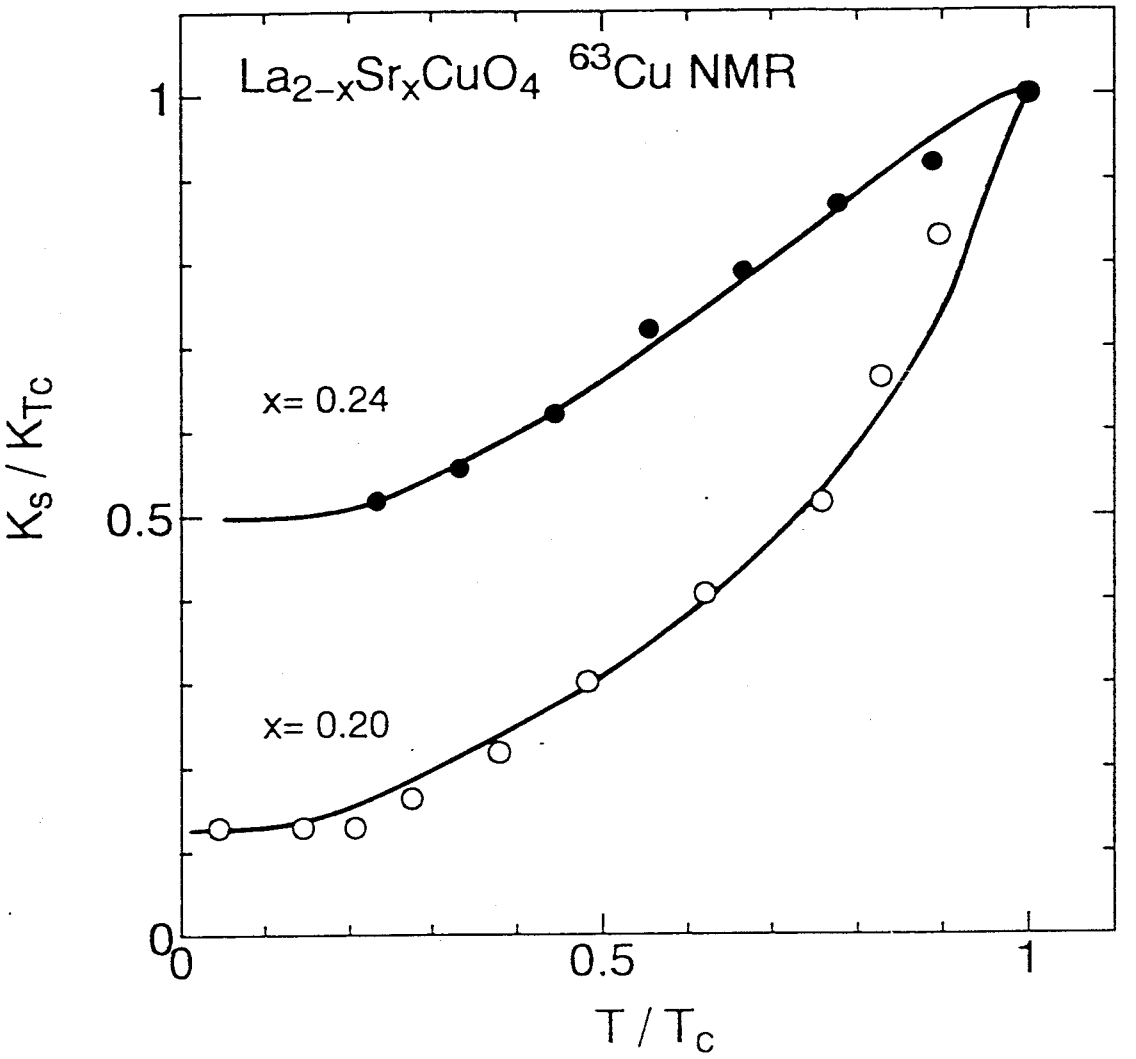

Fig.5-3-2.
T-dependence of K_S/K_{Tc} for x=0.24(●) and 0.20(○) plotted against T/T_c. The spin part of $K_\perp$, K_S, estimated by assuming the orbital part of $K_\perp$, K_{orb}, with 0.24%. K_{Tc} is the value at T_c. The solid lines are the calculation with $2\Delta = 4.5k_BT_c$ and $r=0.32(N_{res}/N_O=0.5)$ for x=0.24, and with $2\Delta = 8k_BT_c$ and $r=0.083(N_{res}/N_O=0.13)$ for x=0.20, respectively.

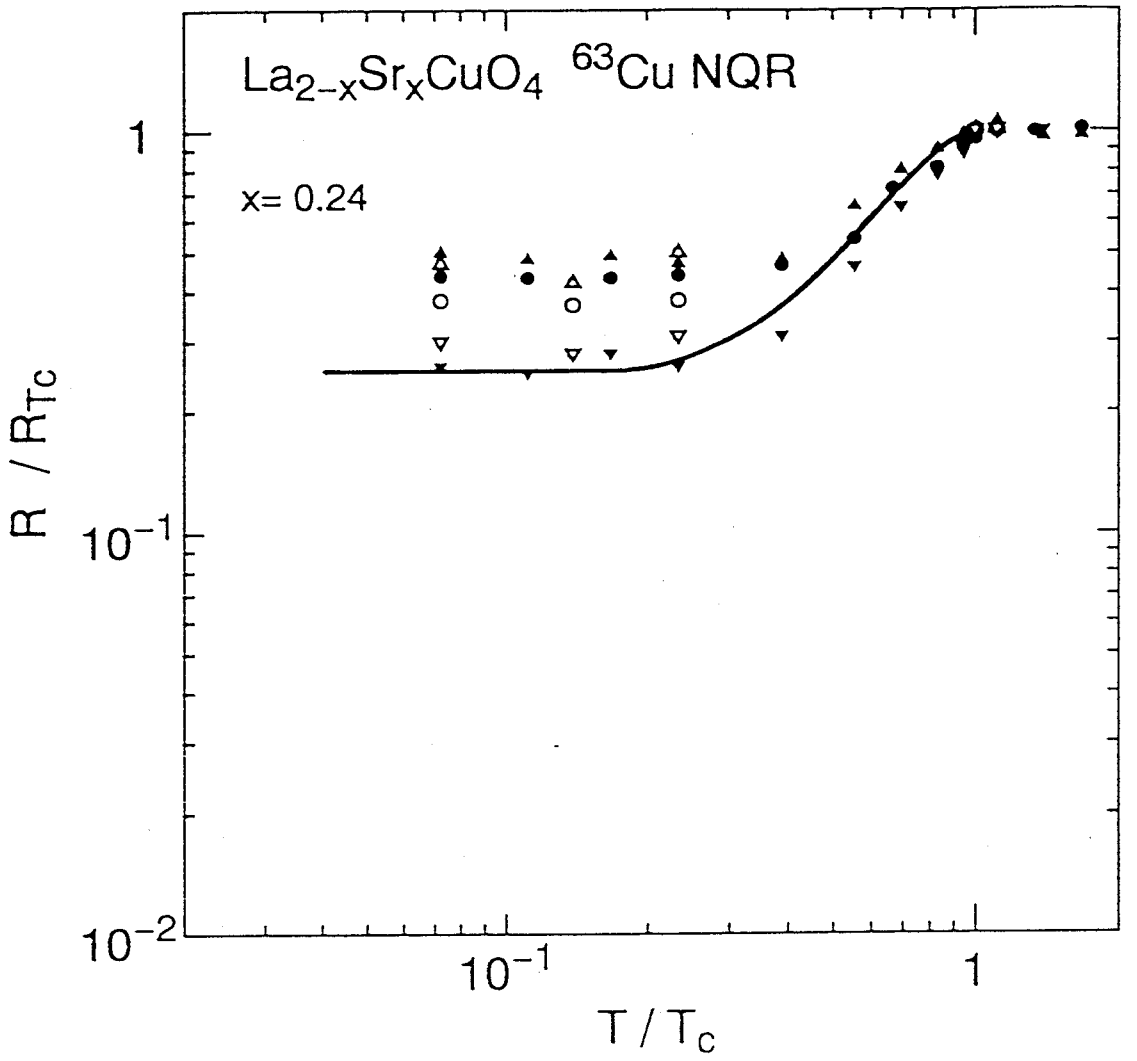

Fig.5-3-3.
Normalized $1/T_1T$ by the value at T_c, $R/R_{Tc}=(1/T_1T)/(1/T_1T)_{Tc}$, of ^{63}Cu for x=0.24, is plotted agaist T/T_c. Here ▲ (△), ● (○) and ▼ (▽) represent T_{1S}, T_1 and T_{1L} for set A(set B) as mentioned in section 4-1, respectively. The solid lines are the calculation with the same parameters as those for the Knight shift in Fig.5-3-2.

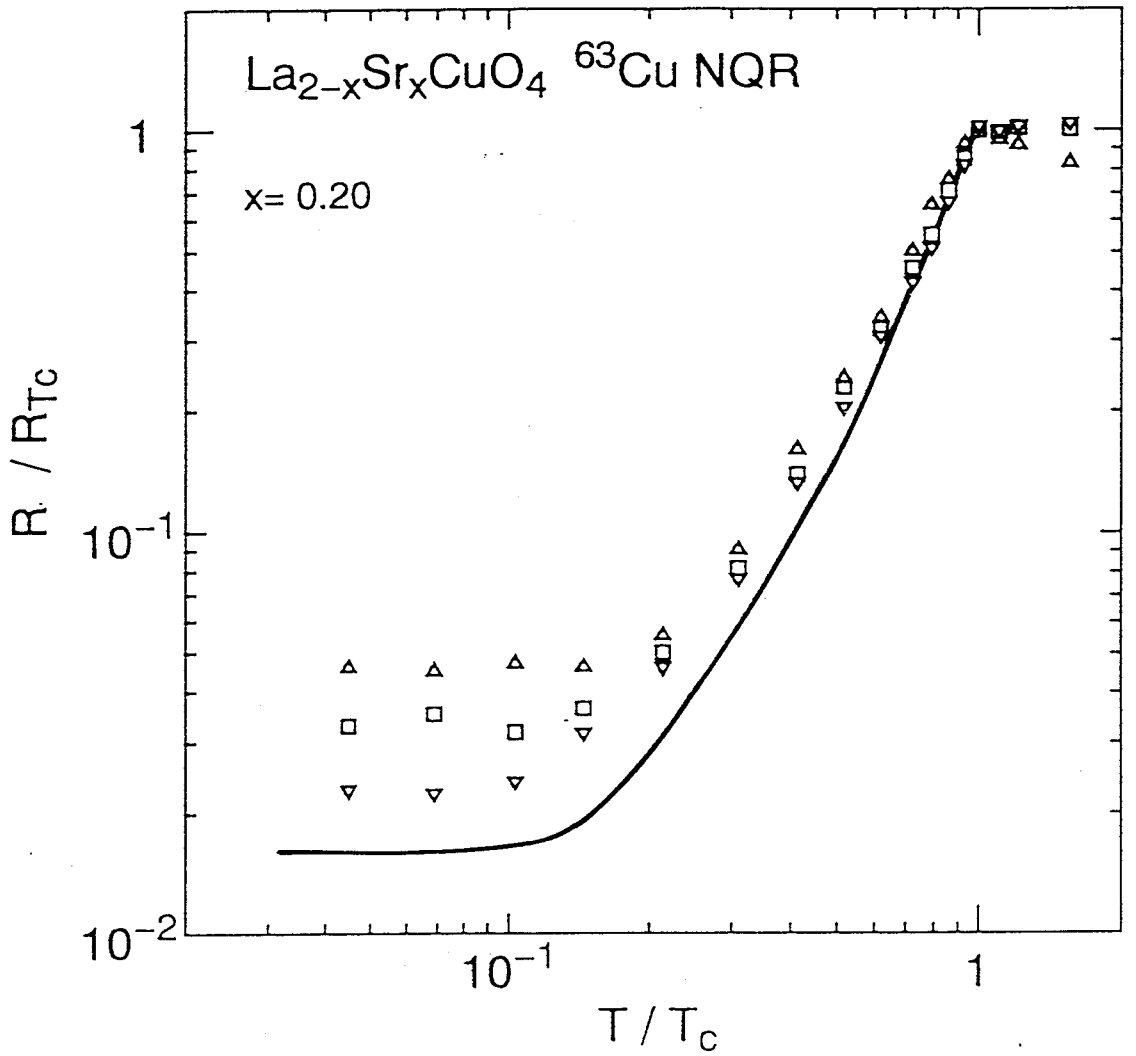

Fig.5-3-4.
Normalized $1/T_1T$ by the value at T_c, $R/R_{Tc}=(1/T_1T)/(1/T_1T)_{Tc}$, of ^{63}Cu for x=0.20 is plotted against T/T_c. Here △, □ and ▽ represent T_{1S}, T_1 and T_{1L}, respectively. The solid lines are the calculation with the same parameters as those for the Knight shift for x=0.20 as shown in **Fig.5-3-2.**

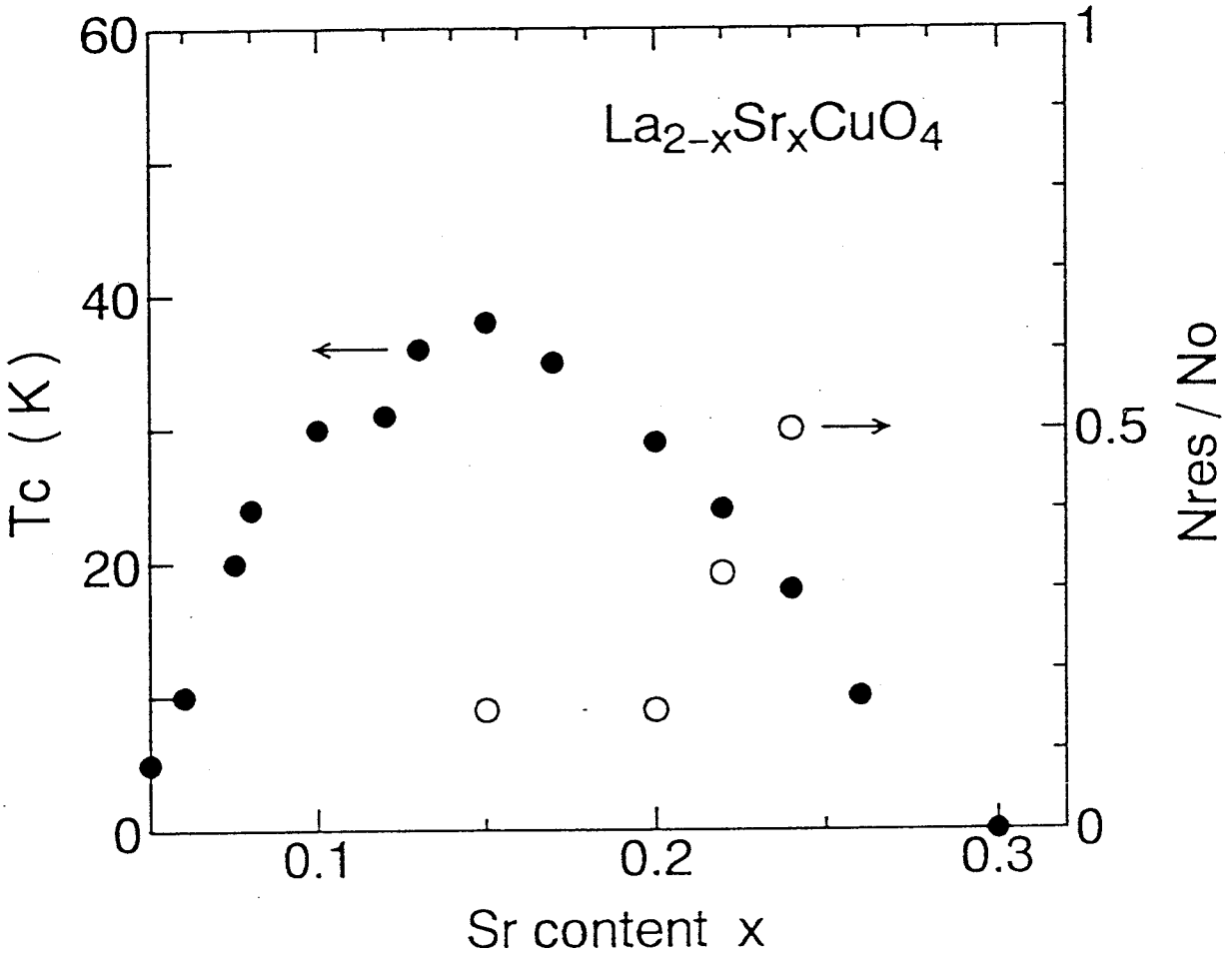

Fig.5-3-5.
N_{res}/N_o(○) and Tc(●) for LSCO plotted against Sr content, x.

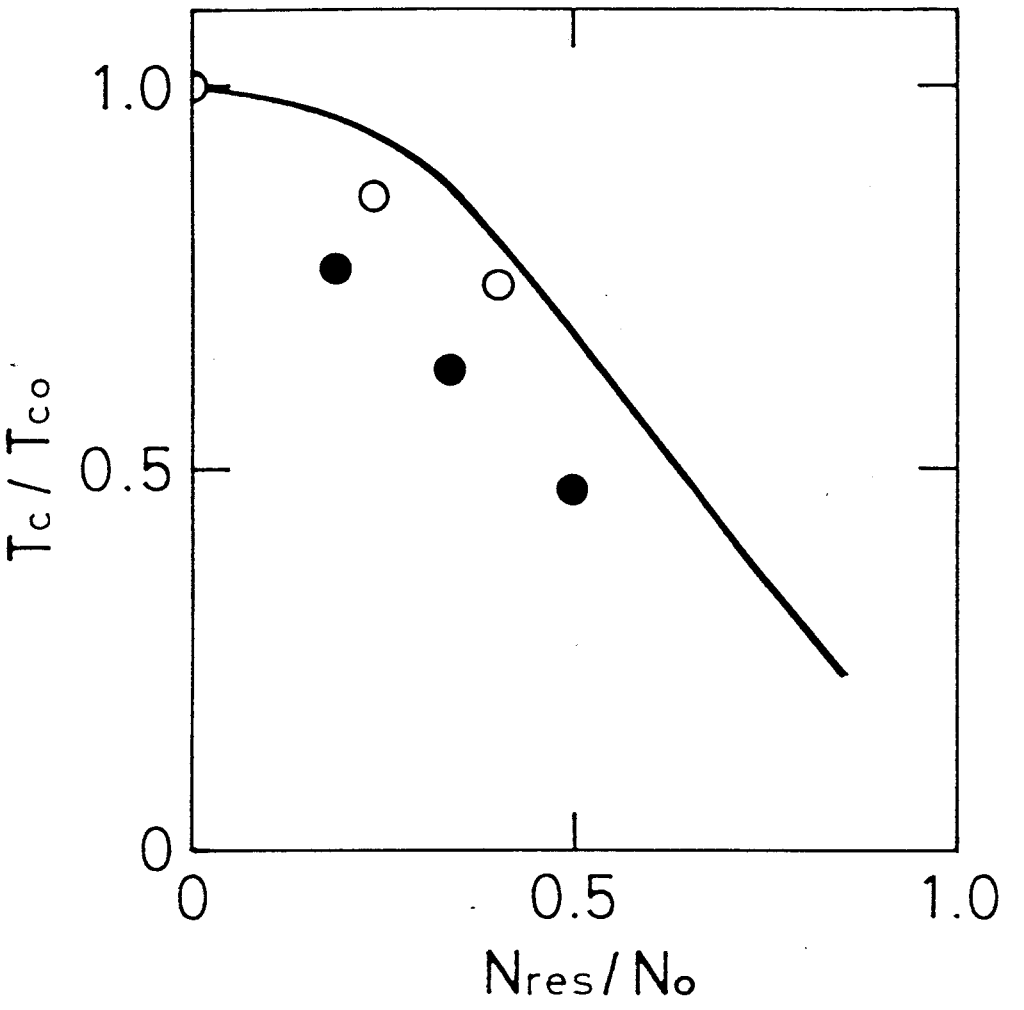

Fig.5-3-6.

T_C/T_{CO} vs N_{res}/N_O plot. Here, ● , ○ represent the data for LSCO in the over doped region and the Zn-doped $YBCO_7$,[72] respectively. T_{CO} for LSCO and $YBCO_7$ are assumed as T_{CO}=38 and 92K, respectively. The solid line is the calculation based on the non-mgnetic impurity scattering in the unitarity limit by Schmitt-Rink, Miyake and Varma.[74]

Chapter 6. Summary

The spin dynamics and the static magnetic properties of $La_{2-x}Sr_xCuO_4$ were systematically investigated by measuring T_1 and Knight shift.

There has been seemingly a doubt that the bulk superconductivity in $La_{2-x}Sr_xCuO_4$ exists in the narrower Sr content region than believed. A systematic NMR study has, however, assured that there exist the superconducting phases with T_c lower than the maximum T_c of 38K in the lightly and over doped region. A steep decrease of $1/T_1$ is seen just below T_c, in addition, a rapid decrease of the spin Knight shift below T_c is clearly deduced from the uniform shift of the NMR spectrum as a whole.

In the over doped region, the observation of a T_1T=const. relation and of the residual spin Knight shift at low-T provides a clear signature that the superconductivity in $La_{2-x}Sr_xCuO_4$ is of a gapless type. A gapless **d-wave** model is useful in interpreting the T-dependence of T_1 and Knight shift below T_c. We have considered that the origin of gapless state is due to the pair braking effect caused by the structural instability from orthorhombic to tetragonal upon hole doping, and T_c is decreased by the pair braking effect and the suppression of AF spin fluctuations in the over doped region.

In the lightly doped region, the Weiss temperature, θ, associated with the strength of the staggered susceptibility, χ_Q, has 0K at the magnetic phase boundary of x=0.05, $1/T_1$ becomes T-independent at low-T below T_c, and the full width at half maximum of the intensity for x=0.10 increases at low-T below

T_c. From above results, it is considered that the AF spin fluctuations at considerably low frequency($\omega \sim 0$) is increased with decreasing hole content near the magnetic phase boundary. Thus we consider that T_c is decreased in the lightly doped region with decreasing hole content and its mobility.

In addition, phonon suppression effect on coherence peak just below T_c in the nuclear spin relaxation rate, $1/T_1$, has been investigated by ^{205}Tl NMR of Chevrel phase superconductor $TlMo_6Se_{7.5}$ with T_c=12.2K. The lack of coherence peak of $^{205}(1/T_1)$ is demonstrated in a strong coupling superconductor $TlMo_6Se_{7.5}$, while the **exponential** decrease of $1/T_1$ is confirmed over four orders of magnitude below $0.8T_c$(10K) with $2\Delta = 4.5k_BT_c$. As argued by Allen and Rainer, the strong electron-phonon decay channels open to excitation cause the unexpectedly strong damping of the quasiparticles in all dynamical properties, being the origin of the depression of coherence peak. From a comparison with an s-wave model in which the quasiparticle damping is taken into account, it is reinforced that the unusual relaxation behavior observed in high-T_c cuprates, i.e. a **power-law** T-dependence with no coherence peak below T_c, cannot be accounted for by the conventional theory of the superconductivity and/or the model based on **s-wave** paring.

From the NMR and NQR studies for the superconducting LSCO and the Chevrel phase superconductors, we conclude that the anisotropic superconducting model is valid for understanding the mechanism of superconductivity for the high-T_c superconductors. Thus it is considered that the superconductivity is due to the spin fluctuations.

Acknowledgments

The auther would like to express his sincere thanks to Professor Kunisuke Asayama for guiding him into this field, and for the continuous advice, enlightening discussions and warmhearted encouragement throughout this study.

He would also like to express his sincere thanks to Associate Professor Yoshio Kitaoka for his kind technical guidance of NMR and useful discussions and encouragement.

He would also like to express his sincere thanks to Professor Tsukio Ohtani and Mr.J.Nakabori in Okayama University of Science for provision of Chevrel compounds with good quality.

He also thanks Dr.K.Ishida, Dr.M.Kyogaku, Dr.G.-q.Zheng, Mr.S.Matsumoto and other colleagues in Asayama laboratory for their cooperation.

References

1) J.G.Bednorts and K.A.Muller: Z. Physik **B64**(1986)189.
2) D.Vaknin et al: Phys. Rev. Lett. **58**(1987)2802.
3) R.J.Birgeneau, D.R.Grabbe, H.P.Jenssen, M.A.Kastner, P.J.Picone, T.R.Thurston, G.Shirane, Y.Endoh, M.Sato, K.Yamada, Y.Hidaka, M.Oda, Y.Enomoto, M.Suzuki and T.Murakami: Phys. Rev. **B38**(1988)6614.
4) Y.Kitaoka, S.Hiramatsu, K.Ishida, T.Kohara and K.Asayama: J. Phys. Soc. Jpn. **57**(1988)30.
5) J.Watanabe et al: J. Phys. Soc. Jpn. **56**(1987)3028.
6) J.B.Torrance et al: Phys. Rev. **B40**(1989)8872.
7) H.Takagi et al: Phys. Rev. **B40**(1989)2254.
8) M.Suzuki: Phys. Rev. **B39**(1989)2312.
9) See, Proc. Int. Conf. Materials and Mechanisms of Superconductivity, Interlaken, 1988: Physica **C153-155**(1987); Stanford, 1989: Physica **C162-164**(1990).
10) K.Ishida, Y.Kitaoka and K.Asayama: J. Phys. Soc. Jpn. **58**(1989)36.; Y.Kitaoka, K.Ishida, T.Kondo and K.Asayama: Proc. 19th. Int. Conf. on Low Temperature Physics 1990: Physica **B165&166**(1990)1309.
11) T.Imai: J. Phys. Soc. Jpn. **59**(1990)2508.
12) D.J.Durand et al: in "Strong Correlation and Superconductivity" eds. H.Fukuyama, S.Maekawa and A.P.Malozemoff: Springer-Verlag, Solid State Science **89**(1989)244.
13) Y.Kitaoka, K.Ishida, K.Fujiwara, T.Kondo, M.Horvatic, Y.Berthier, P.Butaud, P.Segransan, C.Berthier, H.Katayama-Yoshida, Y.Okabe and T.Takahashi: in "Strong Correlation and Superconductivity" eds. H.Fukuyama, S.Maekawa and A.P.Malozemoff: Springer-Verlag, Solid State Science **89**(1989)262.
14) K.Ishida, Y.Kitaoka, G.Zheng and K.Asayama, J. Phys. Soc. Jpn. **60**(1991)3526.
15) K.Fujiwara, Y.Kitaoka, K.Asayama, Y.Shimakawa, T.Manako and Y.Kubo: J. Phys. Soc. Jpn. **59**(1990)3459.
16) J.T.Market, T.W.Noh, S.E.Russek and R.M.Cotts: Solid State State Commun. **63**(1987)847.
17) P.C.Hammel, M.Takigawa, R.H.Heffner, Z.Fisk and K.C.Ott: Phys. Rev. Lett. **63**(1989)1992.
18) F.Mila and T.M.Rice: Phys. Rev. **B40**(1989)11382.: Physica **C157**(1989)561.
19) A.J.Millis, H.Monien and D.Pines: Phys. Rev. **B42**(1990)167.; H.Monien, D.Pines and M.Takigawa: Phys. Rev. **B43**(1991)258.; H.Monien, P.Monthoux and D.Pines: Phys. Rev. **B43**(1991)275.

20) S.Ohsugi, Y.Kitaoka, K.Ishida and K.Asayama:
J. Phys. Soc. Jpn. **60**(1991)2351.
21) R.Chevrel, M.Sergent and J.Prigent: J. Solid State Chem. **3**(1971)515.
22) K.Yvon: Current Topics of Materials Science (North Holland Pub. Co.)
III(1978)53.
23) O.Fisher: App. Phys. **16**(1978)1.
24) J.M.Tarascon, F.J.Disalvo, D.W.Murphy, G.Hull and J.V.Waszczak:
Phys. Rev. **B29**(1984)172.
25) L.C.Hebel and C.P.Slichter: Phys. Rev. **113**(1959)1504.
26) M.Matsumura, N.Sano, T.Taniguchi and K.Asayama:
J. Phys. Soc. Jpn. **50**(1981)3937.
27) H.Nishihara, T.Ohtani, Y.Sano and Y.Nakamura: Proc. Int. Conf. on Materials and Mechanisms of Superconductivity and High-Temperature Superconductors, Kanazawa 1991, to be published in Physica **C**.
28) V.Jaccarino: in " Proc. of Int. School of Physics. Enrico Fermi" ,
Course **37** (Academic Press, New York, 1967).
29) R.E.Watson and A.J.Freeman: in " Hyperfine interactions"
eds. A.J.Freeman and R.B.Frankel (Academic Press, 1967)
30) A.M.Clogston and V.Jaccarino: Phys. Rev. **B121**(1961)1357.
31) D.E.Maclaughlin, J.D.Williamson and J.Butterworth: Phys. Rev. **B4**(1971)60.
32) A.Narath: Phys. Rev. **B13**(1976)3724.
33) J.Korringa: Physica **16**(1950)601.
34) D.E.Maclaughlin: in " Magnetic Resonance in the Superconducting State" ,
Solid State Physics **31**.
35) K.Yosida: Phys. Rev. **110**(1958)769.
36) H.L.Fine, M.Lipsicas and M.Strogin: Phys. Lett. **29A**(1969)366.
37) Y.Masuda and A.G.Redfield: Phys. Rev. **125**(1962)159.
38) G.E.Volvik and L.P.Gor'kov: Sov. Phys. TEPT **61**(1985)843.
39) H.Monien, K.Scharnberg, L.Tewdordt and D.Walker:
Solid State Commun. **61**(1987)581.
40) T.Moriya: J. Phys. Soc. Jpn. **18**(1963)516.
41) R.Balian and N.R.Werthamer: Phys. Rev. **131**(1963)1553.
42) P.W.Anderson and W.F.Brinkman: in " The Physics of Liquid and Solid Helium"
ed. K.H.Benneman and J.B.Koterson (John Wiley & Sons, New York, 1979)
Pt.2 p.177.
43) D.E.Farrel et al: Phys. Rev. **B36**(1987)4025.
44) K.Yoshimura, T.Imai, T.Shimizu, Y.Ueda, K.Kosuge and H.Yasuoka:
J. Phys. Soc. Jpn. **58**(1989).

45) K.Kumagai and Y.Nakamura: Physica **C157**(1989)307.
46) S.Ohsugi, Y.Kitaoka, K.Ishida and K.Asayama: Physica **C185-189**(1991)1099.
47) N.Bulute, D.Hone, D.J.Scalapino and N.E.Bickers: Phys. Rev. **B41**(1990)1797.
48) T.Moriya, T.Takahashi and K.Ueda: J. Phys. Soc. Jpn. **59**(1990)2905.
49) H.Fukuyama and K.Kuboki: to appear in J. Phys. Soc. Jpn.
50) H.Kohno and K.Yamada: Prog. Theor. Phys. **85**(1991) No.1.
51) Y.Kitaoka, S.Ohsugi, K.Ishida and K.Asayama, Physica **C170**(1990)189.
52) K.Ishida et al: unpublished.
53) G.Shirane, R.J.Birgeneau, Y.Endo, P.Gehring, M.A.Kastner, K.Kitazawa, H.Kojima, I.Tanaka, T.R.Thurston and K.Yamada: Phys. Rev. Lett. **63**(1989)330.
54) H.Yasuoka: in "Strong Correlation and Superconductivity" eds. H.Fukuyama, S.Maekawa and A.P.Malozemoff, Springer-Verlag, Solid State Science (1989)254.
55) Y.Kitaoka, S.Ohsugi, K.Asayama and T.Ohtani: Phys. **C192**(1992)272.; S.Ohsugi, Y.Kitaoka, K.Ishida, M.Kyogaku, K.Asayama and T.Ohtani: J. Phys. Soc. Jpn. **61**(1992).
56) K.Ishida, T.Kondo, Y.Kitaoka and K.Asayama: J. Phys. Soc. Jpn. **58**(1989)2638.
57) S.Ohsugi, Y.Kitaoka, K.Ishida, S.Matsumoto and K.Asayama: presented at the SCES 92, Sendai, 1992, to appear in Physica **B**.
58) S.Wada and K.Asayama: J. Phys. Soc.. Jpn. **34**(1973)1168.
59) O.V.Dolgov, A.A.Golubov and A.E.Koshelev: Solis State Commun. **72**(1989)81.
60) L.Coffey: Phys. Rev. Lett. **62**(1990)1071.
61) P.B.Allen and D.Rainer: Nature **349**(1991)349.
62) M.Takigawa: in " Dynamics of Magnetic Fluctuations in High Temperature Superconductors" eds. G.Reiter, P.Horsch and G.Psaltakis(Plenum, New York).
63) M.Mali, D.Brinkmann, L.Pauli, J.Roos and H.Zimmermann: Phys. Lett. **A124**(1987)112.
64) W.W.Warren Jr., R.E.Walstedt, G.F.Brennert, G.P.Espinosa, J.P.Remeika: Phys. Rev. Lett. **59**(1987)1860.
65) Y.Kitaoka, S.Hiramatsu, T.Kondo and K.Asayama: J. Phys. Soc. Jpn. **57**(1988); Y. Kitaoka et al: Physica **C153-155**(1988)83.
66) T.Imai, T.Shimizu, H.Yasuoka, Y.Ueda and K.Kosuge: J. Phys. Soc. Jpn. **57**(1988)2280.
67) K.Asayama, G.q.Zheng, Y.Kitaoka, K.Ishida and K.Fujiwara: Physica **C178**(1991)281.
68) K.Fujiwara, Y.Kitaoka, K.Asayama, Y.Shimakawa, T.Manako and Y.Kubo: Physica **B165-166**(1990)1295.; Y.Kitaoka, K.Fujiwara, K.Ishida, K.Asayama, Y.Shimakawa, T.Manako and Y.Kubo: Physica **C179**(1991)107.

69) B.S.Shastry: Phys. Rev. Lett. **63**(1989)1288.
70) Y.Kitaoka, K.Ueda, T.Kohara, K.Asayama, Y.Onuki and T.Komatsubara: J. Mag. & Magn. Mater. **52**(1985)341.; Y.Kohori, T.Kohara, H.Shibai, Y.Oda, Y.Kitaoka and K.Asayama: J. Phys. Soc. Jpn. **57**(1988)395.; D.E.MacLaughlin, Cheng Tien, W.G.Clerk, M.D.Lan, Z.Fisk, J.L.Smith and M.R.Ott: Phys. Rev. Lett. **53**(1984)1833.
71) K.Miyake: J. Magn, Magn. Mater. **663-64**(1987)411.; S.Schmitt-Rink, K.Miyake and C.M.Varma: Phys. Rev. Lett. **57**(1986)2575.
72) K.Ishida et al: Physica **C179**(1991)29.
73) P.Hirschfeld, D.Vollhardt and P.Wolfle: Solid State Commun. **59**(1986)111.
74) K.Miyake, private commun., S.Schmitt-Rink, K.Miyake and C.M.Varma: unpublished.
75) H.Takagi et al: Phys. Rev. Lett. **68**(1992)3777.
76) M.Oda, H.Matsuki and M.Ido: Solid State Commun. **74**(1990)1321.; M.Oda, T.Nakano, Y.Kamada and M.Ido: Physica **C185-198**(1991)1157.